International Journal of Material Forming (2020) 13:749–787
https://doi.org/10.1007/s12289-020-01580-x

IJMF 10TH ANNIVERSARY - ADVANCES IN MATERIAL FORMING

Advances in anisotropy of plastic behaviour and formability of sheet metals

Dorel Banabic[1] · Frédéric Barlat[2] · Oana Cazacu[3] · Toshihiko Kuwabara[4]

Received: 30 September 2019 / Accepted: 9 July 2020 / Published online: 24 August 2020

Abstract

This paper reviews the most recent models for description of the anisotropic plastic behavior and formability of sheet metals. After a brief review of classic isotropic yield functions, recent advanced anisotropic criteria for polycrystalline materials of various crystal structures and their applications to cup drawing are presented. Next, the discussion focuses on novel formulations of anisotropic hardening. A brief review of the experimental methods used for characterizing and modeling the anisotropic plastic behavior of metallic sheets and tubes under biaxial loading is presented. The experimental methods and theoretical models used for measuring and predicting the limit strains, development of new tests for determining the Forming Limit Curves (FLC), as well as on studying the influence of various material or process parameters on the limit strains are presented.

Keywords Anisotropic yield criteria · Anisotropic hardening · Polycrystals · Biaxial tensile tests · Forming limit · Sheet metals

Introduction

Given the current trends of globalization and active competition on the world market, especially for automotive, the reduction of the lead time can be decisive. Virtual manufacturing using finite element analyses contribute to this reduction. The finite element analysis has been applied extensively to compare design options, understand the influence of process conditions on both formability and structural performance and to reduce the trial and error of tools for optimum performance. For realistic simulations, the use of improved constitutive models for the description of the mechanical behaviour and accurate prediction of formability are essential.

In particular, the use of yield conditions that capture the key features of the plastic behaviour during forming operations are essential. Intrinsic anisotropy associated to a given crystal structure as well as the anisotropy induced by processing of polycrystalline metallic materials place severe restrictions on the form of yield conditions. In Section Anisotropic yield criteria, after a brief review of the classical isotropic yield functions, we discuss the rigorous approaches that enable the extension of isotropic yield criteria such as to account for specific material symmetries. Examples of very versatile anisotropic two-dimensional (2D) and three-dimensional yield criteria (3D) are provided for metallic materials with various crystal structures. For the case of 3-D yield orthotropic yield criteria based on Hershey-Hosford yield criterion involving six anisotropy coefficients, equivalent expressions in terms of stresses and analytical identification procedures which enable to directly correlate the anisotropy parameters to mechanical properties, and consequently standardize their use in F.E. codes are discussed. The capabilities of anisotropic yield functions to describe the plastic behaviour for loading conditions other than those used for parameter identifications are also illustrated for FCC aluminium, HCP magnesium and titanium materials. Specifically, it is shown that currently it is possible to describe with great accuracy the earing profile of certain highly textured aluminium alloys. The importance of

✉ Dorel Banabic
banabic@tcm.utcluj.ro

[1] CERTETA - Research Centre on Sheet Metal Forming Technology, Technical University of Cluj Napoca, 400140 Cluj Napoca, Romania

[2] Graduate Institute of Ferrous Technology, Pohang University of Science and Technology, 77 Cheongam-ro, Nam-gu, Pohang, Gyeongbuk 37673, Republic of Korea

[3] Department of Mechanical and Aerospace Engineering, University of Florida/REEF, Shalimar, FL 32579, USA

[4] Division of Advanced Mechanical Systems Engineering, Institute of Engineering, Tokyo University of Agriculture and Technology, 2-24-16, Nakacho, Koganei-shi, Tokyo 184-8588, Japan

consideration of the combined effects of anisotropy and tension-compression asymmetry in modelling yielding of HCP materials is put into evidence for torsional loadings and bulge forming. The influence of the particularities of yielding on damage evolution and ultimately failure and recent yield functions accounting for plasticity-damage couplings in both FCC and HCP materials are discussed in Section Formability of metallic materials.

The anisotropic yield conditions employed in sheet metal forming simulations usually contain one state variable that account for the strength of the material or the associated plastic work-based effective strain. This means that hardening is isotropic and that the yield surface keeps the same shape during plastic deformation. However, isotropic hardening in not always sufficient to accurately predict plasticity during an entire forming process [1], for instance, for the prediction of sprinbgback [2]. In fact, beside process parameters, it is known that the prediction of springback is very sensitive to material properties including the variations of the elastic modulus as discussed in [3, 4]. Nevertheless, regarding plastic anisotropy, springback strongly depends on the Bauschinger and permanent softening effects that can be mostly observed after one or several load reversals. In these deformation-induced plasticity cases, it is necessary to capture the anisotropic hardening effects. This require the introduction of additional state variables in the formulations allowing drastic changes of the yield condition after severe loading changes. Non-linear kinematic hardening [5] that corresponds to a translation of the yield condition in stress space and / or distortional plasticity have been useful for this purpose. In fact, kinematic models with two or several surfaces [6, 7] have been successfully employed for the modeling of anisotropic hardening effects in forming simulations.

Since the approaches such as those briefly reviewed in Section Anisotropic yield criteria require proper validation to ensure that they are appropriate for given materials and processes, careful uniaxial and multiaxial experiments are required, which is the topic of Section Experimental validation of the anisotropic models. Moreover, it is important to note that the prediction of formability, as discussed in Section Formability of metallic materials, strongly depends on the constitutive model employed in the failure analyses considered [8]. This explains why these three subjects are treated simultaneously in a single review. The plastic deformation behavior of sheet metals is commonly characterized using uniaxial tensile test data, i.e. uniaxial yield stresses and *r*-values with respect to several tensile directions. In addition, a uniaxial compressive yield stress in the thickness direction can be used as the equi-biaxial yield stress for pressure-independent materials [9] [10] (it should be noted that the in-plane stress at the apex of a hydraulic bulge specimen is not necessarily equi-biaxial if the material is anisotropic [11]). The deformation characteristics for other stress states are automatically determined by the material model (yield function) assumed in the analysis. However, there is no guarantee that the assumed material model can accurately reproduce the deformation characteristics of the material under the stress states other than those used for the material characterization. In actual sheet metal forming processes the material is subjected to complex multiaxial stress paths. In addition, unloading makes the material trace multiaxial unloading stress paths (nonlinear unloading behavior of the material significantly affects the magnitude of springback). Therefore, to improve the prediction accuracy of sheet metal forming simulations, the material characterization should be based on the data obtained using multiaxial stress tests.

The shape of the yield surface changes depending on the strain history. It is therefore impossible to formulate the evolution of the yield surface associated with arbitrary strain paths as there are an unlimited number of strain paths occurring during actual metal forming. From this reason a practical material characterization using multiaxial stress tests is usually based on a linear stress path experiment; stress-strain curves are measured for several different linear stress paths and a contour of plastic work and the directions of the plastic strain rates, $\mathbf{D}^{\mathrm{p}}$, associated with a specific value of reference plastic strain are determined. The work contour is assumed to represent a yield surface of the material. The yield function that accurately reproduces the work contour and the direction of the $\mathbf{D}^{\mathrm{p}}$ is identified as a proper material model for the material, e.g. [12–14]. Moreover, it is possible to take into account the evolution of the work contour by changing the material parameters of the yield function as a function of the plastic work per unit volume, or equivalently, of the reference plastic strain, e.g. [13, 15, 16].

The hydraulic bulge test with optical measuring systems and the biaxial tensile test using a cruciform test piece have been standardized as ISO 16808 [17] and ISO 16842 [18], respectively, in 2014. That is an important step in evolving the knowledge about the deformation characteristics of materials under multiaxial stress and in improving the accuracy of material characterization. Shear [19–21] and plane strain tension [22] tests are also effective in material characterization. In particular shear tests are useful to measure the work hardening characteristics in a strain range far exceeding that of uniform elongation in a uniaxial tensile test. The use of full-field measurements, e.g. digital image correlation (DIC), makes it possible to choose complex geometries for the test specimens [23, 24], introducing heterogeneous strain fields. This enables the plastic deformation of the test specimen to be probed at many different stress states at once; a proper material model can be identified by minimizing the difference between the experimental and simulated strain distributions. The virtual fields method (VFM) integrated into a DIC platform is another efficient technique for extracting material parameters from full-field measurements [25–28]. It is computationally time efficient and there is no need to use FEA; therefore, it emerges as a user-friendly tool for identifying proper material models in industrial forming simulations. We present these experimental

methods for material characterization in more detail in the Section Experimental validation of the anisotropic models.

In the last decade, researchers in the field of sheet metal formability analysis have focused their attention on the following directions: the development of new concepts for FLC; refining the method for experimental determination of FLC; improving their prediction models. New concepts such as "Generalized Forming Limit Concept (GFLC)" ([29, 30]) and "polar diagram of the effective plastic strain- PEPS diagram" ([31, 32]) have emerged, promising an increasing applicability in industrial practice, which is essential for the analysis of processes that have a pronounced non-proportional strain-path. The standardization of the FLC determination method in 2008 [33] was an important step in increasing the robustness and accuracy of determining the limit deformations. Subsequently, the German IDDRG Group, based on the experience of companies that developed the Digital Image Correlation (DIC) method, proposed a new method based on a time-dependent technique that was standardized by ISO in 2012 [34]. In recent years, the time-dependent method has been improved by various groups in Germany [35] [36], Spain [37], US [38], Canada [39], Norway [40], etc. Scientists proposed new procedures for FLC determination, such as hydraulic bulging of a double specimen [41] or cruciform specimens test [35, 42] while also analyzing the influences of different parameters on the shape and position of FLC, such as: temperature [43–45]; strain rate [43, 44]; strain path [29] etc. Crystal-plasticity-based FLC prediction is another research area that has recently seen significant results [46–48]. Implementing ductile damage models (Gurson-Tvergaard-Needleman -GTN- model) in FE codes has improved the FLC prediction [49]. Several research groups, especially Iranian and Chinese, have studied the effect of the normal pressure on the formability [50–54] etc. Finally, for topics such as the formability of multi-layer (sandwich) sheets ([55–61]), the extension of the Modified Maximum Force Criterion-MMFC ([62, 63]) or the perturbation approach ([64, 65]) have also seen significant progress in the last decade. We present these approaches in more detail in the following sections of the paper. Due to the volume limitation, this paper does not cover all areas of research in the field. Specifically, topic such as sheared edge fracture [66, 67] is not covered in this paper.

Anisotropic yield criteria

For a fully-dense metallic material, the plastic response is classically considered as independent of the hydrostatic pressure (e.g. for single-crystals, see [68, 69]; for polycrystalline materials, see [70]). Thus, the yield function is a function of $\mathbf{s}$, the deviator of the Cauchy stress tensor, $\boldsymbol{\sigma}$. If the material is isotropic, the yield function should have the same form irrespective of the coordinate frame. This requirement dictates that the yield function depends on $\mathbf{s}$ through its invariants, J_2 and J_3. It follows, that an isotropic yield function should be a symmetric function of the eigenvalues s_j, j = 1…3 of $\mathbf{s}$.

The most used isotropic yield function that satisfies this mathematical requirement was proposed by von Mises in 1913. It states that the material enters the plastic regime when the second-invariant, J_2, reaches a critical limit. Results of tests under combined tension-torsion on various isotropic materials (e.g. [71]) showed the influence of the third-invariant, J_3 on yielding. Examples of classic yield functions depending on both invariants include Tresca, Drucker [72] and Hershey-Hosford (see [73, 74]). Drucker yield function is defined as:

$$J_2^3 - cJ_3^2 = \tau_Y^6, \tag{1}$$

where τ_Y is the yield stress in pure shear, and c is a constant. This constant is expressible as the ratio between the yield stress in uniaxial tension, σ_T, and τ_Y (e.g. see [75]). For $c = 0$, the Drucker [72] yield surface reduces to the von Mises's one while for $c > 0$, it lies between those of von Mises and Tresca's. The Hershey-Hosford yield function is expressed in terms of the eigenvalues s_j as

$$\phi = |s_1 - s_2|^a + |s_2 - s_3|^a + |s_3 - s_1|^a = 2\bar{\sigma}^a \tag{2}$$

where a is a constant larger than 1 while $\bar{\sigma}$ defines the effective stress associated with this criterion (i.e. for simple tension it reduces to the uniaxial yield stress, denoted σ_T). For an exponent $a = 2$ or $a = 4$, Eq. (2) reduces to the von Mises criterion, whereas for a = 1 and the limiting case $a \to \infty$, it leads to Tresca yield condition. For BCC and FCC isotropic materials the recommended values are $a = 6$, and $a = 8$, respectively (e.g. see [76]).Very recently, it has been demonstrated that for any even and positive integer a, the Hershey-Hosford yield function is a homogeneous polynomial of J_2 and J_3^2. In particular, Hershey-Hosford yield function for BCC materials ($a = 6$) and FCC materials ($a = 8$) are is given by:

$$\begin{aligned} (s_1 - s_2)^6 + (s_2 - s_3)^6 + (s_3 - s_1)^6 &= 66\,J_2^3 - 81\,J_3^2, \\ (s_1 - s_2)^8 + (s_2 - s_3)^8 + (s_3 - s_1)^8 &= 258\,J_2^4 - 648\,J_2 J_3^2 \end{aligned} \tag{3}$$

It is clearly seen that Hershey-Hosford with ($a = 6$) is a particular case of Drucker [77] corresponding to $c = 81/66$ (see Eq. (1)). For more details and the new expressions of Hershey-Hosford criterion in terms of invariants for other values of the exponent a, the reader is referred to Cazacu [78] and the monograph of Cazacu, Revil, Chandola [79].

Generally, in polycrystalline metallic sheets the constituent crystals are not randomly oriented, but are distributed along preferred orientations that result from rotations that occur during processing. For a given fabrication process, the textures that develop contain one or several ideal components (e.g. [80,

81]). In the framework of crystal plasticity, the most widely used approach for describing plastic anisotropy and for forming of single crystal or textured polycrystalline sheets is to use Schmid law for modeling slip at the single crystal level, and Taylor's assumption of homogeneous deformation of all crystals ([82, 83], generally known as Taylor-Bishop-Hill model, see also later discussion in the next sections). While increasingly complex homogenization schemes have been proposed, use of such models for large-scale metal forming is still limited, mainly due to the prohibitive computational cost (e.g. see [84]).

Using the new single crystal yield criterion [85], Cazacu et al. [75] showed that for ideal texture components, the yield stress and plastic strain ratios can be obtained analytically. For the case of strongly textured sheets containing a spread about the ideal texture components, these authors showed that the polycrystalline response can be obtained numerically on the basis of the same single-crystal criterion with appropriate homogenization schemes (see [86]). Moreover, it was shown that for textures with misorientation scatter width up to 25°, the numerical predictions are very close to those obtained analytically for an ideal texture and irrespective of the number of grains in the sample Lankford coefficients have finite values for all loading orientations. Illustrative examples for sheets with textures containing a combination of few ideal texture components were also presented in [86, 87]. For examples of applications of this polycrystalline model to industrial textured steel and aluminum alloys, the reader is referred to [79].

Orthotropic yield criteria for textured polycrystalline metals with cubic crystal structure

In the framework of the mathematical theory of plasticity, the plastic anisotropy polycrystalline textured metallic materials is modeled using analytical yield criteria in conjunction with appropriate hardening descriptions (see Section Anisotropic hardening). An extension of the isotropic Mises criterion such as to account for orthotropy was proposed by Hill [88]. For general loadings, this criterion involves six anisotropy coefficients. The use of this yield function in conjunction with associated flow rule, and isotropic or kinematic hardening laws has led to significant advances in metal technology, in particular in forming of certain textured steels ([79, 84]). With the development of new aluminum alloys, it has become evident the need for yield criteria that could describe the observed plastic anisotropy of these materials. To this end, several attempts have been made to extend to orthotropy Hershey-Hosford's yield function given by Eq. (2) (e.g. Hill [89]). The first formulations involving shear stress components that are well-posed and fulfill the mathematical restrictions imposed by orthotropy were developed by Barlat and collaborators, namely Yld89 yield function for plane stress loadings (see [90]), and Yld91 yield function for three-dimensional (3-D) loadings (Barlat et al. [76]). As demonstrated in Karafillis and Boyce [91], Yld91 can be obtained by substituting in Eq. (2) the stress $\bar{\sigma}$ with a transformed stress tensor $\widetilde{\mathbf{S}}$ defined as:

$$\widetilde{\mathbf{S}} = \mathbf{C}\boldsymbol{\sigma} \tag{4}$$

where $\mathbf{C}$ is a symmetric fourth-order tensor, orthotropic, and deviatoric. Similarly, it can be shown that in fact according to Hill [88] criterion the onset of plastic deformation occurs the second-invariant of $\widetilde{\mathbf{S}}$ reaches a critical value. Although Yld91 represents a clear improvement over Hill [88] criterion, its use is more limited than Hill's or Yld89 or more recent 2-D orthotropic yield criteria (for examples of 2-D yield criteria, see the monograph of Banabic [92]).

This is mainly due to the fact that in its original formulation this criterion is expressed in terms of the eigenvalues of the transformed stress tensor $\widetilde{\mathbf{S}}$ and as such the quality of the parametrization depends on the experience of the analyst. Recently, Cazacu [78, 93] derived equivalent explicit expressions of Yld91 [76] and the Karafillis and Boyce [91] orthotropic yield criterion in terms of the Cauchy stress components and established direct correlations between the anisotropy coefficients and mechanical properties. Moreover, it was shown that as in the case of Hill [88] criterion, the anisotropy coefficients involved in these yield criteria can be determined analytically based only on four yield points or only using the three Lankford coefficients and the uniaxial tension yield point along RD. These analytical identification procedures enable to directly correlate the anisotropy parameters to mechanical properties, and consequently standardize their use in finite element (F.E.) codes. Another 3-D orthotropic yield function involving a unique linear transformation was proposed by Cazacu and Barlat [94]. This orthotropic yield function, denoted by these authors YLDLIN, was obtained by substituting in the expression of Drucker's criterion given by Eq. (1), the stress tensor by $\widetilde{\mathbf{S}}$, i.e.

$$\Phi = g\left(\widetilde{\mathbf{S}}\right) \tag{5}$$

It is also important to note that for plane-stress loadings, Hill's criterion or any other orthotropic yield criterion obtained using one linear transformation of type (3) involves four anisotropy coefficients. As a consequence, these criteria cannot predict with accuracy both the anisotropy in r-values and yield stresses. The implications in terms of accuracy of the predictions for various forming processes have been discussed in several review papers (e.g. [84]) and benchmarks.

An important question when modeling anisotropic materials is related to the number of anisotropy coefficients involved in the formulation. This is because material symmetries place severe restrictions on the form of the yield

functions. The number of independent anisotropy coefficients is not arbitrary, the general form of a well-posed yield function and the number of anisotropy coefficients being dictated by invariance properties associated with the material's symmetries. For example, orthotropy dictates that for general 3-D loadings the yield function cannot contain more than 18 anisotropy coefficients (for the full mathematical proof and the orthotropic form of the invariants J_2 and J_3, the reader is referred to Cazacu and Barlat [94]).

A rigorous approach that allows to extend any isotropic criterion such as to account for any material symmetry consists in substituting in the expression of the isotropic yield function, $J_2$and J_3 with their anisotropic counterparts. Using general theorems of representation of tensor functions, Cazacu and Barlat [94, 95] developed orthotropic invariants of the stress tensor, denoted as J_2^o and J_3^o, respectively. J_2^o and J_3^o are homogeneous polynomials of degree two, and three in stresses, respectively; invariant to any transformation belonging to the symmetry group of the material; pressure-insensitive, and for isotropic conditions reduce to J_2 andJ_3, respectively. Irrespective of the mathematical form of the isotropic yield function, the anisotropic yield criterion obtained using the linear transformation approach is a particular form of the extension of the same isotropic criterion obtained using orthotropic invariants (see [79, 84]).

An orthotropic extension of Drucker's yield function expressed in terms of the orthotropic invariants J_2^o and J_3^o was proposed by Cazacu and Barlat [94]. This 3-D yield function involves the maximum admissible number of anisotropy coefficients was derived by Cazacu and Barlat [94]. It has been applied to various aluminum alloys, its predictive capabilities being demonstrated in benchmarks (e.g. Numisheet 2016 benchmark 1, see [77, 96, 97]. Recently, Cazacu [98] proposed the following orthotropic yield function:

$$\phi = \left(J_2^o\right)^4 - \alpha\left(J_2^o\right)\left(J_3^o\right)^2 \tag{6}$$

with α being a parameter. This criterion was mainly used for description of the plastic anisotropy of FCC materials (e.g. [99].

In the last two decades, very versatile orthotropic yield functions were developed using two linear transformations. The corresponding transformed stress tensors are defined as:

$$\widetilde{\mathbf{S}}' = \mathbf{C}'\mathbf{s}, \widetilde{\mathbf{S}}'' = \mathbf{C}''\mathbf{s}, \tag{7}$$

with the fourth-order tensors $\mathbf{C}'$and $\mathbf{C}''$ being orthotropic. For plane stress, the anisotropic Yld2000-2d yield function was defined as (see [100]):

$$F = \left|\widetilde{S}_1' - \widetilde{S}_2'\right|^a + \left|2\widetilde{S}_2'' + \widetilde{S}_1''\right|^a + \left|2\widetilde{S}_1'' + \widetilde{S}_2''\right|^a = 2\bar{\sigma}^a \tag{8}$$

$\widetilde{S}_1', \widetilde{S}_2'$ and $\widetilde{S}_1'', \widetilde{S}_2''$ are the principal values of $\widetilde{s}'$ and $\widetilde{s}''$, respectively. It involves eight independent coefficients, namely three C_{ij}' and five C_{kl}''. The capabilities of this yield function to describe the plastic anisotropy of textured aluminum and steel sheets have been demonstrated for numerous forming applications (see [84, 100]).

Based on the Barlat and Richmond [101] formulation, independently, Banabic and collaborators, developed since 2000 (see for example [102]) the BBC family criteria. The BBC2005 criterion (see [103–105]).) is defined as:

$$\alpha|\Gamma + \Psi|^a + \alpha|\Gamma - \Psi|^a + (1-\alpha)|2\Lambda|^a = \sigma^a \tag{9}$$

where Γ, Ψ and Λ involve the three plane stress components and anisotropy coefficients. It was shown that this yield function contains eight independent coefficients and that, in fact, it is the same as Yld2000-2d only written in a different form (see [106]).

For highly anisotropic sheets, a plane-stress yield function, called BBC2008, expressed in the form of a finite series that can be expanded to retain more or fewer terms, depending on the available experimental data was proposed by Comsa and Banabic [107]. The capabilities of the BBC2008 yield criterion to predict the earing profiles of the aluminum alloys AA5042-H2 and AA2090-T3 were illustrated in Vrh et al. [108].

For certain anisotropic materials for which the microstructure evolution occurs even for the simplest loading conditions (e.g. monotonic simple tension or compression) or for applications where texture evolution during plastic deformation cannot be neglected, the anisotropy coefficients involved in orthotropic yield criteria cannot be considered as being constants. Since it is not possible to perform all the mechanical tests necessary to calibrate evolution laws for all the anisotropy coefficients, instead virtual tests using crystal plasticity codes may be conducted. Such an approach was proposed by Plunkett et al. [109] who used the self-consistent crystal plasticity code VPSC ([110]) to calibrate Cazacu et al. [111] yield function and thus model the evolving anisotropy of hcp zirconium during monotonic loadings. To account for texture evolution during cup drawing of aluminum alloy AA6016, recently, Gawad et al. [112] used the Alamel crystal plasticity model (e.g. [113]) to provide adaptive updates of the local anisotropy in the integration points of a macroscopic F.E. model with yielding described by the BBC 2008 criterion [107]. Moreover, an enhanced yielding description and computationally efficient identification strategy for the anisotropy coefficients involved in the formulation was proposed. For general loadings, Barlat et al. [114] proposed the yield function Yld2004-18p, which extends Eq. (2)

$$\varphi\left(\widetilde{S}_i^{'},\widetilde{S}_j^{''}\right)=\sum_{i,j=1\ldots3}\left|\widetilde{S}_i^{'}-\widetilde{S}_j^{''}\right|^a=4\sigma^a \tag{10}$$

with the fourth-order tensors $\mathbf{C}^{'}$and $\mathbf{C}^{''}$ (see Eq. (7)). Specifically, relative to the orthotropy axes, the transformed stress tensors are written in matrix form as

$$\widetilde{S}\equiv\begin{bmatrix}\widetilde{s}_{xx}\\ \widetilde{s}_{yy}\\ \widetilde{s}_{zz}\\ \widetilde{s}_{yz}\\ \widetilde{s}_{zx}\\ \widetilde{s}_{xy}\end{bmatrix}=\begin{bmatrix}0 & -c_{12} & -c_{13} & 0 & 0 & 0\\ -c_{21} & 0 & -c_{23} & 0 & 0 & 0\\ -c_{31} & -c_{32} & 0 & 0 & 0 & 0\\ 0 & 0 & 0 & c_{44} & 0 & 0\\ 0 & 0 & 0 & 0 & c_{55} & 0\\ 0 & 0 & 0 & 0 & 0 & c_{66}\end{bmatrix}\begin{bmatrix}s_{xx}\\ s_{yy}\\ s_{zz}\\ s_{yz}\\ s_{zx}\\ s_{xy}\end{bmatrix} \tag{11}$$

with the appropriate symbols (prime and double prime) for each transformation. Of the 18 parameters (nine per linear transformation) involved in Yld2004-18p, two can always be set equal to unity (for more details, see van den Boogaard et al. [115]). It was shown that this yield criterion predicts with great accuracy the plastic response of highly anisotropic materials [116, 117] (e.g. see Fig. 1).

Yoshida and collaborators [11] proposed a yield criterion defined as the sum of "n" YLDLIN yield functions. Although the formulation involves 6xn parameters, not all these parameters are independent. For an in-depth discussion of other anisotropic formulations the reader is referred to the recent monographs [79, 92] [118] and reviews presented in (e.g. [84, 117, 119–126].

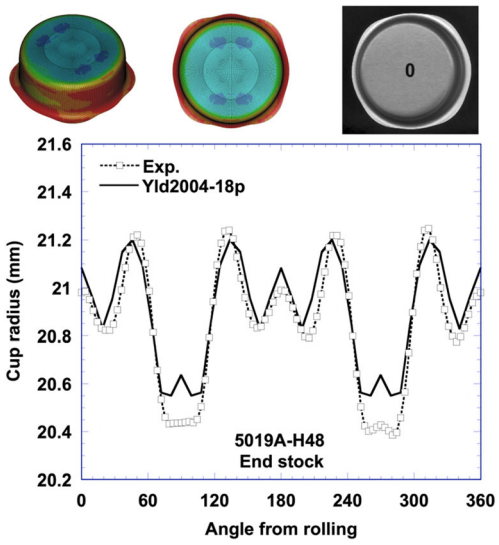

Fig. 1 Finite-element simulations of earing cup profiles for 5019A-H48 aluminum alloy using the Yld2004-18p stress potential in comparison with experimental data (simulation data provided by Prof. Jeong-Whan Yoon) [117]

Anisotropic yield criteria for hexagonal-close packed metals

Improvements in energy efficiency and reduction of greenhouse gas emissions have been one of the central concerns in the last two decades, with light metallic alloys based on magnesium and titanium receiving increased attention. For example, there has been a renewed interest in magnesium alloys in view of potential applications in the automotive, computer, communication and consumer electronic products industries. The global magnesium production each year was about 250,000 tons before 2000, but over the past 5 years an average of more than 650,000 tons of magnesium metal was produced each year (see [127]. However, existing applications are mainly based on cast products. The reasons for the limited use of sheets are related to their comparably poor formability, especially at room temperature (e.g. see [128]. This is because most cold-rolled hexagonal close packed (hcp) alloy sheets have basal or nearly basal textures. As a result, the yield surfaces are not symmetric with respect to the stress free condition (see [129, 130]). Since HCP metal sheets exhibit strong textures (e.g. for AZ31 Mg the c-axis of most grains is oriented predominantly perpendicular to the thickness direction), a pronounced anisotropy in yielding is observed. As mentioned in the previous section, the rigorous methods to extend any isotropic yield criterion such as to account for the initial plastic anisotropy (initial texture) or to describe an average material response over a certain deformation are general, and as such applicable to any material, including hcp metals. The major difficulty encountered in formulating analytic expressions for the yield functions of hcp metals is related to the description of their tension-compression asymmetry. Yield functions in the three-dimensional stress space that describe both the tension-compression asymmetry and the anisotropic behavior of fully-dense hcp metals have been developed. To describe yielding asymmetry in isotropic pressure-insensitive materials that results either from twinning or from non-Schmid slip effects at single crystal level, Cazacu and Barlat [131] proposed an isotropic criterion expressed in terms of all invariants of the stress deviator:

$$f\equiv(J_2)^{\frac{3}{2}}-cJ_3=\tau_Y^3, \tag{12}$$

where τ_Y is the yield stress in pure shear and c is a material constant. For $c=0$, this criterion reduces to the von Mises yield criterion. It was shown that this isotropic yield criterion describes with great accuracy the crystal plasticity simulation results of Hosford and Allen [130] for randomly oriented polycrystals deforming solely by twinning or for isotropic polycrystals with constituent grains deforming by slip governed by a modification of Schmid law involving normal stress components that was proposed by Vitek et al. [132] (for more details, see Cazacu and Barlat [133]). The isotropic

criterion (10) was further extended such as to incorporate orthotropy using the generalized invariants approach. The orthotropic criterion is defined as:

$$f \equiv \left(J_2^o\right)^{\frac{3}{2}} - cJ_3^o \tag{13}$$

where J_2^o and J_3^o denote the orthotropic generalizations of the isotropic invariants J_2, J_3 respectively. For general stress states, the criterion involves 17 anisotropy coefficients. Comparison between this orthotropic criterion and data on magnesium and its alloys (see Graff et al. [134]) and titanium alloys (see Cazacu and Barlat [131]) show that this orthotropic criterion accurately describes both the anisotropy and tension-compression asymmetry in yielding of these materials. If for a given material mechanical data are limited, it is recommended to use the orthotropic criterion of Nixon et al. [135]. This latter criterion is the extension of the isotropic yield function given by Eq. (10). It was obtained using one linear transformation, the fourth-order tensor **C** in Eq. (3) being taken symmetric, orthotropic, and deviatoric.

Cazacu et al. [111] developed another isotropic pressure-insensitive yield criterion that accounts for yielding asymmetry between tension and compression. This isotropic criterion involves all principal values of the stress deviator and is defined as

$$\varphi(s) = (|s_1| - ks_1)^a + (|s_2| - ks_2)^a + (|s_3| - ks_3)^a \tag{14}$$

where k is a material constant while a is an integer. For the yield function to be convex: $-1 \le k \le 1$. It is important to note that for $k \neq 0$, the yield function is not an even function. Therefore, according to the criterion the yielding response in tension and compression are different.

To capture simultaneously anisotropy and tension/compression asymmetry in yielding, the isotropic yield criterion given by Eq. (14) was extended to orthotropy using one linear transformation. The effective stress associated with the orthotropic criterion is:

$$\widetilde{\sigma}_e = B\left[(|\Sigma_1| - k\Sigma_1)^a + (|\Sigma_2| - k\Sigma_2)^a + (|\Sigma_3| - k\Sigma_3)^a\right]^{1/a} \tag{15}$$

In Eq. (15), Σ_1, Σ_2, Σ_3 are the principal values of the transformed stress tensor $\mathbf{\Sigma} = \mathbf{Cs}$, where the fourth-order tensor **C** is not symmetric; B is a constant defined such that the equivalent stress, $\widetilde{\sigma}_e$, reduces to the tensile flow stress along RD. Thus, for full 3-D loadings, 8 anisotropy coefficients are involved in the criterion (15).

The quadratic form of this orthotropic yield criterion (i.e. $a = 2$ in Eq. (15)) was shown to exhibit accuracy in describing the yield loci of a variety of HCP materials. As an example, in Fig. 2a are presented in the (RD-TD) plane the predicted yield loci for a high-purity HCP-Ti material corresponding to several levels of the equivalent plastic strain ε^p. To capture the difference in strain hardening rates between tension and compression loadings observed experimentally (see Nixon et al. [135]), all the material parameters involved in the expression of the yield function, namely the anisotropy coefficients as well as the parameter k were considered to evolve with ε^p. The equivalent plastic strain ε^p was calculated using the expression of $\widetilde{\sigma}_e$ given by Eq. (15) and the work-equivalence principle. The calibration was done using as input the flow stresses in uniaxial tension and uniaxial compression as well as the Lankford coefficients. Additional constraints were imposed such as to ensure that for any given stress state, the yield surface at a given level of equivalent plastic strain is exterior to that corresponding to lower levels of plastic strain (i.e. $\overline{\sigma}\left(L_{ij}^u, k^u, \sigma(\theta_l)^u\right) > \overline{\sigma}\left(L_{ij}^u, k^u, \sigma(\theta_l)^{u-1}\right)$, with $\sigma(\theta_l)^u$ and $\sigma(\theta_l)^{u-1}$ denoting the stress state belonging to the yield surface "u" and "$u-1$", respectively corresponding to same θ_l

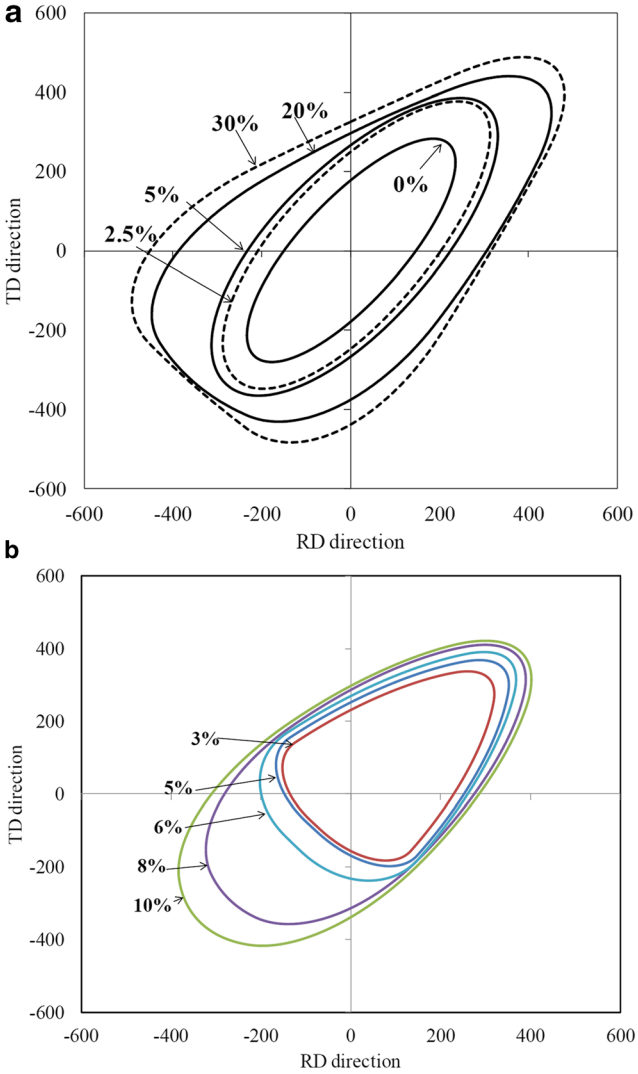

Fig. 2 Theoretical yield surfaces in the (RD, TD) plane according to the quadratic form of the Cazacu et al. [111] orthotropic criterion corresponding to fixed levels of accumulated plastic strain for: **a** high-purity alpha Ti; **b** Mg AZ31 (after [79])

arbitrary stress state in the biaxial planes $(\sigma_{xx}, \sigma_{yy})$ and$(\sigma_{xx}, \sigma_{zz})$, with $\theta_l = 0$ corresponding to uniaxial loadings along the **x**-axis (RD) (for more details, see for example [136]. Because at initial yielding and for strains under 10%, the tension-compression asymmetry of the Ti material is small, according to the criterion the yield surfaces of this material have an elliptical shape. At 20% strain and beyond when the observed difference in response between tension and compression is pronounced, it is predicted that the yield surfaces have a triangular shape. In Fig. 2b are shown the yield surfaces corresponding to different levels of plastic strain for Mg AZ31 that were calculated using the same yield criterion. Note that for Mg AZ31, the criterion predicts that the shape of the surface evolves from a triangular shape for low strain levels to an elliptical shape for large strain levels. The evolution in tension-compression asymmetry with accumulated plastic deformation for AZ31 Mg is completely different from the yield surface evolution for HCP-Ti material. Nevertheless, with the quadratic form of the yield function (15), it is possible to account for these strikingly different yielding evolutions.

Moreover, on the basis of Cazacu et al. [111] criterion a new interpretation and explanation of the development of plastic axial strains under free-end torsion, the so-called Swift phenomenon, was provided in [131]. Moreover, Revil-Baudard et al. [137] showed that axial strains should develop in free-end torsion of AZ31B Mg, the nature of these axial strains (i.e. elongation or contraction) depending on the tension-compression asymmetry ratio in the direction about which the material is twisted. Fig. 3 show comparisons between F.E. predictions obtained with this criterion and Hill's criterion and the data of Guo et al. [138]. Note that if the twist axis is along RD both models predict shortening of the specimen, with the Hill criterion largely underestimating the level of strains. On the other hand, for ND torsion, only Cazacu et al. [111] criterion correctly predicts that the specimen elongates, while the Hill criterion predicts zero axial plastic strains (see Fig. 3).

Considerable efforts have been devoted to the mechanical characterization of the response of titanium and its alloys for quasi-static strain rates under uniaxial loadings (e.g. [135, 139–142], etc.). Despite their outstanding mechanical properties because of high processing and manufacturing costs the use of titanium materials is still limited to applications requiring high performance. It is to be noted that the great majority of formed titanium parts are made by hot forming, with the greatest improvement in formability being for temperatures above 540 C. With these challenges in mind, efforts in the past decade have been done towards developing models that would enable a better description of the mechanical behavior of titanium materials during cold forming operations. As an example, Fig. 4 shows the predicted evolution of the thickness at the pole of the bulge as a function of the fluid pressure according to the Cazacu et al. [111] and Hill [88] criterion

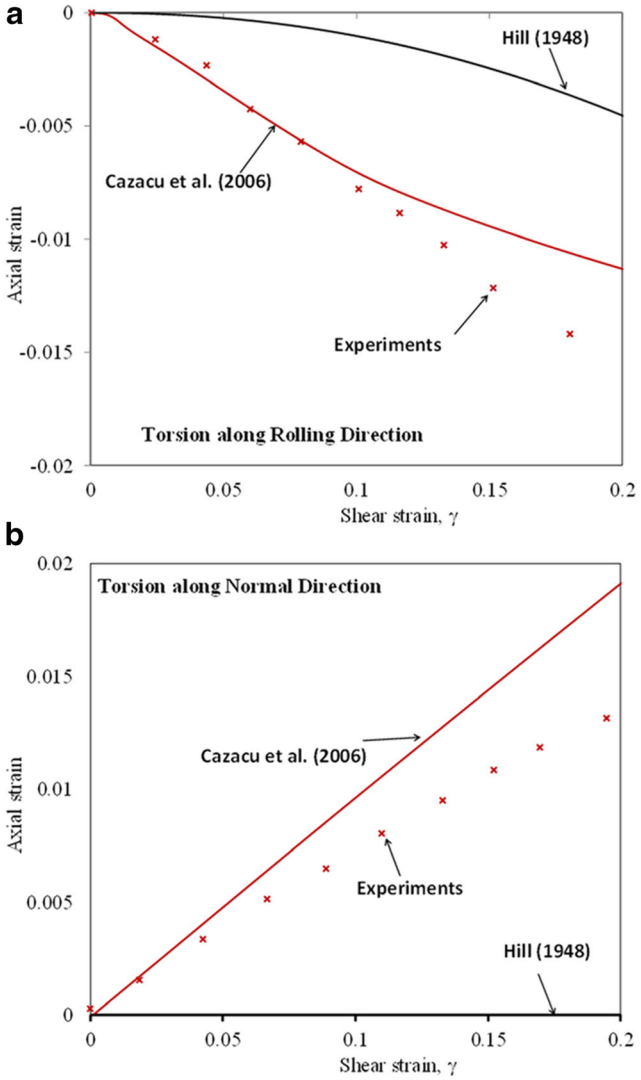

Fig. 3 Variation of the axial strain with the shear strain during free-end torsion along RD and ND directions for AZ31 Mg alloy: Comparison between experimental data by Guo et al. [138] and the F.E. predictions obtained with the Cazacu et al. [111] yield criterion and Hill [88], respectively. Note that depending on the twist direction, the axial strain is either positive (for torsion along ND direction) or negative (for torsion along RD direction) (after [136])

along with the experimental points (represented by symbols) obtained from post-test DIC in two hemispherical bulge tests on a commercially pure hcp titanium T40. Note that Cazacu et al. [111] yield criterion predicts with accuracy the thickness reduction that occurs in the bulge. Most importantly, this criterion captures the almost "vertical" drop in thickness that occurs at a pressure $p = 25.5$ MPa. On the other hand, Hill's criterion greatly underestimates the thickness reduction. According to this model, a thickness of 1.2 mm at the pole would be reached for a fluid pressure $p = 29$ MPa against 24.4 MPa experimentally, and 24.9 MPa according to the Cazacu et al. [111] yield criterion. For a detailed discussion on the importance of consideration of the tension-compression

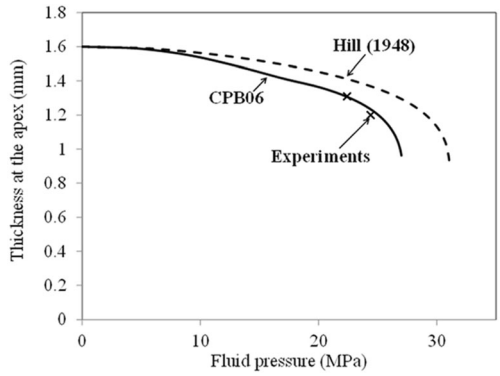

Fig. 4 Thickness at the pole of the bulge as a function of the fluid pressure for CP hcp titanium T40: comparison between the F.E. predictions according to the Hill [88] yield criterion (interrupted line), Cazacu et al. [111] orthotropic yield criterion (solid line), and data obtained in two hemispherical bulge tests (symbols) [after 136]

asymmetry displayed by titanium materials on the predictions of the level of plastic strains at which instabilities occur under hydrostatic bulging for various die inserts geometries, and for the accuracy of the predictions of other cold forming operations, the reader is referred to the monograph [136].

Anisotropic hardening

The anisotropic yield criteria presented above are very useful because they can be implemented relatively easily in FE codes and employed readily for complex applications involving plasticity, including metal forming. Currently, these yield conditions are mostly associated with isotropic hardening or, possibly, with anisotropy coefficients that evolve with the effective strain or any function of the plastic work. However, they cannot handle the anisotropic hardening effects that often occur during strain path changes. In particular, they cannot describe the Bauschinger effect upon load reversal or other transient hardening phenomena that occur during other complex strain path changes. Since it has been shown in many studies that the hardening behavior after reverse loading has a strong effect on springback, anisotropic hardening is important to account for in forming simulations. Typically, kinematic hardening with a back-stress as a tensorial state variable has been used for this purpose, in particular non-linear kinematic hardening as reviewed by Chaboche [143]. Such an approach was developed specifically to account for strain path changes with mutliple tensorial variables by Teodosiu and Hu [144] (see also [145–147]). Often, kinematic hardening has been supplemented by yield surface distortion [148–151]. Other forms of hardening have also been proposed by Kurtyka and Życzkowski [152].

Among the numerous kinematic hardening models available in the literature, the formulation proposed by Yoshida and Uemori (YU) [6] has received much attention in the forming community. This model is based on two surfaces such as in Krieg [153] and Dafalias and Popov [154] with the inner surface called the yield surface and the outer the bounding surface (Fig. 5a). The yield surface only translates in stress space while the bounding surface translates and expands. Therefore, two back-stresses with distinct evolution equations are necessary to describe the translation of the yield and bounding surface centers. The strain hardening rate is also influenced by the contact between the yield and the bounding surfaces and by the expansion rate of the latter. In fact, this framework includes a third surface, the so-called stagnation surface, that controls the amount of permanent softening occurring mostly after reversal, with a center controlled by its

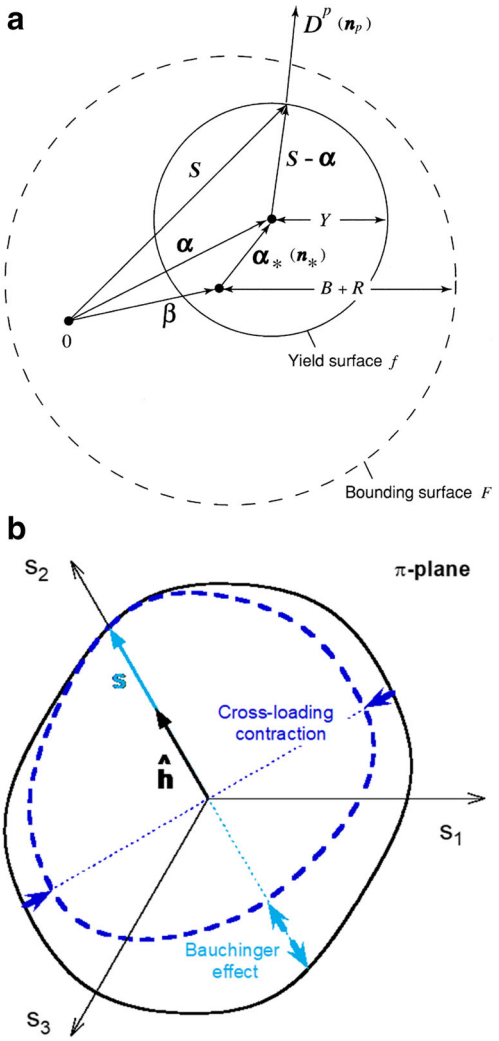

Fig. 5 Deviatoric plane representation of multi-surface kinematic hardening and distortional plasticity models. **a** YU schematic model with yield surface (inner) and bounding (outer) surfaces, reprinted from [6] with permission from Elsevier; **b** HAH distortional model during uniaxial tension with solid line for isotropic (dash line) and distortional (solid line)

own evolution rule. Each of these surfaces can be defined with any isotropic or anisotropic yield function, for instance, one of those described earlier in this Section. The YU model has been used successfully to capture the behavior of materials in forward-reverse loading conditions, in particular, the Bauchinger effect. Its application in finite element simulations of sheet metal forming clearly demonstrated that the prediction of springback was more accurate when the Bauschinger effect was accounted for.

More recently, it has recently been shown that distortional plasticity only i.e., without back-stress, is a viable alternative to account for the Bauschinger effect [114, 150, 155]). The so-called homogeneous anisotropic hardening (HAH) approach proposed by Barlat et al. [114, 156, 157] has been developed in order to employ any isotropic or anisotropic yield conditions as discussed in previous sections and to distort the corresponding shape (see also [155]). One important feature of the HAH approach is that the plastic response under proportional loading is identical to that of the considered yield function under isotropic hardening.

The HAH yield condition can take the form

$$\sigma\left(\mathbf{s}, f_-, f_+, \widehat{\mathbf{h}}\right) = \left\{\overline{\xi}\left(\mathbf{s}\right)^q + \phi_h\left(\mathbf{s}, f_-, f_+, \widehat{\mathbf{h}}\right)\right\}^{\frac{1}{q}} = \sigma_R\left(\overline{\varepsilon}\right) \tag{16}$$

In Eq. (16) $\overline{\sigma}$ is the effective stress, $\mathbf{s}$ the stress deviator, f_- and f_+ two scalar state variables, and q a constant coefficient. $\sigma_R(\overline{\varepsilon})$ is a reference stress-strain curve with $\overline{\varepsilon}$ the plastic work-based effective strain. $\overline{\xi}$ and ϕ_h are two functions defining the isotropic hardening yield condition and the distortion, respectively. The function $\overline{\xi}(\mathbf{s})$ is defined as

$$\overline{\xi}(\mathbf{s}) = \left[\overline{\phi}(\mathbf{s}_L)^2 + \overline{\phi}(\mathbf{s}_X)^2\right]^{1/2} \tag{17}$$

where $\mathbf{s}_L$ and $\mathbf{s}_X$ are two stress deviators obtained by two simple linear transformations of the stress deviator $\mathbf{s}$ to account for latent hardening and cross-loading contraction. When these two effects are inactive, $\overline{\xi}(\mathbf{s})$ reduces to $\overline{\phi}(\mathbf{s})$, the effective stress (yield function) associated with isotropic hardening. ϕ_h determines the amount of distortion that occurs with load reversals

$$\phi_{\mathbf{h}}\left(\mathbf{s}, f_-, f_+, \widehat{\mathbf{h}}\right) = f_-^q\left|\widehat{\mathbf{h}} : \mathbf{s} - \left|\widehat{\mathbf{h}} : \mathbf{s}\right|\right|^q + f_+^q\left|\widehat{\mathbf{h}} : \mathbf{s} + \left|\widehat{\mathbf{h}} : \mathbf{s}\right|\right|^q \tag{18}$$

while $\widehat{\mathbf{h}}$, the so-called microstructure deviator, sets the distortion direction. Other state variables are introduced within the expressions of f_-^q and f_+^q to define permanent softening. All the variables and coefficients of the HAH model are detailed in references [114, 156, 157]. As a convenient feature, the HAH approach was designed in a way that four sets of constitutive coefficients can be determined independently. The stress-strain curve for monotonic loading is approximated with a mathematical model and the yield function coefficients are determined in a classical manner assuming isotropic hardening. Then, the coefficients corresponding to load reversal, including permanent softening, are optimized and, finally, those that control cross-loading.

A recent version of this model [158], called HAH_{20}, was proposed with improved state variable evolution equations. Moreover, it was shown that the substitution of ϕ_h in Eq. (16) by an alternative form taking the yield surface normal into account in the distortion was possible and likely more accurate for anisotropic materials. Finally, HAH_{20} was developed as a pressure-sensitive model in order to account for the higher flow stress in compression (C) than in tension (T) as observed by Spitzig et al. [159]. Note that this influence cannot be clearly observed with only one reversal, e.g. T-C, because permanent softening tends to produce the opposite of a pressure-strengthening effect. However, with two reversals, e.g. T-C-T, the influence of the pressure and permanent softening are more clearly partitioned, particularly for high strength materials.

As an illustration, Fig. 5.b display the normalized yield locus of an EDDQ low carbon steel in the deviatoric plane during pre-strain in uniaxial tension in a direction defined by a unit vector $\mathbf{e}_2$. For isotropic hardening, the normalized yield locus keeps the same shape throughout loading. However, for distortional hardening, the yield locus contract near a stress state opposite to loading, allowing the description of the Bauschinger effect and, possibly, in directions orthogonal to loading, corresponding to cross-loading contraction. If load is suddenly changed to another direction, say uniaxial tension in a direction defined by a unit vector $\mathbf{e}_1$, the strain hardening is subjected to transient effect until it recover the isotropic hardening curve. Possibly, the new stress state might overshoot the isotropic hardening curve because of latent hardening effect, particularly more so in the cross-loading direction. However, in many advanced materials such as high strength steels and aluminum alloys, the latent hardening effect is not observed. Figure 5.b also suggests that when reloading in uniaxial tension occurs, the normal direction of the yield surface fluctuate until the flow stress recovers fully and permanently the isotropic hardening curve. Assuming the associated flow rule, this explains why the Lankford coefficient (r-value) tends to vary drastically just after reloading.

Both YU and HAH models are useful for the prediction of springback. Choi et al. [160, 161] compared FE simulations results of springback of a U-draw channel for a number of advanced high strength steel sheets of strength close to 1 GPa. For this process in which most of the load changes are reversals, these authors observed that, although not identical, both YU and HAH led to springback profiles in better

agreement with the experiments than those predicted with the isotropic hardening model.

Experimental validation of the anisotropic models

In sheet or tube forming processes, materials are subjected to multiaxial loads. Such multiaxial loading experiments are highly desirable for validating the plasticity models to be used in accurate numerical simulations. This section reviews the experimental studies, published after 2010, that investigated the anisotropic plastic deformation behavior of metal sheets and tubes under multiaxial loading to check the validity of anisotropic plasticity constitutive models. See [121, 162] for the related papers published before 2010.

Hydraulic bulge test

The hydraulic bulge test is effective in measuring the work hardening behavior of sheet metals at significantly larger strain levels than those reached in the uniaxial tension test. Readers can see excellent reviews on the previous studies on hydraulic bulge test in [163, 164].

The stress and strain are not uniform in the specimen for the hydraulic bulge test. Therefore, the accuracy of these measurements depends on the uniformity of deformation within the gauge lengths for strain and curvature measurement. They should be small enough relative to the diameter of the die cavity. Yoshida [164] performed a FEA of the hydraulic bulge test using a higher order yield function proposed by Barlat and coworkers [76, 106]. He concluded that for an isotropic specimen accuracy of the stress measurement is within 1% if (i) the meridional strain is evaluated at the middle layer (the bending strain is necessary to be subtracted from the outer surface strain), (ii) the meridional stress is estimated considering the internal pressure acting on the inner surface, and (iii) the geometry of the experimental setup satisfies $R_\rho/D \leq 0.1$, $R_\varepsilon/D \leq 0.05$, and $t_0/D \leq 0.01$, where D and t_0 are the specimen's initial diameter and thickness, respectively, $2R_\rho$ is the distance of the two edges of the spherometer for measuring the radius of curvature of the bulging specimen, and $2R_\varepsilon$ is the initial gauge length for measuring the meridional strain on the outer surface of the specimen. Moreover, he demonstrated that for typical orthotropic sheet metals, the stress state at the apex deviates from the equibiaxial stress state; $1.01 < \sigma_{yy}/\sigma_{xx} < 1.05$, depending on the degree of anisotropy of the material, where σ_{xx} and σ_{yy} are the stress components at the apex in the RD and TD, respectively [164].

An international standard on the determination of biaxial stress–strain curves by means of the hydraulic bulge test with optical measuring systems has been published as ISO 16808 [17]. Mulder et al. [163] performed a detailed analysis of the hydraulic bulge test with optical measuring systems, as suggested by ISO 16808 [17], to evaluate the validity of all assumptions and simplifications applied to the test. They concluded that a highly accurate stress-strain curve can be obtained by fitting the surface coordinates to an ellipsoid shape function and by considering the local strain data to approximate the curvature for the midplane. Moreover, they have demonstrated that the fitting procedure is robust even when the bulge surface geometry includes a realistic revel of measurement noise. Min et al. [165] developed a new method to accurately calculate stresses and strains for both isotropic and orthotropic sheet materials. The new method takes the elastic volume change into account, the bending effect, and the non-balanced biaxial curvatures in the principal directions when calculating the effective stress at the specimen pole. The accuracy is improved in comparison with previous methods including the ISO 16808 [17], which underestimate the thickness at the specimen pole and lead to an overestimation of stresses by up to several percent.

Some authors used the hydraulic bulge test to verify the validity of anisotropic yield functions. Yanaga et al. [166] measured the thickness strain along the meridian directions of the bulged specimens of 6000 series aluminum alloy sheets with high and low cube texture densities. They found that the difference in the thickness strain distributions between the two samples were in good agreement with the FEA results obtained using the Yld2000-2d yield functions identified for the samples using cruciform specimens. Chen et al. [167] developed a methodology for incorporating anisotropy in the extraction of the material stress–strain response from a bulge test. Williams and Boyle [168] applied the elliptical bulge test to the calibration of anisotropic yield functions coefficients for commercially pure titanium and an exhaust grade titanium alloy sheet.

Biaxial stress test using cruciform specimen

Cruciform specimen design

Biaxial tensile testing method using a cruciform specimen and a proper geometry of the cruciform specimen has been standardized by ISO 16842 [18] in 2014 (Fig. 6). Hanabusa et al. [169, 170] performed FEAs of the ISO cruciform specimen to quantitatively evaluate the error of stress measurement, assuming that the material follows the Yld2000-2d yield function [169] or the von Mises yield function [170]. They concluded that the stress measurement error with the ISO specimen is less than 2% when the following conditions are satisfied:

a) $a \leq 0.08B$, where a is the thickness of the test sample and B is the arm width.
b) $N \geq 7$, where N is the number of slits per arm.

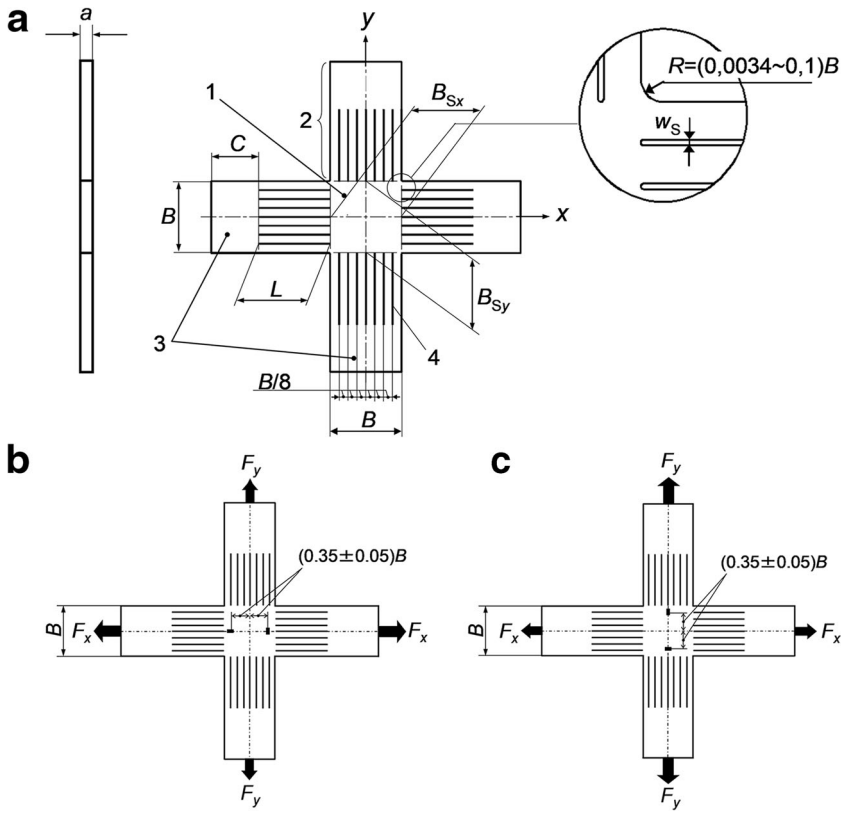

Fig. 6 **a** Geometry of the cruciform specimen, **b** and **c** optimum positions for measuring the normal strain components when **b** $F_x \geq F_y$ and **c** $F_x < F_y$, where F_x and F_y are the tensile forces in the x- and y- directions, respectively. (ISO 16842 [18])

c) $L \geq B$, where L is the length of slits made in the arm.
d) $w_S \leq 0.01B$, where w_S is the width of slits.
e) The positions where strain components are measured are on the centerline of a specimen, approximately $0.35B$ away from the center of the specimen, parallel to the maximum stress direction.

The maximum plastic strain, ε^{p}_{max}, applicable to the ISO cruciform specimen depends primarily on the work hardening rate (n-value) of the test material; $\varepsilon^{p}_{max} \leq 0.1$ in most cases for materials with $0 \leq n \leq 0.3$ [18, 170]. A specimen with a reduced-thickness gauge area have been developed to increase ε^{p}_{max} (see [171, 172]).

A methodology is proposed to optimize a cruciform specimen shape for the identification of constitutive laws based on full-field measurements [173]. The effective cross-sectional area of a cruciform specimen for an accurate determination of the stress components from the tensile forces has been discussed [174].

Measurement of forming limit curve using cruciform specimen

Some authors applied cruciform specimens with a reduced-thickness gauge area to the measurement of the forming limit curves (FLC) of an aluminum alloy 5086 with linear and nonlinear strain paths [42, 175, 176] and DP600 with quasi-static and dynamic biaxial tensile tests [177, 178]. The biaxial tensile testing of a titanium alloy was performed to measure the FLC at elevated temperatures [179]. A method for measuring a FLC using a cruciform specimen and a blank holder with adjustable draw beads has been developed [180]. Equibiaxial tensile testing of commercially pure (CP) titanium up to fracture was performed using an optimized cruciform specimen to investigate the ductility, strain hardening exponent, and texture evolution of the test sample [181].

Material modeling based on the biaxial tensile test using cruciform specimen

Biaxial tensile testing using cruciform specimens were applied to measure and model the biaxial deformation behavior of sheet metals: an ultra-low carbon interstitial free (IF) high strength steel [182], cold rolled DDQ steels [183–185], a hot rolled steel [186], a precipitation hardened 590 MPa steel [187, 188], a DP 590 steel under continuous loading and unloading [189], DP 780 [190], DP 980 [191, 192] and DP 980 MPa multiphase steel sheet [193]), annealed stainless steel SUS304 foils [194], aluminum alloy sheets (5000 series [192, 195–197], 6000-series with different cube textures densities [166] and 6016-O and -T4 [16]), an AZ31 magnesium alloy [198], a pure titanium (JIS Grade 1) [13, 199], a high

strength titanium alloy Ti-6Al-4 V [200], and a GH738 nickel-based super alloy at elevated temperatures [201].

The validity of the material models identified using the cruciform tests has been assessed by comparing the experimental results with the numerical analysis results for hole expansion forming [13, 16, 184, 186, 188, 190, 202], Marciniak-Kuczyński-type punch stretching test [183, 187], hemispherical punch stretching test (Nakajima test) [14], the strain distribution on a cruciform specimen [177, 196, 197], and hydraulic bulge forming [166, 194].

Biaxial loading-unloading test

Andar et al. [203] investigated the deformation behavior of BH340 and DP590 steel sheets subjected to biaxial tension with constant stress ratios followed by biaxial unloading with the same stress ratios. An exponential decay model was proposed that provides good reproduction of the unloading stress–strain relations. Sumikawa et al. [204] experimentally obtained the unloading stress-strain curves of high strength steels under four stress states: uniaxial tension, plane strain tension, biaxial tension and shear (in-plane torsion test [205]). Kulawinski et al. [206] investigated a metastable austenitic stainless steel under different biaxial-planar load paths by using a cruciform specimen geometry. The stress state within the cruciform specimens was evaluated by an elastic unloading procedure with subsequent calculation of the stress components. Isotropic initial yielding and non-isotropic hardening were found.

Multiaxial stress test using tubular specimen

In order to increase the magnitude of ε^{p}_{max} that can be attained experimentally the multiaxial tube expansion testing method (MTET) has been developed [183, 199]. A tubular specimen is fabricated by bending and welding, and then combined internal pressure P and axial force T are applied to the tubular specimen using a servo-controlled testing machine. The axial and circumferential true stress components applied to the tubular specimen can be determined and controlled using the measured P, T, the biaxial strain components, and the radius of curvature in the axial direction. For example, the MTET has been applied to a pure titanium sheet (JIS grade #1) [199], a cold rolled interstitial-free steel sheet [183, 184], a DP590 steel sheet [187], a 304 L stainless steel microtube [207] an A5182-O aluminum alloy sheet [195], and A6016-O and -T4 aluminum alloy sheet [16].

Figure 7a shows the results of biaxial stress tests of an aluminum alloy sheet 6016-O using the ISO cruciform specimens for $0.002 \leq \varepsilon^{p}_{0} \leq 0.04$ and MTET for $0.04 < \varepsilon^{p}_{0} \leq 0.08$, where ε^{p}_{0} is the logarithmic uniaxial tensile plastic strain in RD (see [16]). The isocontours of plastic work measured

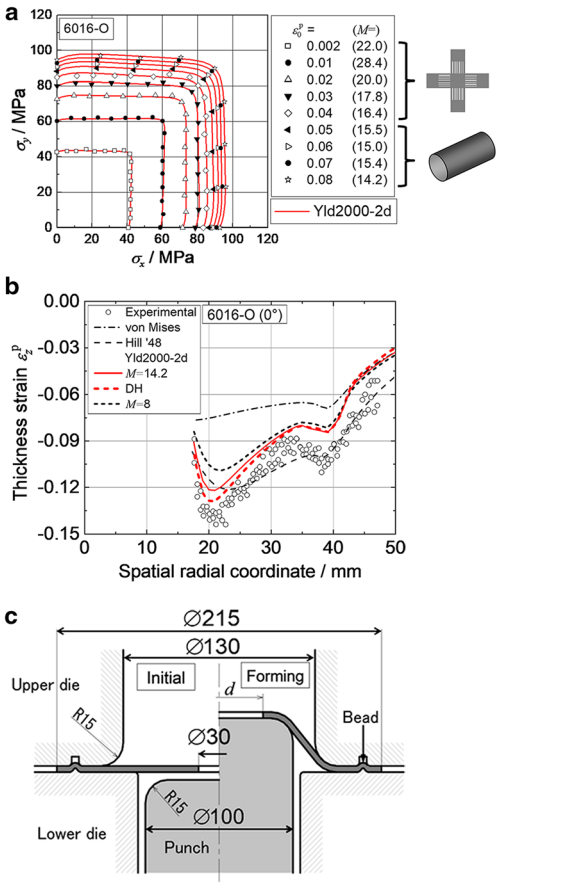

Fig. 7 **a** Stress points forming contours of plastic work of aluminum alloy sheet 6016-O compared with the yield loci determined using the Yld2000-2d yield function [100, 208]. M is an exponent of the Yld2000-2d yield function. **b** Thickness strain distribution along the RD of a hole expanded test specimen at a punch stroke of 15 mm. **c** Experimental apparatus for the hole expansion forming (after [16])

using biaxial tensile tests are reported for increments of 0.01. The solid lines are the yield loci determined using the Yld2000-2d [100, 208]. The material exhibits differential hardening (DH) as the shapes of the work contours change with work hardening. Figure 7b shows the thickness strain along the radial line parallel to the RD of a hole expansion test specimen (A6016-O) at a punch stroke of 15 mm, compared with those calculated using selected material models. It is clearly seen that the choice of the model has a significant effect on the FEA prediction of the thickness strain distribution. The Yld2000-2d (DH), which reproduces the DH behavior of the material, leads to the closest agreement with the experimental results.

Dick and Korkolis [209] proposed an experimental method for generating combined tension and shear stress states in thin-walled tubes, with the purpose of calibrating anisotropic yield functions. Two notches that form the test-section between them are machined. By controlling the orientation of the notches infinite combinations of tension and shear on the test-section can be created.

Yoshida and Tsuchimoto [210] measured the elastoplastic deformation behaviors of thin-walled tubes made of pure aluminum and steel under various combined tension–torsion loadings. They found that the stress state and the strain rate direction are essential parameters characterizing the plastic flow and proposed a pseudo-corner model capable of reproducing experimentally observed plastic deformation behavior. Khalfallah et al. [211] identified the constitutive parameters of several yield criteria, von Mises, Hill [88], Cazacu and Barlat [94] orthotropic criterion calibrated using reduced experimental data obtained from uniaxial tensile tests and a free bulge test and compared the FEA results for height vs. internal pressure curve, thickness distribution and axial bulge profiles to experimental results on tubular materials (mild steel S235 seamed tube and aluminium alloy AA6063 extruded tube).

Shear test and plane strain tension test

Simple shear tests are widely used for material characterization of sheet metals to achieve large deformation without plastic instability. Yin et al. [212] showed that shear stress vs. shear strain curves obtained from different test setups (Miyauchi specimen [162], ASTM [213], and in-plane torsion test [205] are consistent with each other, provided that strains are measured using a DIC system. Fu et al. [214] applied the VFM to a forward-reverse simple shear test to identify the parameters of the homogeneous anisotropic hardening (HAH) model [114] for advanced high strength steel (AHSS) sheets.

Peirs et al. [215] developed a novel shear specimen geometry for sheet metals that can be used over a wide range of strain rates using traditional tensile test device. The specimen has notches with eccentric position that leads to an almost pure-shear stress state up to large strains. Rahmaan et al. [216] applied this specimen geometry to the investigations of fracture behavior of DP600 and 5182-O aluminum alloy sheets with a range of strain rates from 0.01 s^{-1} to 600 s^{-1} using in situ digital image correlation (DIC) strain measurement techniques. Abedini et al. [217] investigated the failure behavior of a highly anisotropic magnesium alloy (ZEK100) and a dual phase steel (DP780) at room temperature using two different shear specimen geometries: the butterfly type specimen [218] and that developed by Peirs et al. [215]. They found that the fracture strains obtained using the butterfly specimen were lower for both alloys. Abedini et al. [219] performed simple shear tests for three orientations of 0° (or 90°), 45°, and 135° with respect to the RD of a magnesium alloy (ZEK100-O) to show the asymmetry of flow stress not only in tension-compression regions represented by the 1st and 3rd quadrants of yield locus but also in shear regions represented by the 2nd and 4th quadrants. Moreover, the CPB06 yield criterion with two linear transformations was calibrated with the experimental data.

Rahmaan et al. [220] characterize the high strain rate constitutive behavior and the anisotropic plasticity of three high strength aluminum sheet alloys, 6013-T6, 7075-T6 and a developmental 7xxx-T76, using uniaxial tension, simple shear and through-thickness compression at various strain rates ranging from 10^{-3} to 10^{3} s^{-1}. The experimental force-displacement curves of a hemispherical punch stretching test and a simple shear test were consistent with the FEA results based on higher order yield functions.

Butcher and Abedini [221] showed that plane strain conditions of pressure-independent metals occur when the third deviatoric stress invariant is zero which leads to a maxima (for plane strain tension) or minima (for shear) in the second deviatoric invariant, and that the data from stress-controlled cruciform tests [16, 183, 190, 191] and simple shear tests [216, 217, 220, 222], support the existence of the generalized plane strain constraints for shear and plane strain tension for FCC and BCC materials. Moreover, they suggested that the generalized plane strain constraints must be enforced upon the plastic potential function during the calibration procedures in order for generalized plane strain loading conditions to be physically-consistent with the assumptions of pressure-independent plasticity.

Flores et al. [223] quantified the influence of the geometry of the plane strain tension specimen proposed by An et al. [22] and material anisotropy on the stress computation error. Aretz et al. [224] proposed a calibration method for identifying yield functions using three directional uniaxial tensile tests and two plane strain tensile tests. They demonstrated that calculated forming limit curves for three materials (IF steel, low carbon steel and 5000-series aluminum alloy) depends strongly on the accuracy of the experimental plane strain tensile test data used for the calibration. Therefore, they suggest that the specimen geometry must be optimized so that the desired plane strain state can be realized.

Combined use of simple mechanical tests

Tian et al. [225] determined a proper material model for an aluminum alloy Al-6022-T4, using uniaxial and plane-strain tension, as well as disk compression experiments. The model is applied to the FEA of a cup drawing process of the material. The thickness and earing profile predictions are in good agreement with the experiments. Abspoel et al. [226] determined the yield loci (contours of equal plastic work) of a wide range of steel sheets and 5xxx, 6xxx and 7xxx series aluminium alloy sheets by the combined use of uniaxial tension, plane strain tension, equibiaxial tension, uniaxial compression in the thickness direction, and simple shear tests. Baral et al. [227] determined the yield loci (contours of equal plastic work) of a 12.7 mm thick CP titanium sheet by the combined use of in-plane and through-thickness uniaxial tension and compression, and plane-strain tension tests.

Zillmann et al. [228] performed biaxial, in-plane compressive testing of deep drawing steel sheets with and without skin-pass treatment, together with biaxial tension and simple shear tests, to determine full yield loci in the principal stress space and to evaluate the tension–compression asymmetry of the test samples.

Mohr et al. [229] evaluated the accuracy of quadratic plane stress plasticity models for a dual phase and a TRIP-assisted steel using both associated and non-associated quadratic formulations. The response of the materials subjected to combined normal and tangential loads were measured. They found that both the associated and non-associated quadratic formulations provide good estimates of the stress–strain response under multi-axial loading.

Application of digital image correlation (DIC) to material modeling

The use of full-field measurements, e.g. digital image correlation (DIC), makes it possible to choose complex geometries for the test specimens, introducing heterogeneous strain fields. That enables the plastic deformation of the test specimen to be probed at many different stress states at once. Coppieters et al. [230] developed a new method to identify the post-necking hardening behavior of sheet metals without using a finite element model. The strain fields in the central zone of a tensile specimen are measured using DIC to calculate the stress fields by assuming a certain yield criterion and hardening behavior. The stress fields are used to compute the internal work in the necking zone, which should be equal to the work exerted by the external forces if the assumed hardening behavior and yield criterion is correct. Based on this hypothesis, the post-necking hardening behavior of a mild steel sheet (DC05) is determined by minimizing the discrepancy between the internal and external work in the necking zone. Coppieters and Kuwabara [27] determined the post-necking stress-strain curve of a cold rolled mild steel sheet (SPCD), assuming the Yld2000-2d yield function. The results were experimentally validated beyond the point of maximum uniform strain using the MTET [183] [199] up to an equivalent plastic strain of 0.35.

The virtual fields method (VFM) [25] is a very efficient technique for extraction of material parameters from full-field measurements. It is fast in the computational time, no need to use FEA, and can be integrated directly into a DIC platform making it more accessible to engineers.

Grédiac and Pierron [231] applied the VFM to the identification of elasto-plastic constitutive coefficients using simulated full-field kinematic data obtained from a thin notched tensile specimen. Experimental validations of the VFM in elasto-plasticity were performed at small strains by Pannier et al. [232], and Pierron et al. [233]. Rossi and Pierron [26] provided a general procedure to extract the constitutive parameters of a plasticity model starting from displacement measurements and using the VFM, which applies to a general three-dimensional displacement field leading to large plastic deformations. The method was validated using a simulated post-necking tensile experiment. Kim et al. [234] characterize the post-necking strain hardening behavior of for three types of sheet metals, DP780, TRIP780 and EDDQ, assuming von Mises yield criterion to retrieve the relationship between stress and strain. Knysh and Korkolis [235] developed a method for identifying the material hardening curves past the limit of necking in uniaxial tension and across a range of strain-rates and temperatures in a fully-coupled way, using full-field measurements of the strain and temperature during testing.

Marth et al. [236] developed an effective and computationally fast method to determine the relationship between true stress and true plastic strain, including post-necking behavior, by using an optical full-field measurement of the localized deformation field. Marek et al. [28] extend the sensitivity-based virtual fields (SBVF) developed by Marek et al. [237] to large deformation anisotropic plasticity. The main advantage of the SBVFs comes from the automation of virtual fields generation.

Teaca et al. [238] measured heterogeneous biaxial strain fields on a non-standard cruciform specimen using an image correlation method and compared them with those calculated from the FEA based on the 8-parameter anisotropic yield function proposed by Ferron et al. [239]. The parameters of the yield function were determined to minimize the difference between the measured and calculated stain fields. Güner et al. [240] applied an optical strain measurement to sheet specimens with varying notch radii. An inverse parameter identification scheme which minimizes the differences between the numerical simulation results and the measurements for principal strains, forces, and biaxial flow stress σ_b was developed to identify the parameters of the Yld2000-2d yield function. Tardif and Kyriakides [241] developed a systematic methodology to extract the material stress-strain behavior at much larger strains. This was achieved by accurately following the deformation in the necked region of a custom made tensile test specimen. The test was simulated numerically using a 3D FE model and the material response was iteratively extrapolated until the calculated and measured force-elongation matched. The results were used to calibrate the 18-parameter non-quadratic Yld2004-3D yield function [242]. Tsutamori et al. [243] performed biaxial tensile tests using a cruciform specimen with a hole at the center to evaluate the predictive accuracy of the spline yield function they developed. The thickness strain distribution around the hole measured using a DIC system was consistent with the prediction.

Validation of polycrystal plasticity models

Multiaxial stress tests are effective in evaluating the validity of polycrystal plasticity models. An et al. [244] measured yield loci of several forming steel grades using plane strain

tension, balanced biaxial tension and simple shear tests. The measured yield loci were consistent with those calculated using a polycrystal plasticity model combining the Taylor full constraint model and the Taylor relaxed pancake model. Yoshida et al. [245] investigated the work hardening behavior of a thin-walled tubular specimen of A3003-O using an axial load-internal pressure-torsion type test machine. They found that the amount of work hardening of the specimen depends on the plastic work and the applied stress path. They concluded that the source of such work-hardening behavior is attributed to the path dependency of the evolution rate of the dislocation density, using a crystal plasticity analysis with hardening models based on accumulated slip and dislocation density. Yamanaka et al. [246] performed numerical biaxial tensile tests based on the crystal plasticity finite element (CPFE) method and the mathematical homogenization approach. The biaxial tensile deformation behavior of a 5182 aluminum alloy predicted by the numerical biaxial tensile tests were consistent with that measured using the ISO-type cruciform specimens [18]. Coppieters et al. [247] performed the biaxial tension tests of a low carbon steel sheet using cruciform [18] and tubular specimens [183]. The measured biaxial deformation behavior of the sample subjected to linear stress paths in the first quadrant of stress space was consistent with that predicted by the ALAMEL multiscale plasticity model [113]. However, the differential hardening behavior of the sample at a small strain range ($\varepsilon_0^{\mathrm{p}} < 0.05$) could not be reproduced by the ALAMEL model. Upadhyay et al. [248] investigated the deformation behavior of 316 L stainless steel cruciform samples subjected to different biaxial load path change to interpret the material response (biaxial Bauschinger effect) using the anisotropic viscoplastic self-consistent polycrystalline model. Hama et al. [249] reproduced the differential hardening under biaxial loadings and tension-compression asymmetry of a pure titanium sheet (JIS Grade 1) using crystal-plasticity FEA. Steglich et al. [250] simulated the plastic deformation of Mg AZ31 under monotonic biaxial loadings using VPSC and successfully reproduced the differential strain hardening character of the sample for a small strain range (less than 0.008). Kim et al. [251] performed nonlinear strain path experiments for a cold-rolled high-strength steel sheet and DP780. The strain paths consist of uniaxial tension (UT) in TD followed by UT in RD and DD, and biaxial tension. The measured data were compared with those calculated using VPSC and the HAH model [114].

In-plane compression and reverse loading tests for sheet metals

Optimum specimen geometry for the in-plane compression and reverse loading test for sheet metals has been proposed [252]. The tension-compression asymmetry of flow stress of steel sheets and its effects on forming simulations was investigated for an ultra-low carbon IF steel sheet [182, 253], cold rolled interstitial-free steel sheet and dual phase high strength steel sheet [254], DP590 steel sheet [255], and DP980 steel sheets [9, 191]. Gröge and Vitek [256] hypothesized that the onset of yielding of single crystals of bcc metals is governed by the yield criterion that is represented as a linear combination of the Schmid stress and three other (non-Schmid) shear stress components, and that the individual non-Schmid stresses contribute differently towards the effective stress in tension and compression, which results in the experimentally observed tension-compression asymmetry of the yield stress in certain bcc metals.

The tension-compression asymmetry of hcp metals was also recently experimentally investigated for magnesium alloy sheets [10, 257–261], pure titanium [142, 199, 262], and titanium alloy sheets [200, 263, 264].

Dietrich et al. [265] designed a new anti-buckling fixture that allows tension–compression cyclic loading tests on sheet metals. The fixture can be mounted on a conventional tensile testing machine.

Marcadet and Mohr [266] investigated the effect of loading direction reversal on the onset of ductile fracture of DP780 steel sheets using continuous compression-tension experiments on flat notched specimens to identify the parameters of several plasticity models for reproducing the reverse loading stress-strain curves. Moreover, the model is used to estimate the local strain and stress fields in monotonic fracture experiments covering plane stress states ranging from pure shear to plane strain tension.

A new test equipment has been developed to measure the in-plane cyclic behavior of sheet metals at elevated temperatures up to 400 °C [267].

Zecevic et al. [268] developed a comprehensive polycrystal plasticity model capable of predicting the elasto–plastic cyclic deformation behavior of multi-phase polycrystalline metals deforming by crystallographic slip. The model successfully captures the flow response of a DP590 steel sheet under cyclic tension–compression–tension deformation to various levels of plastic pre-strains.

Stress measurement using X-ray diffraction

Jeong et al. [269] investigated the equibiaxial flow behavior of an IF free steel sample was investigated using Marciniak punch test with in situ X-ray diffraction for stress analysis. An experimental technique using a combination of in-situ X-ray diffraction and digital image correlation (DIC) was applied for an IF steel sheet to measure contours of plastic work in stress space up to strain levels of 0.1 [270].

Formability of metallic materials

Formability describes the capability of a sheet metal to undergo plastic deformation in order to get some shape without defects. During the last decades different assessment methods of metal sheets formability have been developed. The most useful tool used to assess the formability is the Forming Limit Diagram (FLD). This method meets both manufacturer and user's requirements and is widely used in factory and research laboratories. Due to the vastness of the analyzed domain, this paper does not cover all types of defects that limit the formability of sheet metals (necking, fracture, sheared edge, wrinkling, modification of the roughness, etc.). Four main mechanisms limit the deformation of metal sheets: necking, fracture, shearing and wrinkling [271, 272] (see Fig. 8 [272]). The appearance of one or the other of the four ways depends on the type of material and on the deformation process of the sheets. The interplay between necking and fracture is still not well understood and needs further research. We have limited ourselves in this paper only to necking as a defect that limits deformation. A detailed presentation of the FLD method can be found in the literature [32, 92, 120, 273–280].

During the last decades, the development in the field of sheet metal forming has been focused on the use of new materials (high strength steels, new aluminum alloys, magnesium alloys, sandwich materials, etc.), materials exhibiting phase transitions during the forming process, innovative forming procedures (nano-micro forming, hydroforming, incremental forming, etc.), use of neural networks, intensive use of numerical simulation, etc. In order to follow this trend, both experimental and theoretical research has been performed in the field of formability. The experimental research has been focused on refining the experimental methods used for detecting and measuring the limit strains (with the aim of enhancing the accuracy and robustness of experimental methods),

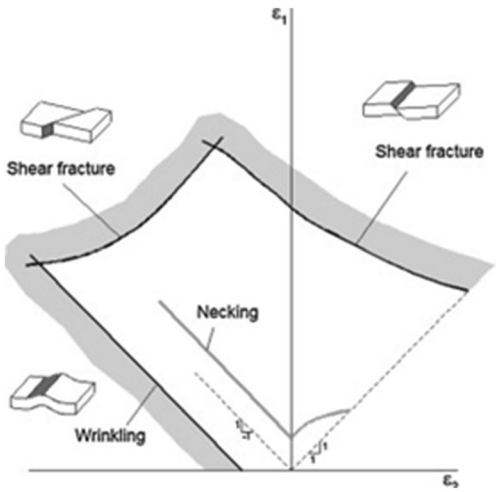

Fig. 8 Forming limit curves with respect to shear fracture/necking and wrinkling [272]

development of new laboratory tests for determining the Forming Limit Curves (FLC), as well as on studying the influence of various material or process parameters on the limit strains. The theoretical research aimed to improve the predictive capabilities of plasticity models by refining the numerical techniques used for their solution, as well as by incorporating ductile fracture and crystal plasticity models in FLC approaches. The influence of some process parameters (such as temperature or normal pressure) on the limit strains has been also analyzed from a theoretical point of view. The most significant results obtained during the last decade in this domain will be presented in the following subsections.

Advances in experimental investigation of FLC

New concepts related to the manner of defining the Forming Limit Curves have been introduced during the last decade: the Generalized Forming Limit concept (GLFC) [281], as well as a concept based on combining a limit strain model with a fracture model [282]. In the same time, the concepts of Stress-Based Forming Limit Curve (σFLC) (introduced for the first time by the research group of Embury [283, 284] and later developed by Arrieux [285]) and Extended Stress-Based Forming Limit Curve (XSFLC) [286, 287] defined at the end of 1970's and in 2007, respectively, have got further developments. A detailed description of these concepts can be found in [32]. The most significant limitation of the Strain Forming Limit Curve consists in the difficulty of applying it to non-linear load paths. The FLSD concept therefore appears to be useful, particularly in multistage forming, for predicting the failure of metal tubes and sheets.

In order to extend the application of stress limit curves to a 3-D stress state (presence of through-thickness components of compressive stress), Simha et al. [286] has introduced a new concept, namely Extended Stress-Based Limit Curve (XSFLC). The XSFLC represents the equivalent stress and mean stress at the onset of necking during in-plane loading. Figure 9 shows the three formulations of the Forming Limit Curve concept, namely: strain-based FLC (εFLC), stress-based FLC (σFLC) and Extended Stress-Based FLC (XSFLC), respectively. Figure 9 also presents the loading paths for the three cases: uniaxial stress, plane strain and biaxial stress. A thorough analysis of the conditions for the use of the XSFLC as a Formability Limit Curve under three-dimensional loading is presented in [286].

The most important drawback of the FLC is the strain path dependency. During the last decade, the efforts of the scientists have been oriented towards finding a model that overcomes this disadvantage. The Generalized Forming Limit concept (GFLC) has been proposed by Müschenborn and Sonne [288] and revisited by Volk [29, 30, 281, 289] and consists of the conventional FLC and an acceptable number of experiments with bi-linear strain history. The concept is

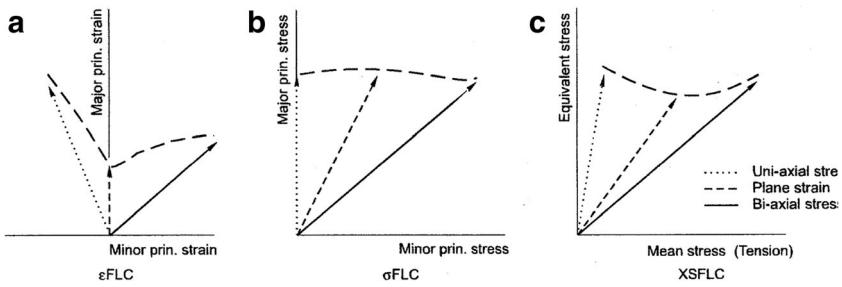

Fig. 9 Schematic of the Strain-Based Forming Limit Curve (εFLC), the Stress-Based Forming Limit Curve (σFLC) and the Extended Stress-Based Forming Limit Curve (XSFLC) [287]

based on the idea that all points with an equivalent pre-strain have the same remaining formability at the defined post-forming direction. This concept allows an easy evaluation of the formability for a multi-step deformation history with different changes of forming direction. This concept is currently implemented in the AutoForm FE commercial code.

By combining the stress-based forming limit curve (σFLC) and the maximum shear stress (MSS) criterion, Stoughton and Yoon [282] proposed a new criterion for failure prediction. This criterion is able to take the stress distribution through the thickness of the sheet into account. Based on the ideas of Yoshida et al. [290] and Zeng et al. [291], Stoughton and Yoon [31] proposed a new concept, the so-called "polar diagram of the effective plastic strain- PEPS diagram". This diagram is a polar diagram with effective plastic strain EPS as the radial variable and the arc tangent of the ratio of the principal plastic strain rates as angle. The graphical illustration of the PEPS diagram for a complex strain path is presented in Figure 10. The advantages of this new representation of the limit strains are: its insignificant path dependence, its independence on the stress-strain relationship, and its similar shape with the strain FLC [32]. The PEPS method has been successfully implemented into user material interfaces for PAMSTAMP and LS-DYNA 3D commercial codes [292].

Both stress-based FLC (σFLC) and the polar diagram of the effective plastic strain (PEPS) are very efficient in the FE simulation code because the path dependency of SFLCs is much less significant than that of strain-based FLCs. Stoughton [293] present the methodology to convert non-linear strain paths FLC into a single stress-based forming limit curve (σFLC) (see Fig. 11 [125]).

Advanced methods used to determine the limit strains

Since the proposal of the FLC concept, many researchers have been actively involved in the development of experimental methods for the accurate and objective determination of the limit strains. These experimental aspects have been the most important obstacles limiting the practical use of the FLC's. During the last years, the digital processing of the images has allowed the development of refined methods for the experimental measurement of the limit strains. These methods aim to remove the subjective perturbations induced by the human operator in the process of image analysis. More precisely, new algorithms for the detection of the defect occurrence on the deformed part have been developed. They have contributed to the increased accuracy of the limit strain measurement and to the reduction of the discrepancy between the

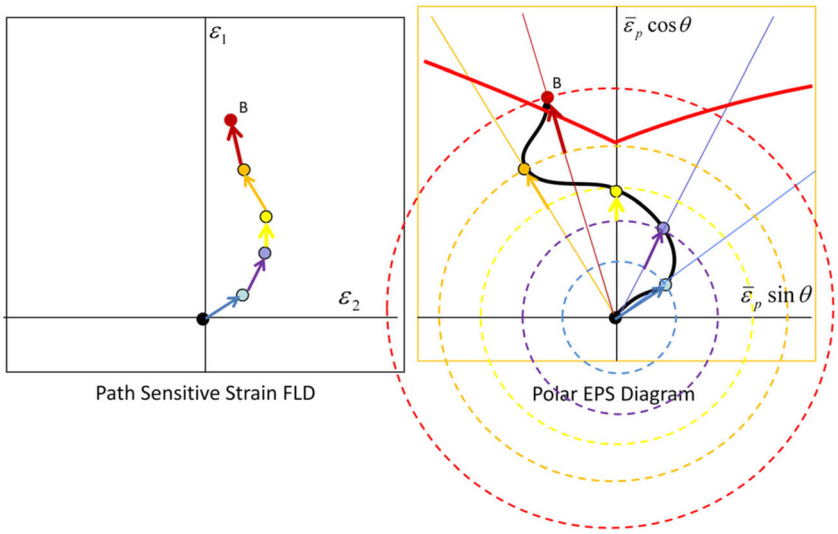

Fig. 10 Graphical illustration of the PEPS diagram for a complex strain path [31]

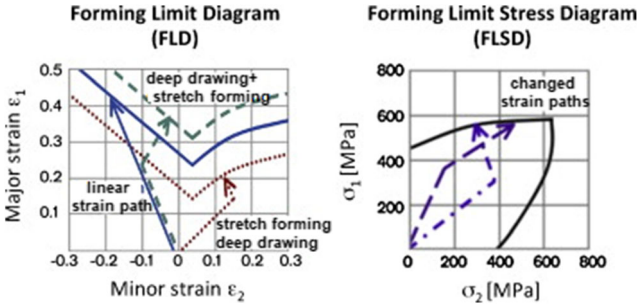

Fig. 11 From a path-dependent FLD to a non-path dependent FLSD [125]

experimental data obtained in different laboratories. In the following, we shall present some of these methods. Further details related to this problem can be found in [32, 92, 120, 273–280].

The first methods used for determining limit strains were proposed by Takashina [294] (the so-called "three circle method"), Veerman [295], Bragard [296] and d'Hayer [297] (the so-called "double profile method"), Hecker [298], Kobayashi [299], IDDRG Group [300] (known as the "Zürich Nr.5 method"). A review of these methods can be found in references [92, 273].

Together with the development "of online" video strain measuring methods, new methods of determining the limit strains have been proposed in the last years. A new criterion based on the evolution of the strain rate as a function of time during the forming process has been proposed by the SOLLAC team [301]. The method is based on the observation that the beginning of the necking is accompanied by a considerable increase of the strain rate (see Fig. 12a).

According to this method the start of necking corresponds to the dramatic change in the strain-rate versus time variation (characteristic point). This point could be determined by intersecting the straight lines corresponding to the first and the last sector of the curve. The strain – rate evolution is automatically determined by image analysis. The strain-rate method has been intensively studied over the past decade to improve the accuracy of detecting the limit strains and to increase the robustness of the method Volk [302–304], Merklein [34, 35], Wang [38], Hashemi [305], Dicecco [39], Lumelskyj [306, 307]. Situ et al. [308] proposed a method based on the major strain acceleration criterion. Volk and Hora [36] proposed an improved method based on recording the strain rate history with the aim of enhancing the capability of detecting the necking initiation and, by consequence, the accuracy of determining the limit strains. The improvement consists in applying a three-stage procedure: The necking region is identified in the first stage (using a 2D evaluation of the strain distribution); the necking initiation is identified in the second stage (by analyzing the strain-rate versus time diagram); finally, in the third stage, the limit strains are evaluated. The method proposed by Volk and Hora is physically founded

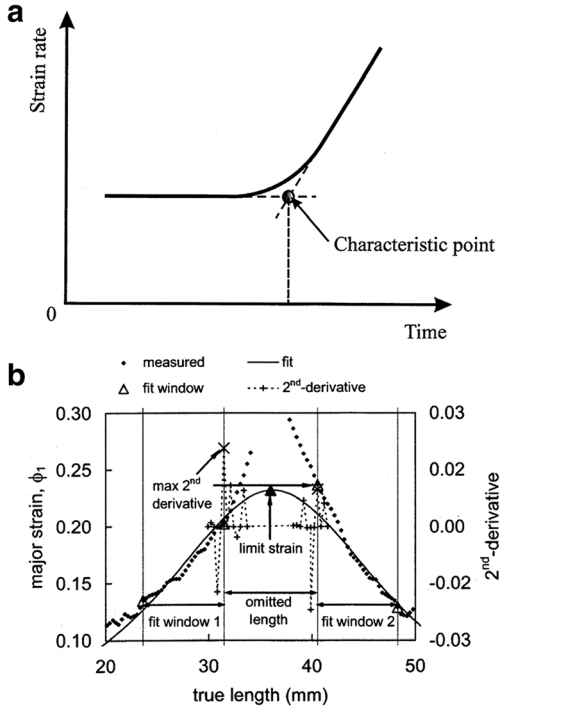

Fig. 12 Methods to determine the limit strains: **a** Strain-rate versus time; **b** IDDRG method

and ensures an enhanced robustness of the limit strain measurement.

The Nakajima workgroup of the IDDRG developed a new procedure [309], the so-called "in-process measurement" method (see Fig. 12b). A guideline for the FLC determination based on this method is presented in [310, 311]. The method is similar to that proposed by Bragard (see [296]). Using a video camera system, a film of the forming process is made. Based on the film of the forming process, the development of the strain distribution starting from the onset of necking and ending with the fracture occurrence is analyzed. The method is very robust and leads to a good repeatability of the results. Based on this achievement, the Nakajima workgroup proposed a revision of the ISO 12004-2 standard "Metallic materials-sheet and strip-Determination of the forming limit curves" [32]. The formability of a wide range of materials was assessed using traditional Nakajima FLD testing at different labs and compared with the results obtained using the analysis method in the revised ISO/DIS 12004–2 standard, for position dependent testing after fracture [312]. Leppin et al. [313] proposed a method to correct the effect of non-proportional strain paths on the Nakajima test and Hogström at al [314] optimized the ISO method. A comparison of different algorithms used to detect the necking onset was made by Hotz et al. [34]. The limitations of these methods are that they are static, do not describe the development of the strains, and are not applicable to materials characterized by a heterogeneous evolution of the thickness strain (for example in the case of small-radius

bending). Vysochinskiy et al. [40] proposed thickness-control method, a robust method for the case of multiple local necks in the sheet. According to this method, the onset of local necking occurs when the local thinning exceeds the allowable tolerance. Dicecco et al. [315] proposed a curvature-based necking criterion to determine the limit strains for aluminium alloy at elevated temperature.

Vallellano and his co-workers [37, 316, 317] developed a method to determine the limit strain based on the strain rate variations near the necking zone. A schematic of the method proposed by Vallellano et al. [37] is presented in Fig. 13. The method has been successfully used later by Zahedi et al. [318]. Recently, Iquilio et al. [319] improved the method proposed by Vallellano and proposed a novel experimental method to determine the limit strain by capturing the heterogeneity of the strain distribution at the local necking site. The limit strains are determined when a non-homogeneous decrease in the thickness necking area begins.

Min et al. [320] propose an original method to compensate the process depend effects, based on the measured surface geometry of the test specimen using digital image correlation (DIC) techniques. This method has been improved by Min et al. [321, 322] by using a change in the surface curvature in order to detect a geometric effect associated with the onset of localized necking. Figure 14 [321] presents the curvature evolution during the necking and the change of surface curvature C_{AB} between the points A and B. The method captures the effects of curvature, non-linear strain path and contact pressure. This enables compensating for these effects and reconciling the forming limits determined using the methods of Marciniak (in-plane test) and Nakazima (out of plane test). By using this method, both tests (Marciniak and Nakazima) give identical limit curves.

Elangovan et al. [323, 324] used the Artificial Neural Network (ANN) model to predict the Forming Limit Curves. Abspoel et al. [226] proposed a new semi-empirical method for predicting Forming Limit Curves from mechanical properties namely, total elongation, anisotropy coefficients and sheet thickness.

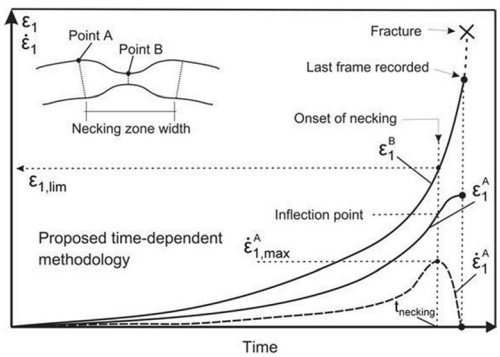

Fig. 13 Schematic of the time dependent methodology [37]

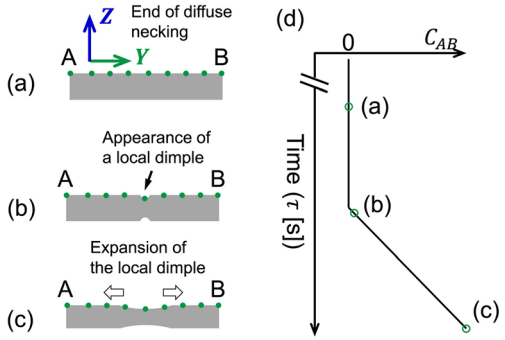

Fig. 14 Cross-sectional views showing the evolution of surface curvature during localized necking. **a** end of diffuse necking, **b** initiation and **c** expansion of a local dimple, **d** illustration of the change of surface curvature [321]

New tests used to determine the FLC

Banabic et al. [41] proposed a new procedure for the experimental determination of the FLCs. The methodology is based on the hydraulic bulging of a double specimen (Fig. 15).

The most important advantages of the method are the capability of investigating the whole strain range specific to the sheet metal forming processes, simplicity of the equipment, reduction of the parasitic effects induced by the friction, as well as the occurrence of the necking in the polar region. The comparison between the FLCs determined using the new procedure and the Nakazima test shows minor differences. Figure 16 compares the FLCs obtained using the methodology proposed by Banabic and the Nakazima test (according to the specifications of the international standard ISO 12004-2) [41]. The test was performed by Mitukiewicz [325] and Karadogan [326].

Another research direction in this field was oriented toward the use of biaxial traction tests performed on cruciform specimens. This type of mechanical test was proposed at the beginning of 1950's as a method for determining the biaxial yield stress [327]. The development of the biaxial traction test became more intense at the end of 1990's (see Section Experimental validation of the anisotropic models) of the paper. Yu at al [328] designed and optimized cruciform specimens to be used for FLC determination. The NIST team designed cruciform specimens and built a biaxial traction

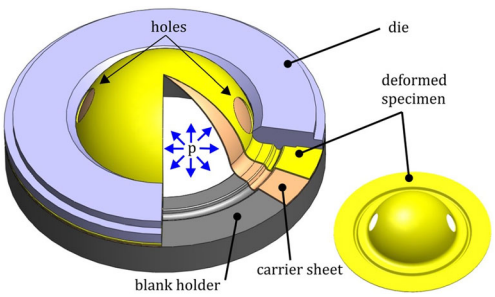

Fig. 15 Schematic view of the new test [41]

machine [329]. During the last decade, this type of mechanical test has been used and developed by Letoing et al. [42, 175, 176, 178, 196, 197], Merklein et al. [35], Shao et al. [330, 331]. In this test the strain path is very easily controlled by the displacements in the two main directions of the cruciform specimen. The main advantages of the test are the flexibility, the fact that it is an in-plane test which is not perturbed by friction.

Influence of different factors on the limit strains

Influence of bending A comparative study between the Nakazima and Marciniak tests for aluminum killed steel, brass and cold rolled aluminum [332] showed a clear overestimation of the limit strains obtained from Nakazima tests. It is however too early to conclude from this study that sheet curvature during forming is the reason for the overestimation. Charpentier [333] reported the influence of punch curvature on the stretching limits of sheet steel. Several researchers have investigated the influence of the bending radius on the limit strains during the last decade. The results obtained by the groups coordinated by Vallellano [37, 316, 334–338], van den Boogaard [339–341], Stoughton [320, 322], as well as by other groups [155, 342–345], etc. are relevant from this point of view. Figure 17 illustrates the influence of the bending radius on the limit strains [336].

Influence of temperature During the last years, the intense utilization of advanced high strength steels (AHSS), aluminum alloys, magnesium alloys, and titanium alloys has determined an active investigation of the temperature influence on the limit strains. Significant results in this domain were reported by a number of researchers: [346, 347] with reference to different steel sorts; papers published by the groups of Dean and Lin ([44, 330, 331, 348–350] etc.), Bariani and Bruschi ([125, 351]), Leotoing and Guines ([43, 352]), Worswick et al. ([315, 353]), Wang et al. [45], etc., as well as some groups from China [354–356], etc. with reference to aluminum alloys. The influence of the temperature on the formability of magnesium alloys was

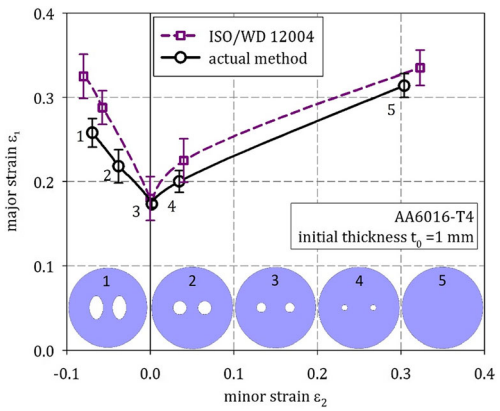

Fig. 16 FLD of the AA6016-T4 alloy [41]

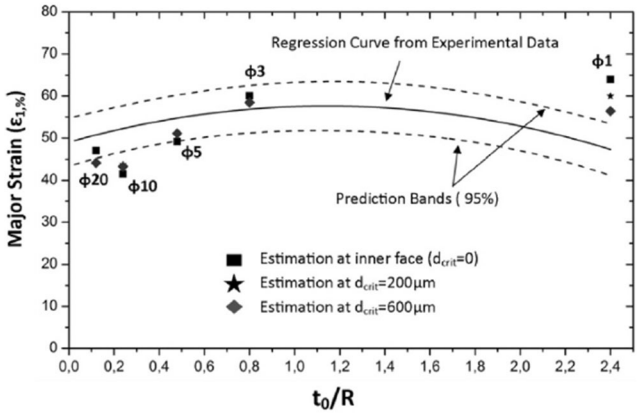

Fig. 17 Experimental and predicted forming limit strains versus t_0/R [336]

investigated by Sorgente et al. [357], Ghiotti [358], Zhang et al. [359], Huang et al. [360], Ambrogio et al. [361], Boba et al. [362], Berge et al. [363], Koh et al. [364], Kim et al. [365], Stutz et al. [366], Mekonen [367] etc. Yang et al. [368], Bodunrin [369], etc. studied the influence of the temperature on the formability of titanium alloys. Further details on this topic can be found in the synthesis papers [125, 350, 370–372]. Figure 18 [44] illustrates the influence of the temperature on the formability of an aluminum alloy.

Influence of strain rate The strain-rate effects should consider both room temperature and elevated temperature. Drewes and Martini [373], Ayres and Wenner [374] and Percy [375] initiated the research concerning the influence of the strain rate on the limit strain at room temperature. In the last decade this influence has been analyzed especially at elevated temperature by Chu [43], Gao [44], Ding [352], Koh et al. [364], Li [376], Yamashida [377], etc. In general, the authors reported that with the increase of the strain rate the FLCs move downward

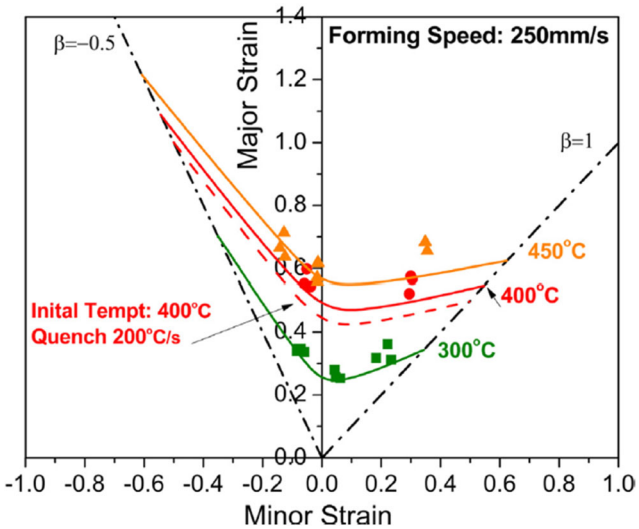

Fig. 18 Predicted versus experimental FLCs for AA2060 at different temperatures [44]

(which means the formability decreases), both for steels and aluminum alloys. The influence of the strain-rate on the FLC for an aluminum alloy deformed at elevated temperature is presented in Fig. 19 [44]. In this case the influence of the strain-rate on the FLC is significant due to the high strain-rate sensitivity of the tested material at warm. At room temperature, the strain rate effect is important for the high speed forming processes (for example, electromagnetic forming [378]. Increases in formability for several materials have been reported in high-speed forming processs ([379–381]). Jacques [382] extended the Marciniak model to include the contribution of inertia. For this purpose, it was introduced in the model the Bridgman correction factor [70] in order to account for triaxiality effects.

Influence of strain path Several researchers Nakazima [383], Müschenborn [288], Graf [384] have noticed that the strain path has a strong influence on the shape and position of FLC. This topic was recently investigated by Volk [29, 30, 281, 289] who developed a theoretical model based on Müschenborn and Sonne [288] proposal for calculating the limit strains along complex strain paths [281]. Stoughton and his coworkers [31, 32, 292], also contributed to this domain by developing an original method for determining FLC's along complex strain paths [31]. Contributions on the determinations of forming limit curves for complex strain paths were also reported by Gao [44], Erfanian [51], Leotoing [175], Rojek et al. [385], El Fakir [386], Mattiasson [387], Suttner [388], Nurcheshmeh [389], Wang [355],, etc.

Advances in the FLC prediction

Various theoretical models have been developed for the calculation of forming limit curves (FLC). The first ones were proposed by Swift [390] and Hill [391] assuming homogeneous sheet metals (the so-called models of diffuse necking and localized necking, respectively). The Swift model has been later developed by Hora (the so-called Modified Maximum Force Criterion - MMFC) [392, 393]. Marciniak and Kuczynski (MK model) [394] proposed a model assuming that sheet metals were non-homogeneous from both the geometrical and the microstructural point of view. Barata and Jalinier [395] extended the MK model for non-linear strain path. Stören and Rice [396] developed a model based on the bifurcation theory. Dudzinski and Molinari [397] used the method of linear perturbations for analyzing the strain localization and computing the limit strains. Bressan and Williams [398] introduced the so-called "Through Thickness Shear Instability Criterion" in order to take the shear fracture mode into account. Based on the analysis of the influence of the stress distribution through the thickness on the mode of failure, Stoughton [293, 399] proposed a generalized failure criterion. Since the theoretical models are rather complex and need a profound knowledge of continuum mechanics and mathematics while their results are not always in agreement with experiments, some semi-empirical models have been developed in recent years. The models used for FLC prediction are detailed (formulation of the model, solution methods, numerical aspects, advantages and limitations) in [92].

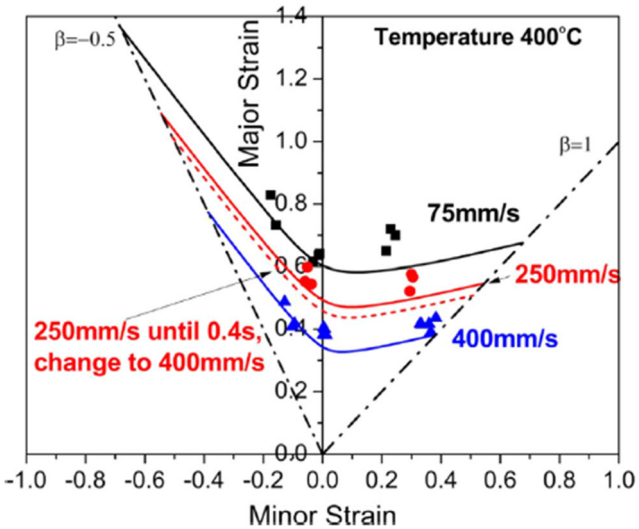

Fig. 19 Predicted versus experimental FLCs for AA2060 for different speeds [44]

At present, the most widely used models for the computation of the limit strains are those proposed by Marciniak and Kuczynski [394] and Hora [392, 393], respectively. As a consequence, the models previously mentioned will be briefly discussed in the following (see also [92, 400]). The Forming Limit Stress Diagram (FLSD) proposed by Arrieux et al. [285] has been also intensively studied during the last decade.

During the last decade the research in the field of forming limits prediction has been oriented along the same directions as in the previous decade. As an observation we mention that the research regarding the physical understanding of the phenomena of strain localization using polycrystalline, ductile damage models and the influence of the through-thickness stress have more significant weight. Therefore, we will focus our attention only on these three areas.

Because a book chapter devoted to the description of advanced models used for FLC prediction has been recently published [275] we will give here only a synthetic presentation of the research papers published during the last decade, with an emphasis on the papers published after the issuance of the book chapter mentioned above.

Crystal plasticity based FLC prediction

During the last years, two different approaches have been mainly followed to couple crystal plasticity calculations to sheet formability prediction, namely the MK framework and FE modelling.

The adaptability of the texture-based models to the MK theory of the strain localization has been proved in the 1980's by Bassani [401], Bate [402], Asaro [403], Barlat [8, 101] and later by van Houtte [404] and Neale [405] teams. The early studies often adopt the Taylor-Bishop-Hill plasticity model. During the last decade, Signorelli's team [47, 48, 406–408] has showed that FLDs predicted using coupled models of VPSC and M–K method (MK-VPSC) [110] are able to provide a better agreement with the measured FLDs as compared with the Taylor based M–K models (see Fig. 20 [47]).

Apart from the above models, the full-field approaches, namely crystal plasticity–finite element (CPFEM) have been used by Inal's group to predict the limit strains [409, 410]. Recently, this group has used the rate tangent based crystal plasticity–fast Fourier transform model (RTCP-FFT) [411]. This model, which may account for the 3D microstructure, grain interactions, and intragranular texture evolution, has been implemented recently in the M–K framework [46] to improve the accuracy of FLD predictions as compared with Taylor models (a homogenous deformation is assumed throughout the material) and VPSC.

Ductile damage and fracture models

It is well accepted that in metals, damage and ultimately failure is the result of nucleation, growth, and coalescence of voids (e.g. [412]). Since voids grow due to the plastic deformation of the fully-dense material, early on it has been recognized that the rate of void growth can be deduced once the plastic potential of the porous solid is known. One of the most widely used models are those derived by Gurson [413, 414] by conducting limit-analysis of a hollow sphere or hollow cylinder obeying von Mises yield criterion. It was proven that the presence of voids in a von Mises matrix induces dependence of the plastic flow on the mean stress, or hydrostatic pressure. To better account for void evolution, various modifications of Gurson's criteria have been proposed (e.g. [415–417], etc.), the most used being the Gurson-Tvergaard-Needleman (GTN) model. Recently, efforts have been devoted towards describing the role played by the particularities of the yielding behavior on void evolution. Cazacu et al. [418, 419] demonstrated that if the yielding behavior of the void-free material is described by either von Mises, Tresca, or Drucker criterion (see Eq. (1)), the dependence of the plastic potential and ultimately the fracture locus on the stress invariants cannot be arbitrary Specifically, it was mathematically proven that with the exception of purely hydrostatic and purely deviatoric loadings (triaxiality zero), there is dependence on $J_3$and moreover there exists a very specific coupling between the signs of the pressure and that of the third invariant J_3such that:

$$\mathrm{F}(\sigma_m, J_2, J_3) = \mathrm{F}(-\sigma_m, J_2, -J_3) \tag{19}$$

Furthermore, it was shown that for positive triaxialities the rate of void growth is faster for loadings at $J_3>0$ (e.g. uniaxial tension) than for loadings at $J_3 \leq 0$ (e.g. equibiaxial tension); the reverse holds true in the case of void closure (i.e. loadings corresponding to negative triaxialities). It was also shown that the rate of void growth is much faster in a Tresca material than in a von Mises material. Recently Cazacu and Stewart [420] used limit-analysis to derive the plastic potential for isotropic materials with matrix displaying tension-compression asymmetry. This model predicts that irrespective of loading there is an effect of the sign of the mean stress while the effect of J_3 is very strong for any loadings except hydrostatic tension or compression. In the absence of porosity, this model reduces to the isotropic Cazacu et al. [111] criterion. For materials with $k > 0$ (matrix softer in compression than in tension), the rate of void growth is much faster than for materials characterized by $k < 0$ (matrix harder in compression than in tension).

In the case of a textured material, it is extremely difficult or impossible to obtain the plastic potential of the damaged material in closed-form. Benzerga and Besson [421] developed such a potential for the case when the matrix is described by the Hill [88] while Stewart and Cazacu [422] developed an orthotropic plastic potential for the case when the matrix is described by the orthotropic Cazacu et al. [111] criterion .

With the availability of High-Resolution X-ray Computed Tomography (XRCT), in the past decades it has become possible to quantify the porosity in the bulk of a given material. Specifically, void nucleation and growth can be clearly visualized during continuous or interrupted in-situ tests. Recently, Maire and collaborators used this technique to measure porosity evolution in several commercial aluminum alloys. For example, for AA 6016-T4 tensile test results on both smooth and notched samples of the material as well as damage measurements by XRCT for several orientations in the plane of the sheet were reported in [423]. It was shown that the observed rate of void growth is well predicted using the Cazacu and Stewart [422] model for all notch acuities (see Revil et al. [424]. For XCRT data on 2000, 5000 and 7000 series aluminum alloys, the reader is referred to Maire et al. [425].

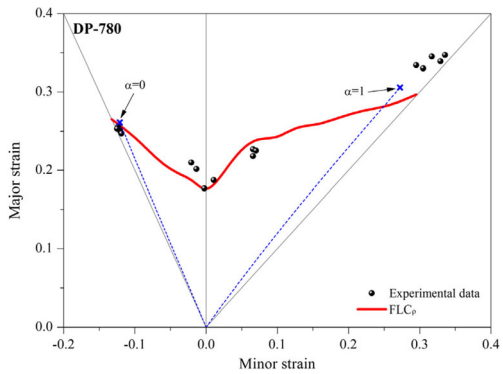

Fig. 20 Experimental and predicted FLDs for the DP-780 steel samples taken along the RD [47]

In the case of hcp materials, every aspect of damage and its evolution are completely different than in materials with very little tension-compression asymmetry. As an example, Fig. 21a shows the reconstructed 2-D views in the (TD, TT) plane, and in the (RD, TD) plane of a smooth RD specimen of a strongly textured Ti material, respectively, which was subjected to uniaxial tension very close to failure. For comparison purposes, in Fig. 21b are shown the respective views extracted from an XCMT scan done for a copper specimen, scan which was taken at the same level of axial displacement (see Revil et al. [142]). Note that for the same axial displacement, the Cu material is much damaged than the Ti material shows. Specifically, for the Ti specimen the average porosity over the specimen volume and minimal cross-section is of 0.052% and 0.25%, respectively.

In situ scans on a notched RD specimen subjected to uniaxial tension were also reported in [142]. It was observed that damage initiates at the outer surface of the specimen and further grows from the outer surface to the center of the specimen. Stewart and Cazacu [422] model predicts these trends as well as the fact that damage accumulates differently in the TD and ND directions of the cross section (see [136, 142] for comparisons between model and data). To evaluate the importance of the consideration of the tension-compression asymmetry on the damage predictions, these authors also performed simulations with k = 0, as shown in Fig. 22a. Note that in this case, the maximum porosity is at the center of the specimen. Only if the tension-compression asymmetry in plastic deformation is accounted for, the experimental porosity distribution is captured (see Fig. 22b).

For examples of other damage models and approaches for modeling damage in metallic materials the reader is referred to the monographs [79, 426].

The GTN damage model has been used by many researchers interested in the prediction of FLC's. The papers published by Zahedi [318], Hu [346], Lin [427], Malcher [428], Yang [429], Tang [430], etc. can be mentioned here. Recently, the CERTETA team used the Gurson's model with some recent extensions to model porous materials, following both the evolution of a homogeneous sheet and the evolution of the distribution of voids [431]. The Gurson-Tvergaard-Needleman (GTN) model has been used by Kami et al. [49, 432] to determine the FLC of AA6016-T4 aluminum alloy. Figure 23 shows that the results obtained by numerical simulation using the GTN model are in good agreement with experimental data. The comparison becomes even more favorable when confronted with the predictions of the Marciniak-Kuczynski (M-K) model and the modified maximum force criterion (MMFC) (see Fig. 23) [432].

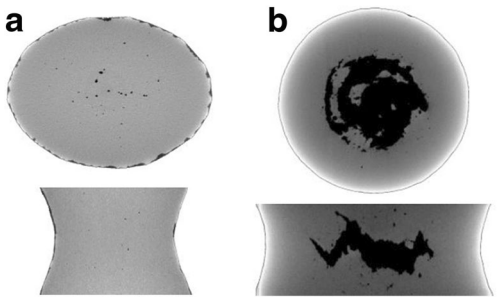

Fig. 21 Post-test XCMT scans of smooth specimens subjected to uniaxial tension: **a** Ti specimen; **b** Cu specimen (after [142]). (a)Anisotropic model with k = 0 (b) Stewart and Cazacu [422] model

Fracture laws that expressed by relations between the fracture strain and the stress triaxiality have been frequently used during the last decade. Furthermore, Wierzbicki and his group introduced a new concept to define the formability based on the dependence of the equivalent strain at fracture on the stress triaxiality [433–436]. This has been intensively studied in the last decade by the groups of Wierzbicki [437–442] anh Huh and Yoon [443–446] and also by Li [447], Lou [448] etc. A review of the most popular laws used for the prediction of fracture forming limit curves was conducted by Habibi [344]. Lou proposed in 2012 [443] a ductile fracture condition extended in 2014 [444] and 2017 [448]. The fracture locus for plane stress proposed by Lou is presented in Fig. 24 [444]. A fracture polygon based on the maximum shear stress (MSS) fracture criterion has been proposed by Stoughton and Yoon [282] and used to predict the necking limit. To describe yielding and fracture of pressure-sensitive metallic materials [449] introduced in the expression of the orthotropic yield function of Nixon et al. [135] an additional hydrostatic pressure term.

Effect of the normal pressure on the formability

The effect of the normal pressure on the formability of sheet metals is well known and has been exploited in industry for a long time [450]. Banabic and Soare [451], Wu et al. [452] and Allwood and Shouler [453] analyzed independently the influence of the normal pressure on the Forming Limit Curve using an enhanced MK model. The effect of the through-thickness normal stress on the forming limit diagram has been studied extensively in the last 5 years especially by Iranian and Chinese groups: Assempour et al. [50], Liu [454], Zhang et al. [54, 455, 456], Nurcheshmeh and Green [457], Lang et al. [458], Hashemi [52, 459, 460], Mirfalah [461, 462], Ma [53, 463], Bettaieb [464], Shi [465], Erfanian [51], Hu [466] etc. The influence of the hydro-static pressure on the yield and flow of metallic materials was also investigated by Soare and Barlat in [467]. The study of the influence of through-thickness shear on the limit strains was initiated by Eyckens et al. [468] and continued in the last decade by Eyckens [469], Fatemi [470], Mirfalah [461, 462], etc.

Besides the above-mentioned domains, systematic investigations have been recently performed along the following directions: formability of multi-layer (sandwich) sheets ([55–61, 471–473], etc.), extension of the Modified

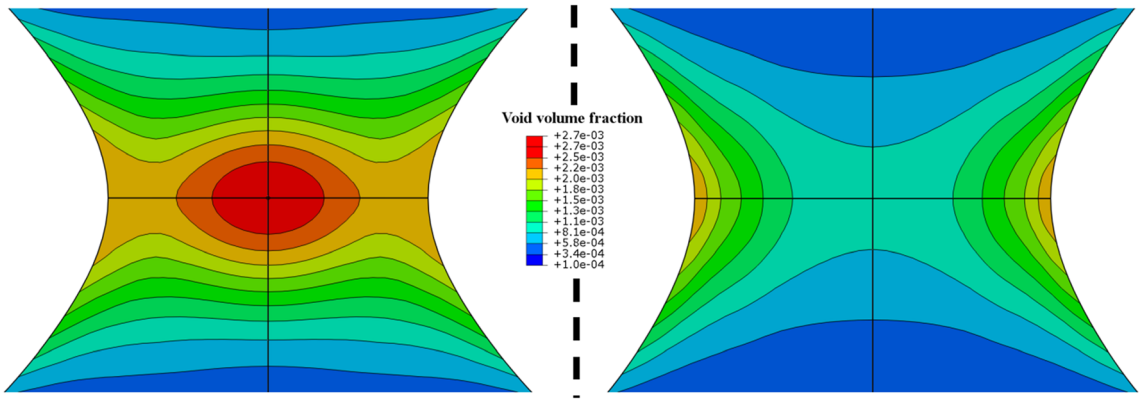

Fig. 22 Importance of accounting for tension-compression asymmetry: comparison of the F.E. isocontours of porosity in the (RD-TD) of a notched Ti specimen subjected to uniaxial tension along RD for an axial displacement of 1.2 mm: **a** predictions according to anisotropic model with no tension-compression asymmetry (k = 0); **b** Stewart and Cazacu [422] model (after [142])

Maximum Force Criterion-MMFC model [61, 63, 260, 392, 393, 474–476] etc.), formability of sheet metals at micro-meso scale [477], as well as revisiting the perturbation approach ([64, 65, 478, 479]), etc.

Concluding remarks and future directions

In this paper we have presented and discussed recent advances in modeling the yielding and hardening behavior, and damage of metallic materials, innovative experiments aimed at providing verification/validation of these models, and illustrative examples and applications to metal forming. Further discussion, concluding remarks, and future directions are presented in the following.

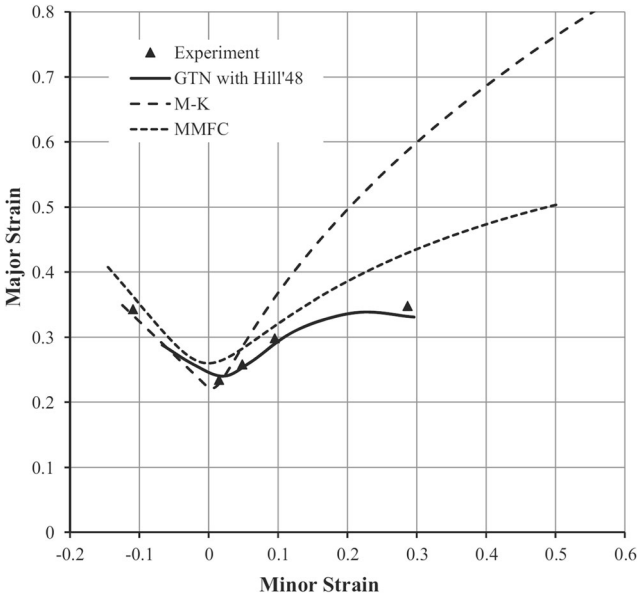

Fig. 23 Comparison between the FLC calculated with different methods and experimental data [432]

At present, there are 3-D yield functions (or strain rate potentials, e.g. see [79, 100],) for single crystals, and polycrystalline FCC, BCC or HCP materials that take the distinctive features of the mechanical behavior of these materials into account (see also [136]). For instance, for HCP materials there exist pressure-insensitive yielding formulations that account for the difference in yielding behavior in tension and compression observed experimentally for these materials. Due to a correct modelling of material symmetries, anisotropic yield functions available nowadays are more versatile than those used in the past. Examples of the capabilities of representative plane stress or general three-dimensional formulations were presented.

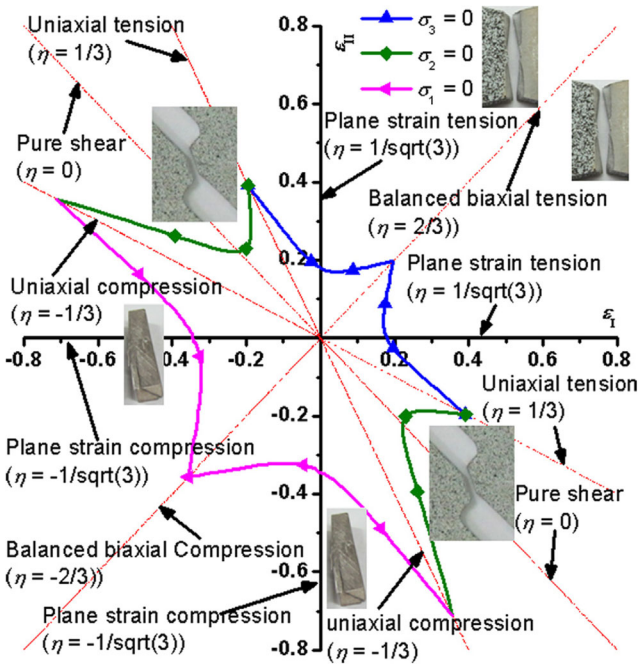

Fig. 24 Fracture locus for plane stress in the in the space ε1-εh determined by using Lou criterion [444]

Any isotropic or anisotropic yield condition, including any of those described in this article, can be used as a plastic potential though the associated flow rule (AFR) in order to determine the plastic strain increment. Many authors have used the AFR, also called normality rule, based on the strain hardening stability expressed in the Drucker postulate [480]. Critical experimental investigations as reviewed by Hecker [481] could not find any clear violation of the rule. Nevertheless, the non-associated flow rule (NAFR) made a resurgence during the last two decades and its applications to sheet metal forming simulations have been increasing because the NAFR allows the use of simpler functional forms with improved calibration accuracy [482]. In this respect, the NAFR is interesting for industrial applications where simpler approaches are preferred. Moreover, the work of Stoughton and Yoon [483] on the development of stability constraints has also been essential for allowing a wider application of the NAFR. In fact, the recent version of the homogeneous anisotropic hardening model HAH_{20} is non-associated in the direction of the hydrostatic stress to preserve plastic incompressibility but associated in the deviatoric hyperplane as implied in [159, 484] and demonstrated in Soare and Barlat [467]. This is because, for metals, the AFR is supported by theoretical arguments based on crystal plasticity set forth by Bishop and Hill [82] with a minimum number of assumptions. Although AFR models might appear more complex, numerical optimization methods are available through commercial software to calibrate constitutive models with high accuracy. Moreover, the use of numerical derivation techniques such as in [485, 486], which do not require the analytical derivation of the flow rule from the potential, are very accurate and greatly simplify the finite element implementation of the AFR-based models.

In the future, the evolution of yield function coefficients will be self-contained in the formulation for any linear and non-linear loading. Therefore, as in the case of crystal plasticity, it will be possible to describe the evolution of anisotropy as deformation proceeds. However, the computation time will be much lower than what is at present required for calculations when crystal plasticity models are directly linked to FE codes.

In conventional multiaxial stress tests many linear stress paths are applied to test samples to determine the contours of the plastic work and the directions of the plastic strain rates. Proper material models (anisotropic yield functions) are identified using the experimental data, assuming that the normality flow rule (NFR) associated with the work contours is satisfied. When the contours of plastic work are similar with the increase of plastic work an isotropic hardening (IH) model is applied to the material while if it is not the case a differential hardening (DH) model should be used. To the author's knowledge this procedure of material modeling is effective to enhance the predictive accuracy of sheet metal forming simulations, although IH is assumed in most industrial forming simulation.

In reality, however, most materials exhibit DH [12, 13, 15, 16, 183, 184, 187, 189, 195, 198, 199, 247, 267]. Moreover, some materials do not follow NFR with respect to work contours [16, 221]. To quantitatively evaluate the DH of sheet metals and the validity of NFR for a lager strain range up to immediately before a localized neck occurs, MTET is a useful testing method. In particular, it is capable of applying arbitrary nonlinear stress/strain paths to a specimen, which sheet metals very often undergo in industrial forming operations. The main issue of MTET is that it requires a special testing apparatus that can simultaneously apply internal pressure and axial force to a tubular specimen using a feedback control system. Even preparing a tubular specimen could be problematic for high strength materials and materials with poor weldability. Therefore, the development of a systematic and user-friendly multiaxial stress testing method is crucial to the identification and the development of highly-accurate material models. The VFM integrated into a DIC platform will be a powerful experimental tool for the establishment of the testing method.

Regarding the formability of metallic materials, in the past, the FLC models provided an approximate description of the experimental results. Such models were used especially for obtaining qualitative information concerning the necking/tearing phenomena. At present, the FLC models allow a sufficiently accurate prediction of the limit strains, but each model suffers from its own limitations (see Section Advanced methods used to determine the limit strains). There is no model that can be applied to any sort of sheet metal, any type of crystallographic structure, any strain-path or any variation range of the process parameters (strain rate, temperature, pressure, etc.).

During the last decade, the experimental research has been mainly focused on refining the experimental methods used for detecting and measuring the limit strains, developing new laboratory tests for FLC determination, as well as on investigating the influence of various material and process parameters on the limit strains. The theoretical research has been oriented toward improving the predictive capabilities of various models by refining the numerical methods used to solve the models and including new material or process parameters in the models (temperature, strain rate, pressure, shear stresses, strain path effect, bending effect, etc.). An intense research activity can be noticed in the field of investigating the effect of the normal pressure and through-thickness shear on the formability. The research on ductile fracture and crystal plasticity models has gained an increased weight during the last decade. These models have contributed to the clarification of some phenomena taking place at micro-meso scale directly linked to the necking and fracture processes, thus ensuring an enhanced accuracy in the FLC prediction. The industrial utilization of sandwich materials has also intensified the research regarding their formability.

The future research will be focused on a more in-depth analysis of the phenomena accompanying the necking and

fracture of the sheet metals. On the basis of the analysis, more realistic models will be developed in order to obtain better predictions of the limit strains. New models will be developed for prediction of the limit strains for special sheet metal forming processes: superplastic forming, forming at very high pressure, incremental forming etc. Commercial codes allowing the quick and accurate calculation of the FLC's both for linear and complex strain-paths will be developed. The texture models will be also implemented in such commercial programs. The FLC computation will be included in the finite element codes used for the simulation of the sheet metal forming processes. The aim is to develop automatic decision tools (based on artificial intelligence methods) useful in the technological design departments. The stochastic modeling of the FLC's will be developed in order to increase the robustness of the sheet metal forming simulation programs. Comparing different FLC detection methods for the same material is a usefull research topic. More refined, accurate and objective experimental methods for the experimental determination of the limit strains (e.g. methods based on thermal, acoustic effects, X-ray tomography) will be also developed.

Acknowledgments FB is very grateful to POSCO for generous financial support. OC gratefully acknowledges partial support for this work provided by the Air Force Office of Scientific Research (AFOSR) grant FA9550-18-1-0517.

Compliance with ethical standards

Conflict of interest None.

References

1. Morestin F, Boivin M (1996) On the necessity of taking into account the variation in the young modulus with plastic strain in elastic-plastic software. Nucl Eng Des 162:107–116
2. Wagoner RH, Lim H, Lee M-G (2013) Advanced issue in springback. Int J Plast 45:3–20
3. Sun L, Wagoner RH (2011) Complex unloading behavior: nature of the deformation and its consistent constitutive representation. Int J Plast 27:1126–1144
4. Yoshida F, Amaishi T (2020) Model for description of nonlinear unloading-reloading stress-strain response with special reference to plastic-strain dependent chord modulus. Int J Plast 130:102708
5. Chaboche JL (1986) Time-independent constitutive theories for cyclic plasticity. Int J Plast 2:149–188
6. Yoshida F, Uemori T (2002) A model of large-strain cyclic plasticity describing the Bauschinger effect and workhardening stagnation. Int J Plast 18:661–686
7. Yoshida F, Uemori T (2003) A model of large-strain cyclic plasticity and its application to springback simulation. Int J Mech Sci 45:1687–1702
8. Barlat F (1987) Crystallographic texture, anisotropic yield surfaces and forming limits of sheet metals. Mater Sci Eng 91:55–72
9. Maeda T, Noma N, Kuwabara T, Barlat F, Korkolis YP (2018) Measurement of the strength differential effect of DP980 steel sheet and experimental validation using pure bending test. J Mater Process Technol 256:247–253
10. Steglich D, Tian X, Bohlen J, Kuwabara T (2014) Mechanical testing of thin sheet magnesium alloys in biaxial tension and uniaxial compression. Exp Mech 54:1247–1258
11. Aretz H, Keller S (2011) On the non-balanced biaxial stress state in bulge-testing. Proc. 10th Int Conf Technol plasticity, steel research international, Special Edition: 738–743
12. Kuwabara T, Van Bael A, Iizuka E (2002) Measurement and analysis of yield locus and work hardening characteristics of steel sheets with different *r*-values. Acta Mater 50:3717–3729
13. Nagano C, Kuwabara T, Shimada Y (2018) Kawamura R, (2018) measurement of differential hardening under biaxial stress of pure titanium sheet. IOP Conf Ser Mater Sci Eng 418:012090
14. Hippke H, Hirsiger S, Berisha B, Hora P (2020) Optimized and validated prediction of plastic yielding supported by cruciform experiments and crystal plasticity. Int J Mater Form. https://doi.org/10.1007/s12289-020-01569-6
15. Suh YS, Saunders FI, Wagoner RH (1996) Anisotropic yield functions with plastic-strain- induced anisotropy. Int J Plast 12:417–438
16. Kuwabara T, Mori T, Asano M, Hakoyama T, Barlat F (2017) Material modeling of 6016-O and 6016-T4 aluminum alloy sheets and application to hole expansion forming simulation. Int J Plast 93:164–186
17. ISO 16808 (2014) Metallic materials −Sheet and strip − Determination of biaxial stress-strain curve by means of bulge test with optical measuring systems
18. ISO 16842 (2014) Metallic materials −Sheet and strip −Biaxial tensile testing method using a cruciform test piece
19. Rusinek A, Klepaczko JR (2001) Shear testing of a sheet steel at wide range of strain rates and a constitutive relation with strain-rate and temperature dependence of the flow stress. Int J Plast 17:87–115
20. Bouvier S, Haddadi H, Levee P, Teodosiu C (2006) Simple shear tests: experimental techniques and characterization of the plastic anisotropy of rolled sheets at large strains. J Mater Process Technol 172:96–103
21. Rauch EF (2009) Plastic behavior of metals at large strains: experimental studies involving simple shear. J Eng Mater Technol 131:011107
22. An YG, Vegter H, Elliott L (2004) A novel and simple method for the measurement of plane strain work hardening. J Mater Process Technol 155–156:1616–1622
23. Hu JJ, Chen GW, Liu YC, Hsu SS (2014) Influence of specimen geometry on the estimation of the planar biaxial mechanical properties of cruciform specimens. Exp Mech 54:615–631
24. Nasdala L, Husni AH (2020) Determination of yield surfaces in accordance with ISO 16842 using an optimized cruciform test specimen. Exp Mech. https://doi.org/10.1007/s11340-020-00601-9
25. Pierron F, Grédiac M (2012) The virtual fields method: extracting constitutive mechanical parameters from full-field deformation measurements. Springer, New-York
26. Rossi M, Pierron F (2012) Identification of plastic constitutive parameters at large deformations from three dimensional displacement fields. Comput Mech 49:53–71
27. Coppieters S, Kuwabara T (2014) Identification of post-necking hardening phenomena in ductile sheet metal. Exp Mech 54:1355–1371
28. Marek A, Davis FM, Rossi M, Pierron F (2019) Extension of the sensitivity-based virtual fields to large deformation anisotropic plasticity. Int J Mater Form 12:457–476
29. Gaber C, Jocham D, Weiss HA, Böttcher O, Volk W (2017) Evaluation of non-linear strain paths using generalized forming

limit concept and a modification of the time dependent evaluation method. Int J Mat Form 10:345–351
30. Volk W, Hoffmann H, Suh J, Kim J (2012) Failure prediction for nonlinear strain paths in sheet metal forming. CIRP Ann Manuf Technol 61:259–262
31. Stoughton TB, Yoon JW (2012) Path independent forming limits in strain and stress spaces. Int J Solids Struct 49:3616–3625
32. Stoughton TB, Yoon JW (2014) Stress-based forming limit curves. In: Hashmi MSJ (ed) Comprehensive Materials Processing (vol 1), Elsevier, Amsterdam, pp. 71–84
33. ISO 12004-1; 12004–2 (2008) Metallic materials-sheet and strip-Determination of the Forming Limit Curves. Part 1: Measurement and application of forming-limit diagrams in the press shop Part 2: Determination of forming-limit curves in the laboratory
34. Hotz W, Merklein M, Kuppert A, Friebe H, Klein M (2013) Time dependent FLC determination – comparison of different algorithms to detect the onset of unstable necking before fracture. Key Eng Mater 549:397–404
35. Merklein M, Biasutti M (2013) Development of a biaxial tensile machine for characterization of sheet metals. J Mater Process Technol 213:939–946
36. Volk W, Hora P (2011) New algorithm for a robust user-independent evaluation of beginning instability for the experimental FLC determination. Int J Mat Form 4:339–346
37. Martínez-Donaire A, Garcia-Lomas F, Vallellano C (2014) New approaches to detect the onset of localised necking in sheets under through-thickness strain gradients. Mat Des 57:135–145
38. Wang K, Carsley JE, He B, Li J, Zhang L (2014) Measuring forming limit strains with digital image correlation analysis. J Mater Process Technol 214:1120–1130
39. Dicecco S, Butcher C, Worswick M, Boettcher E, Chu F, Shi C (2016) Determination of forming limit diagrams of AA6013-T6 aluminum alloy sheet using a time and position dependent localized necking criterion. Mater Sci Eng 159:012009
40. Vysochinskiy D, Coudert T, Hopperstad OS, Lademo OG, Reyes A (2016) Experimental detection of forming limit strains on samples with multiple local necks. J Mater Process Technol 227:216–226
41. Banabic D, Lazarescu L, Paraianu L, Ciobanu I, Nicodim I, Comsa DS (2013) Development of a new procedure for the experimental determination of the forming limit curves. CIRP Ann Manuf Technol 62:255–258
42. Leotoing L, Guines D, Zidane I, Ragneau E (2013) Cruciform shape benefits for experimental and numerical evaluation of sheet metal formability. J Mater Process Technol 213:856–863
43. Chu X, Leotoing L, Guines D, Ragneau E (2014) Temperature and strain rate influence on AA5086 forming limit curves: experimental results and discussion on the validity of the M-K model. Int J Mech Sci 78:27–34
44. Gao H, El Fakir O, Wang L, Politis DJ, Li Z (2017) Forming limit prediction for hot stamping processes featuring non-isothermal and complex loading conditions. Int J Mech Sci 131–132:792–810
45. Wang N, Ilinich A, Chen M, Luckey G, D'Amours G (2019) A comparison study on forming limit prediction methods for hot stamping of 7075 aluminum sheet. Int J Mech Sci 151:444–460
46. Nagra JS, Brahme A, Mishra R, Lebensohn RA, Inal K (2018) An efficient full-field crystal plasticity-based M–K framework to study the effect of 3D microstructural features on the formability of polycrystalline materials. Model Simul Mater Sci Eng 26: 075002
47. Schwindt C, Schlosser F, Bertinetti MA, Stout M, Signorelli JW (2015) Experimental and viscoplastic self-consistent evaluation of forming limit diagrams for anisotropic sheet metals: an efficient and robust implementation of the M–K model. Int J Plast 73:62–99
48. Signorelli J W, Bertinetti MA (2012) Self-consistent homogenization methods for predicting forming limits of sheet metal in: metal forming—process, Tools, Design, InTech, London, pp. 175–210
49. Kami A, Mollaei Dariani B, Sadough Vanini A, Comsa DS, Banabic D (2014) Prediction of the forming limit curves using GTN damage model. Rom J Tech Sciences – App Mech 59: 253–264
50. Assempour A, Nejadkhaki HK, Hashemi R (2010) Forming limit diagrams with the existence of through-thickness normal stress. Comput Mater Sci 48:504–548
51. Erfanian F, Hashemi R (2018) A comparative study of the extended forming limit diagrams considering strain path, through-thickness normal and shear stress. Int J Mech Sci 148:316–326
52. Hashemi R, Abrinia K (2014) Analysis of the extended stress-based forming limit curve considering the effects of strain path and through-thickness normal stress. Mat Des 54:670–677
53. Ma B, Diao K, Wu X, Li X, Wan M, Cai Z (2016) The effect of the through-thickness normal stress on sheet formability. J Manuf Process 21:134–140
54. Zhang F, Chen J, Chen J, Zhu X (2014) Forming limit model evaluation for anisotropic sheet metals under through-thickness normal stress. Int J Mech Sci 89:40–46
55. Bagherzadeh S, Mirnia MJ, Mollaei DB (2015) Numerical and experimental investigations of hydro-mechanical deep drawing process of laminated aluminum/steel sheets. J Manuf Process 18: 131–140
56. Gorji M, Berisha B, Manopulo N, Hora P (2016) Effect of through thickness strain distribution on shear fracture hazard and its mitigation by using multilayer aluminum sheets. J Mater Process Technol 232:19–33
57. Jalali Aghchai A, Shakeri M, Mollaei Dariani B (2013) Influences of material properties of components on formability of two-layer metallic sheets. Int J Adv Manuf Technol 66:809–823
58. Kami A, Mollaei Dariani B, Comsa DS, Banabic D, Sadough Vanini A, Liewald M (2017) An experimental study on the formability of a vibration damping sandwich sheet (Bondal). Proc. Rom Acad 18A:281–290
59. Kim D, Kim H, Kim JH, Lee MG, Kim KJ, Barlat F, Lee Y, Chung K (2015) Modeling of forming limit for multilayer sheets based on strain-rate potentials. Int J Plast 75:63–99
60. Liu J, Liu W, Xue W (2013) Forming limit diagram prediction of AA5052/polyethylene/AA5052 sandwich sheets. Mater Des 46: 112–120
61. Parsa MH, Ettehad M, Matin PH, Al Ahkami SN (2010) Experimental and numerical determination of limiting drawing ratio of Al3105-polypropylene-Al3105 sandwich sheets. J Eng Mater Technol 132:31004
62. Hora P, Tong L, Berisha B (2013) Modified maximum force criterion, a model for the theoretical prediction of forming limit curves. Int J Mat Form 6:267–279
63. Lian J, Shen F, Jia X, Ahn DC, Chae DC, Münstermann S, Bleck W (2018) An evolving non-associated Hill48 plasticity model accounting for anisotropic hardening and r-value evolution and its application to forming limit prediction. Int J Solids Struct 151: 20–44
64. Hu Q, Li X, Zhu X, Chen J (2018) Investigations on the effects of hardening law and yield criterion on the forming limit prediction with perturbation approach. Acta Mech Solids Sin (in press)
65. Yoshida K, Kuroda M (2012) Comparison of bifurcation and imperfection analyses of localized necking in rate-independent polycrystalline sheets. Int J Solids Struct 49:2073–2084
66. Butcher C, Anderson D, Worswick M (2013) Predicting failure during sheared edge stretching using a damage-based model for the shear-affected zone. SAE Int J Mater Manf 6:304–312

67. Ilinich A, Smith L, Golovashchenko S (2011) Analysis of methods for determining sheared edge formability, SAE technical paper 2011-01-1062
68. Karnop R, Sachs G (1928) Festigkeitseigenschaften von Kristallen einer veredelbaren Aluminiumlegierung. Z Phys 49:480–497
69. Polanyi M, Schmid E (1923) Ist die Gleitreibung vom Druck normal zu den Gleitflächen abhängig. Z Phys 16:336–339
70. Bridgman P (1952) W:studies in large plastic flow and fracture. McGraw-Hill, New York
71. Lode W (1926) Versuche über den Einflus der mittleren Hauptspannung auf das Fliessen der Metalle Eisen, Kupfer und Nickel. Z Phys 36:913–939
72. Drucker DC (1949) Relation of experiments to mathematical theories of plasticity. J Appl Mech 16:349–357
73. Hershey AV (1954) The plasticity of an isotropic aggregate of anisotropic face centred cubic crystals. J Appl Mech 21:241–249
74. Hosford WF (1972) A generalized isotropic yield criterion. J Appl Mech 39:607–609
75. Cazacu O, Chandola N, Revil-Baudard B (2018) Analytical expressions for the yield stress and Lankford coefficients of polycrystalline sheets based on a new single crystal model. Int J Mater Form 11:571–581
76. Barlat F, Lege DJ, Brem JC (1991) A six-component yield function for anisotropic materials. Int J Plast 7:693–712
77. Watson M, Dick R, Huang Y H, Lockley A, Cardoso R, Santos A (2016) Benchmark 1 – failure prediction after cup drawing, reverse redrawing and expansion: part D: responses, NUMISHEET 2016, 10th Int Conf workshop numerical simulation of 3D sheet metal forming processes, J of physics: Conf series Cardoso R, Adetosro OB (Eds.), Vol. 734. https://doi.org/10.1088/1742-6596/734/2/022001
78. Cazacu O (2019) New mathematical results and explicit expressions in terms of the stress components of Barlat et al. (1991) orthotropic yield criterion. Int J Solids Struct 176–177:86–95
79. Cazacu O, Revil-Baudard B, Chandola N (2019) Plasticity-damage couplings:from single crystal to polycrystalline materials. Springer, Berlin Heidelberg
80. Dillamore I, Roberts W (1964) Rolling textures in fcc and bcc metals. Acta Metall 12:281–293
81. Hirsch J (2005) Texture and anisotropy in industrial applications of aluminium alloys. Arch Metall Mater 50:21–34
82. Bishop J, Hill R (1951) A theoretical derivation of the plastic properties of a polycrystalline face-centred metal. Philos Mag J Sci 42:1298–1307
83. Taylor GI (1938) Analysis of plastic strain in a cubic crystal. In: Stephen Timoshenko 60 th anniversary volume pp 218–224
84. Barlat F, Cazacu O, Życzowski M, Banabic D, Yoon JW (2004) Yield surface plasticity and anisotropy. In: Raabe D, Roters F, Barlat F, Chen LQ (eds) Continuum scale simulation of engineering materials–fundamentals– microstructures – process applications. Wiley VCH, Manheim, pp 145–177
85. Cazacu O, Revil-Baudard B, Chandola N (2018) A yield criterion for cubic single crystals. Int J Solids Struct 151:9–19
86. Chandola N, Cazacu O, Revil-Baudard B (2017) New polycrystalline modeling as applied to textured steel sheets. Mech. Res Commun 84:98–101
87. Chandola N, Cazacu O, Revil-Baudard B (2017) Predictions of plastic anisotropy of textured polycrystalline sheets using a new single crystal model. C R Mecanique 346:756–769
88. Hill R (1948) A theory of the yielding and plastic flow of anisotropic metals. Proc Roy Soc A193:281–297
89. Hill R (1990) Constitutive modelling of orthotropic plasticity in sheet metals. J Mech Phys Solids 38:405–417
90. Barlat F, Lian J (1989) Plastic behavior and stretchability of sheet metals. Part I: Yield function for orthotropic sheets under plane stress conditions. Int J Plast 5:51–66
91. Karafillis AP, Boyce MC (1993) A general anisotropic yield criterion using bounds and a transformation weighting tensor. J Mech Phys Solids 41:1859–1886
92. Banabic D et al (2010) Sheet metal forming processes. Springer, Berlin Heidelberg
93. Cazacu O (2019) New expressions and calibration strategies for Karafillis and Boyce (1993) yield criterion. Int J Solids Struct 185–186:410–422
94. Cazacu O, Barlat F (2001) Generalization of Drucker's yield criterion to orthotropy. Math Mech Solids 6:613–630
95. Cazacu O, Barlat F (2003) Application of representation theory to describe yielding of anisotropic aluminum alloys. Int J Eng Sci 41:1367–1385
96. Barros PD, Neto DM, Alves JL, Oliveira MC, Menezes LF (2015) DD3IMP, 3D fully implicit finite element solver: implementation of CB2001 yield criterion. Rom J Techn Sci App Mech 60(1–2):105–136
97. Neto DM, Oliveira MC, Dick RE, Barros PD, Alves JL, Menezes LF, Neto DM, Oliveira MC, Dick RE, Barros PD, Alves JL, Menezes LF (2017) Numerical and experimental analysis of wrinkling during the cup drawing of an AA5042 aluminium alloy. Int J Mater Form 10:125–138
98. Cazacu O (2018) New yield criteria for isotropic and textured metallic materials. Int J Solids Struct 139:200–210
99. Revil-Baudard B (2020) Forming of materials with cubic crystal structure. Procedia Manuf 47:1300–1307
100. Barlat F, Brem JC, Yoon JW, Chung K, Dick RE, Lege DJ, Pourboghrat F, Choi S-H, Chu E (2003) Plane stress yield function for aluminum alloy sheet-part I: theory. Int J Plast 19:1297–1319
101. Barlat F, Richmond O (1985) Prediction of tricomponent plane stress yield surfaces and associated flow and failure behavior of strongly textured FCC sheets. Mater Sci Eng 95:15–29
102. Banabic D, Comsa DS, Balan T (2000) A new yield criterion for orthotropic sheet metals under plane –stress conditions. In: Banabic, D. (ed.): Proc. of the 7th Conf. "TPR2000". Cluj Napoca, pp 217-224
103. Banabic D, Kuwabara T, Balan T, Comsa DS, Julean D (2003) Non-quadratic yield criterion for orthotropic sheet metals under plane-stress conditions. Int J Mech Sci 45:797–811
104. Banabic D, Aretz H, Comsa DS, Paraianu L (2005) An improved analytical description of orthotropy in metallic sheets. Int J Plast 21:493–512
105. Pilthammar J, Banabic D, Sigvant M (2020) BBC05 with non-integer exponent and ambiguities in Nakajima yield surface calibration. Int J Mater Form. https://doi.org/10.1007/s12289-020-01545-0
106. Barlat F, Yoon JW, Cazacu O (2007) On linear transformations of stress tensors for the description of plastic anisotropy. Int J Plast 23:876–896
107. Comsa DS, Banabic D (2008) Plane-stress yield criterion for highly-anisotropic sheet metals. Proc Numisheet 2008 Conf, Interlaken, Switzerland, pp 43–48
108. Vrh M, Halilovič M, Starman B, Štok B, Comsa DS, Banabic D (2014) Capability of the BBC2008 yield criterion in predicting the earing profile in cup deep drawing simulations. Eur J Mech A/Solids 45:59–74
109. Plunkett B, Lebensohn RA, Cazacu O, Barlat F (2006) Anisotropic yield function of hexagonal materials taking into account texture development and anisotropic hardening. Acta Mater 54:4159–4169
110. Lebensohn RA, Tomé CN (1993) A self-consistent approach for the simulation of plastic deformation and texture development of polycrystals: application to zirconium alloys. Acta Metall Mater 41:2611–2624

111. Cazacu O, Plunkett B, Barlat F (2006) Orthotropic yield criterion for hexagonal close packed metals. Int J Plast 22:1171–1194
112. Gawad J, Banabic D, van Bael A, Comsa DS, Gologanu M, Eyckens P, van Houtte P, Roose D (2015) An evolving plane stress yield criterion based on crystal plasticity virtual experiments. Int J Plast 75:141–169
113. van Houtte P, Li S, Seefeldt M, Delannay L (2005) Deformation texture prediction: from the Taylor model to the advanced Lamel model. Int J Plast 21:589–624
114. Barlat F, Gracio JJ, Lee M-G, Rauch EF, Vincze G (2011) An alternative to kinematic hardening in classical plasticity. Int J Plast 27:1309–1327
115. van den Boogaard T, Havinga J, Belin A (2016) Parameter reduction for Yld2004-18p yield criterion. Int J Mater Form 9: 175–178
116. Yoon JW, Barlat F, Dick RE, Karabin ME (2006) Prediction of six or eight ears in a drawn cup based on a new anisotropic yield function. Int J Plast 22:174–193
117. Yoon JW, Barlat F (2006) Modeling and simulation of the forming of aluminium sheet alloys. In: Semiatin SL (ed) ASM Handbook, Metalworking: sheet forming, vol 14B. ASM International, Materials Park, OH, pp 792–826
118. Skrzypek JJ, Ganczarski AW (2015) Mechanics of anisotropic materials. Springer, London
119. Banabic D (2000) Anisotropy of sheet metals. In: Banabic D (ed) Formability of metallic materials. Springer, Berlin Heidelberg, pp 119–172
120. Banabic D, Barlat F, Cazacu O, Kuwabara T (2007) Anisotropy and formability. In: Chinesta F, Cueto E (eds) Advances in material forming-ESAFORM 10 years on. Springer, Berlin, Heidelberg, pp 143–173
121. Banabic D, Barlat F, Cazacu O, Kuwabara T (2010) Advances in anisotropy and formability. Int J Mat Form 3:165–189
122. Barlat F (2007) Constitutive modeling for metals. In: Banabic D (ed) Advanced methods in material forming. Springer, Berlin, Heidelberg, pp 5–25
123. Barlat F, Lee M-G (2015) Constitutive description of isotropic and anisotropic plasticity for metals. In: Altenbach H, Sadowski T (eds) Failure and damage analysis of advanced materials. Course and lectures at the International Center for Mechanical Sciences (CISM), Udine, Italy. Springer, Berlin, pp 67–118
124. Barlat F, Kuwabara T, Korkolis Y (2017) Anisotropic plasticity and application to plane stress. In: Encyclopedia of Continuum Mechanics, Springer, Berlin
125. Bruschi S, Altan T, Banabic D, Bariani PF, Brosius A, Cao J, Ghiotti A, Khraisheh M, Merklein M, Tekkaya AE (2014) Testing and modelling of material behaviour and formability in sheet metal forming. CIRP Ann Manuf Technol 63:727–749
126. Yu MH (2002) Advances in strength theories for materials under complex stress state in the 20th century. Appl Mech Rev 55:198–218
127. Nie JF (2014) Physical metallurgy of light alloys. In: Laughlin DE, Hono K (eds) Physical metallurgy. Elsevier, Amsterdam, pp 2009–2156
128. Bohlen J, Nürnberg MR, Senn JW, Letzig D, Agnew SR (2007) The texture and anisotropy of magnesium–zinc–rare earth alloy sheets. Acta Mater 55:2101–2112
129. Hosford WF (1985) Comments on anisotropic yield criteria. Int J Mech Sci 27:423–427
130. Hosford WF, Allen TJ (1973) Twining and directional slip as a cause for strength differential effect. Met Trans 4:1424–1425
131. Cazacu O, Barlat F (2004) A criterion for description of anisotropy and yield differential effects in pressure-insensitive metals. Int J Plast 20:2027–2045
132. Vitek V, Mrovec M, Bassani JL (2004) Influence of non-glide stresses on plastic flow: from atomistic to continuum modeling. Mater Sci Eng A 365:31–37
133. Cazacu O, Barlat F (2008) Modeling plastic anisotropy and strength differential effects in metallic materials. In: Cazacu O (eds.) Multiscale modeling of heterogeneous materials: from microstructure to macroscale properties, ISTE ltd and John Wiley & Sons Inc, pp 71-91
134. Graff S, Brocks W, Steglich D (2007) Yielding of magnesium: from single crystals to polycrystalline aggregates. Int J Plast 23: 1957–1978
135. Nixon ME, Cazacu O, Lebensohn RA (2010) Anisotropic response of high-purity α-titanium: experimental characterization and constitutive modeling. Int J Plast 26:510–532
136. Cazacu O, Revil-Baudard B (2020) Plasticity of metallic materials: modelling and applications to metal forming. Elsevier, Amsterdam
137. Revil-Baudard B, Chandola N, Cazacu O, Barlat F (2014) Correlation between Swift effects and tension–compression asymmetry in various polycrystalline materials. J Mech Phys Solids 70:104–115
138. Guo XQ, Wu W, Wu PD, Qiao H, An K, Liaw PK (2013) On the Swift effect and twinning in a rolled magnesium alloy under free-end torsion. Scr Mater 69:319–322
139. Khan Aszmi R, Farrokh B (2007) Multiaxial and non-proportional loading responses, anisotropy and modeling of Ti–6Al–4V titanium alloy over wide ranges of strain rates and temperatures. Int J Plast 23:931–950
140. Gilles G, Tuninetti V, Bettaïeb MB, Cazacu O, Habraken A, Duchene L (2011b) Experimental characterization and constitutive modeling of TA6V mechanical behavior in plane strain state at room temperature. In: AIP Conf Proc. American Inst Physics, pp. 78–85
141. Bouvier S, Benmhenni N, Tirry W, Gregory F, Nixon M, Cazacu O, Rabet L (2012) Hardening in relation with microstructure evolution of high purity α-titanium deformed under monotonic and cyclic simple shear loadings at room temperature. Mater Sci Eng A 535:12–21
142. Revil-Baudard B, Cazacu O, Flater P, Chandola N, Alves JL (2016) Unusual plastic deformation and damage features in titanium: experimental tests and constitutive modeling. J Mech Phys Solids 88:100–122
143. Chaboche JL (2008) A review of some plasticity and viscoplasticity constitutive theories. Int J Plast 24:1642–1693
144. Teodosiu C, Hu Z (1998) Microstructure in the continuum modeling of plastic anisotropy. In: Cartensen JV, Leffers T, Lorentzen T, Pedersen OB, Sørensen BF, Winther G (eds) Proc. Risø international symposium on material science: modelling of structure and mechanics of materials from microscale to products. Risø National Laboratory, Roskilde, pp 149–168
145. Mánik T, Holmedal B, Hopperstad OS (2015) Strain-path change induced transients in flow stress, work hardening and r-values in aluminum. Int J Plast 69:1–20
146. Peeters B, Seefeldt M, Teodosiu C, Kalidindi SR, Van Houtte P, Aernoudt (2001) Work-hardening/softening behaviour of b.c.c. polycrystals during changing strain paths: I. An integrated model based on substructure and texture evolution, and its prediction of the stress–strain behaviour of an IF steel during two-stage strain paths. Acta Mater 49, 1607–1619
147. Wang J, Levkovitch V, Svendsen B (2006) Modeling and simulation of directional hardening in metals during non-proportional loading. J Mater Process Technol 177:430–432
148. Feigenbaum HP, Dafalias YF (2007) Directional distortional hardening in metal plasticity within thermodynamics. Int J Solids Struct 44:7526–7542
149. Levkovitch V, Svendsen B (2007) Accurate hardening modeling as basis for the realistic simulation of sheet forming processes with complex strain-path changes. AIP conference proceedings 907, Cueto, E. and Chinesta, F., (Eds.), pp. 358–363

150. Qin J, Holmedal B, Zhang K, Hopperstad OS (2017) Modeling strain-path changes in aluminum and steel. Int J Solids Struct 117: 123–136
151. Qin J, Holmedal B, Hopperstad OS (2018) A combined isotropic, kinematic and distortional hardening model for aluminum and steels under complex strain-path changes. Int J Plast 101:156–169
152. Kurtyka T, Życzkowski M (1996) Evolution equations for distortional plastic hardening. Int J Plast 23:191–213
153. Krieg RD (1975) A practical two surface plasticity theory. Trans ASME J App Mech 42:641–646
154. Dafalias YF, Popov EP (1975) A model of nonlinearly hardening materials for complex loading. Acta Mecanica 21:173–192
155. He J, Xia ZC, Zeng D, Li S (2013) Forming limits of a sheet metal after continuous bending-under-tension loading. J Eng Mater Technol 135:031009
156. Barlat F, Ha J, Grácio JJ, Lee M-G, Rauch EF, Vincze G (2013) Extension of homogeneous anisotropic hardening model to cross-loading with latent effects. Int J Plast 46:130–142
157. Barlat F, Vincze G, Grácio JJ, Lee M-G, Rauch E, Tomé C (2014) Enhancements of homogenous anisotropic hardening model and application to mild and dual phase steels. Int J Plast 58:201–218
158. Barlat F, Yoon SY, Lee SY, Kim JH (2020) Distortional plasticity framework with application to advanced high strength steel. Int J Solids Struct. https://doi.org/10.1016/j.ijsolstr.2020.05.014
159. Spitzig WA, Sober RJ, Richmond O (1975) Pressure dependence of yielding and associated volume expansion in tempered martensite. Acta Metall 23:885–893
160. Choi J, Lee J, Bae GH, Barlat F, Lee MG (2016) Evaluation of springback for DP980 S-rail part by anisotropic hardening models. JOM 68:1850–1857
161. Choi J, Lee J, Bong HJ, Lee MG, Barlat F (2018) Advanced constitutive modeling of AHSS sheets for springback prediction after double stage U-draw bending. Int J Solids Struct 151:152–164
162. Kuwabara T (2014) Biaxial stress testing methods for sheet metals. In: comprehensive materials processing; van Tyne CJ (ed) Elsevier, Vol. 1, pp. 95–111
163. Mulder J, Vegter H, Aretz H, Keller S, van den Boogaard AH (2015) Accurate determination of flow curves using the bulge test with optical measuring systems. J Mater Process Technol 226: 169–187
164. Yoshida K (2013) Evaluation of stress and strain measurement accuracy in hydraulic bulge test with the aid of finite-element analysis. ISIJ Int 53:86–95
165. Min J, Stoughton TB, Carsley JE, Carlson BE, Lin J, Gao X (2017) Accurate characterization of biaxial stress-strain response of sheet metal from bulge testing. Int J Plast 94:192–213
166. Yanaga D, Kuwabara T, Uema N, Asano M (2012) Material modeling of 6000 series aluminum alloy sheets with different density cube textures and effect on the accuracy of finite element simulation. Int J Solids Struct 49:3488–3495
167. Chen K, Scales M, Kyriakides S, Corona E (2016) Effects of anisotropy on material hardening and burst in the bulge test. Int J Solids Struct 82:70–84
168. Williams BW, Boyle KP (2016) Characterization of anisotropic yield surfaces for titanium sheet using hydrostatic bulging with elliptical dies. Int J Mech Sci 114:315–329
169. Hanabusa Y, Takizawa H, Kuwabara T (2010) Evaluation of accuracy of stress measurements determined in biaxial stress tests with cruciform specimen using numerical method. Steel Res Int 81:1376–1379
170. Hanabusa Y, Takizawa H, Kuwabara T (2013) Numerical verification of a biaxial tensile test method using a cruciform specimen. J Mater Process Technol 213:961–970
171. Deng N, Kuwabara T, Korkolis YP (2015) Cruciform specimen design and verification for constitutive identification of anisotropic sheets. Exp Mech 55:1005–1022
172. Tiernan P, Hannon A (2014) Design optimisation of biaxial tensile test specimen using finite element analysis. Int J Mat Form 7:117–123
173. Bertin M, Hild F, Roux S (2016) Optimization of a biaxial tensile specimen geometry for the identification of constitutive parameters based upon full field measurements. Strain 52:307–323
174. Härtel M, Pfeiffer S, Schmaltz S, Söhngen B, Kulawinski D, Willner K, Henkel S, Biermann H, Wagner MFX (2018) On the identification of an effective cross section for a cruciform specimen. Strain 54:1–12
175. Leotoing L, Guines D (2015) Investigations of the effect of strain path changes on forming limit curves using an in-plane biaxial tensile test. Int J Mech Sci 99:21–28
176. Song X, Leotoing L, Guines D, Ragneau E (2016) Investigation of the forming limit strains at fracture of AA5086 sheets using an in-plane biaxial tensile test. Eng Fract Mech 163:130–140
177. Liu W, Guines D, Leotoing L, Ragneau E (2016) Identification of strain rate-dependent mechanical behaviour of DP600 under in-plane biaxial loadings. Mater Sci Eng A 676:366–376
178. Song X, Leotoing L, Guines D, Ragneau E (2017) Characterization of forming limits at fracture with an optimized cruciform specimen: application to DP600 steel sheets. Int J Mech Sci 126:35–43
179. Xiao R, Li XX, Lang LH, Song Q, Liu KN (2017) Forming limit in thermal cruciform biaxial tensile testing of titanium alloy. J Mater Process Technol 240:354–361
180. Jocham D, Gaber C, Böttcher O, Wiedemann P, Volk W (2017) Experimental prediction of sheet metal formability of AW-5754 for non-linear strain paths by using a cruciform specimen and a blank holder with adjustable draw beads on a sheet metal testing machine. Int J Mat Form 10:597–605
181. Srinivasan N, Velmurugan R, Kumar SSK, Pant B (2016) Deformation behavior of commercially pure (CP) titanium under equi-biaxial tension. Mater Sci Eng A674:540–551
182. Verma RK, Kuwabara T, Chung K, Haldar A (2011) Experimental evaluation and constitutive modeling of non-proportional deformation for asymmetric steels. Int J Plast 27:82–101
183. Kuwabara T, Sugawara F (2013) Multiaxial tube expansion test method for measurement of sheet metal deformation behavior under biaxial tension for a large strain range. Int J Plast 45:103–118
184. Kuwabara T, Ichikawa K (2015) Hole expansion simulation considering the differential hardening of a sheet metal. Rom J Tech Sci Appl Mech 60:63–81
185. Merklein M, Suttner S, Brosius A (2014) Characterization of kinematic hardening and yield surface evolution from uniaxial to biaxial tension with continuous strain path change. CIRP Ann Manuf Technol 63:297–300
186. Nomura S, Kuwabara T (2020) Material modeling of hot-rolled steel sheet considering differential hardening and hole expansion simulation. ISIJ Int 106 (in Japanese)
187. Hakoyama T, Kuwabara T (2015) Effect of biaxial work hardening modeling for sheet metals on the accuracy of forming limit analyses using the Marciniak-Kuczynski approach. In: Altenbach H, Matsuda T, Okumura D (eds) From Creep Damage Mechanics to Homogenization Methods. Springer, Cham, pp 67–95
188. Hashimoto K, Kuwabara T, Iizuka E, Yoon JW (2010) Effect of anisotropic yield functions on the accuracy of hole expansion simulations for 590 MPa grade steel sheet. J Iron Steel Inst Jpn 96: 557–563 (in Japanese)
189. Deng N, Kuwabara T, Korkolis YP (2018) On the non-linear unloading behavior of a biaxially loaded dual-phase steel sheet. Int J Mech Sci 138–139:383–397

190. Kuwabara T, Hashimoto K, Iizuka E, Yoon JW (2011) Effect of anisotropic yield functions on the accuracy of hole expansion simulations. J Mater Process Technol 211:475–481
191. Kuwabara T, Nakajima T (2011) Material modeling of 980MPa dual phase steel sheet based on biaxial tensile test and in-plane stress reversal test. J Solid Mech Mater Eng 5:709–720
192. Zhang S, Léotoing L, Guines D, Thuillier S (2015) Potential of the cross biaxial test for anisotropy characterization based on heterogeneous strain field. Exp Mech 55:817–835
193. Min J, Carsley JE, Lin J, Wen Y, Kuhlenkötter B (2016) A non-quadratic constitutive model under non-associated flow rule of sheet metals with anisotropic hardening: modeling and experimental validation. Int J Mech Sci 119:343–359
194. Cheng C, Wan M, Meng B, Zhao R, Han WP (2019) Size effect on the yield behavior of metal foil under multiaxial stress states: experimental investigation and modelling. Int J Mech Sci 151: 760–771
195. Kawaguchi J, Kuwabara T, Sakurai T (2015) Formulation of the differential hardening of 5000 series aluminum alloy sheet for enhancing the predictive accuracy of sheet metal forming simulations. J Jpn Inst Light Metals 65:554–560 (in Japanese)
196. Liu W, Guines D, Leotoing L, Ragneau E (2015) Identification of sheet metal hardening for large strains with an in-plane biaxial tensile test and a dedicated cross specimen. Int J Mech Sci 101-102:387–398
197. Zhang S, Leotoing L, Guines D, Thuillier S, Zang SL (2014) Calibration of anisotropic yield criterion with conventional tests or biaxial test. Int J Mech Sci 85:142–151
198. Andar MO, Kuwabara T, Steglich D (2012) Material modeling of AZ31 Mg sheet considering variation of r-values and asymmetry of the yield locus. Mater Sci Eng A 549:82–92
199. Ishiki M, Kuwabara T, Hayashida Y (2011) Measurement and analysis of differential work hardening behavior of pure titanium sheet using spline function. Int J Mat Form 4:193–204
200. Badr OM, Barlat F, Rolfe B, Lee MG, Hodgson P, Weiss M (2016) Constitutive modelling of high strength titanium alloy Ti-6Al-4V for sheet forming applications at room temperature. Int J Solids Struct 80:334–347
201. Xiao R, Li XX, Lang LH, Chen YK, Yang YF (2016) Biaxial tensile testing of cruciform slim superalloy at elevated temperatures. Mat Des 94:286–294
202. Lee JY, Lee KJ, Lee MG, Kuwabara T, Barlat F (2019) Numerical modeling for accurate prediction of strain localization in hole expansion of a steel sheet. Int J Solids Struct 156–157:107–118
203. Andar MO, Kuwabara T, Yonemura S, Uenishi A (2010) Elastic-plastic and inelastic characteristics of high strength steel sheets under biaxial loading and unloading. ISIJ 50:613–619
204. Sumikawa S, Ishiwatari A, Hiramoto J, Yoshida F, Clausmeyer T, Tekkaya E (2017) Stress state dependency of unloading behavior in high strength steels. Procedia Eng 207:179–184
205. Brosius A, Yin Q, Güner A, Tekkaya AE (2011) A new shear test for sheet metal characterization. Steel Res Int 82:323–328
206. Kulawinski D, Ackermann S, Seupel A, Lippmann T, Henkel S, Kuna M, Weidner A, Biermann H (2015) Deformation and strain hardening behavior of powder metallurgical TRIP steel under quasi-static biaxial-planar loading. Mat Sci Eng A 642:317–329
207. Ripley PW, Korkolis YP (2016) Multiaxial deformation apparatus for testing of microtubes under combined axial-force and internal-pressure. Exp Mech 56:273–286
208. Yoon JW, Barlat F, Dick RE, Chung K, Kang TJ (2004) Plane stress yield function for aluminum alloy sheets–part II: FE formulation and its implementation. Int J Plast 20:495–522
209. Dick CP, Korkolis YP (2015) Anisotropy of thin-walled tubes by a new method of combined tension and shear loading. Int J Plast 71:87–112
210. Yoshida K, Tsuchimoto T (2018) Plastic flow of thin-walled tubes under nonlinear tension-torsion loading paths and an improved pseudo-corner model. Int J Plast 104:214–229
211. Khalfallah A, Oliveira MC, Alves JL, Zrib T, Belhadjsalah H, Menezes LF (2015) Mechanical characterization and constitutive parameter identification of anisotropic tubular materials for hydroforming applications. Int J Mech Sci 104:91–103
212. Yin Q, Zillmann B, Suttner S, Gerstein G, Biasutti M, Tekkaya A, Wagner M, Merklein M, Schaper M, Halle T, Brosius A (2014) An experimental and numerical investigation of different shear test configurations for sheet metal characterization. Int J Solids Struct 51:1066–1074
213. ASTM 2005 Test method for shear testing of thin aluminum alloy products. ASTM Int.
214. Fu J, Barlat F, Kim JH, Pierron F (2017) Application of the virtual fields method to the identification of the homogeneous anisotropic hardening parameters for advanced high strength steels. Int J Plast 93:229–250
215. Peirs J, Verleysen P, Degrieck J (2012) Novel technique for static and dynamic shear testing of Ti6Al4V sheet. Exp Mech 52:729–741
216. Rahmaan T, Abedini A, Butcher C, Pathak N, Worswick MJ (2017) Investigation into the shear stress, localization and fracture behavior of DP600 and AA5182-O sheet metal alloys under elevated strain rates. Int J Impact Eng 108:303–321
217. Abedini A, Butcher C, Worswick MJ (2017) Fracture characterization of rolled sheet alloys in shear loading: studies of specimen geometry, anisotropy, and rate sensitivity. Exp Mech 57:75–88
218. Dunand M, Mohr D (2011) Optimized butterfly specimen for the fracture testing of sheet materials under combined normal and shear loading. Eng Fract Mech 78:2919–2934
219. Abedini A, Butcher C, Nemcko M, Kurukuri S, Worswick MJ (2017) Constitutive characterization of a rare-earth magnesium alloy sheet (ZEK100-O) in shear loading: studies of anisotropy and rate sensitivity. Int J Mech Sci 128-129:54–69
220. Rahmaan T, Noder J, Abedini A, Zhou P, Butcher C, Worswick MJ (2020) Anisotropic plasticity characterization of 6000- and 7000-series aluminum sheet alloys at various strain rates. Int J Impact Eng 135:103390
221. Butcher C, Abedini A (2019) On anisotropic plasticity models using linear transformations on the deviatoric stress: physical constraints on plastic flow in generalized plane strain. Int J Mech Sci 161–162:105044
222. Abedini A, Butcher C, Rahmaan T, Worswick MJ (2018) Evaluation and calibration of anisotropic yield criteria in shear loading: constraints to eliminate numerical artefacts. Int J Solids Struct 151:118–134
223. Flores P, Tuninetti V, Gilles G, Gonry P, Duchene L, Habraken AM (2010) Accurate stress computation in plane strain tensile tests for sheet metal using experimental data. J Mater Process Technol 210:1772–1779
224. Aretz H, Hopperstad OS, Lademo OG (2007) Yield function calibration for orthotropic sheet metals based on uniaxial and plane strain tensile tests. J Mater Process Technol 186:221–235
225. Tian H, Brownell B, Baral M, Korkolis YP (2017) Earing in cup-drawing of anisotropic Al-6022-T4 sheets. Int J Mater Form 10: 329–343
226. Abspoel M, Scholting ME, Droog JMM (2013) A new method for predicting forming limit curves from mechanical properties. J Mater Process Technol 213:759–769
227. Baral M, Hama T, Knudsen E, Korkolis YP (2018) Plastic deformation of commercially-pure titanium: experiments and modeling. Int J Plast 105:164–194
228. Zillmann B, Wagner MFX, Schmaltz S, Schmidl E, Lampke T, Willner K, Halle T (2015) In-plane biaxial compression and tension testing of thin sheet materials. Int J Solids Struct 66:111–120

229. Mohr D, Dunand M, Kim KH (2010) Evaluation of associated and non-associated quadratic plasticity models for advanced high strength steel sheets under multi-axial loading. Int J Plast 26: 939–956
230. Coppieters S, Cooreman S, Sol H, Van Houtte P, Debruyne D (2011) Identification of the post-necking hardening behaviour of sheet metal by comparison of the internal and external work in the necking zone. J Mater Process Technol 211:545–552
231. Grédiac M, Pierron F (2006) Applying the virtual fields method to the identification of elasto-plastic constitutive parameters. Int J Plast 22:602–627
232. Pannier Y, Avril S, Rotinat R, Pierron F (2006) Identification of elasto-plastic constitutive parameters from statically undetermined tests using the virtual fields method. Exp Mech 46:735–755
233. Pierron F, Avril S, Tran VT (2010) Extension of the virtual fields method to elasto-plastic material identification with cyclic loads and kinematic hardening. Int J Solids Struct 47:2993–3010
234. Kim JH, Serpanti A, Barlat F, Pierron F, Lee MG (2013) Characterization of the post-necking hardening behaviour using the virtual fields method. Int J Solids Struct 50:3829–3842
235. Knysh P, Korkolis YP (2017) Identification of the post-necking hardening response of rate- and temperature-dependent metals. Int J Solids Struct 115-116:149–160
236. Marth S, Häggblad HÅ, Oldenburg M, Östlund R (2016) Post necking characterisation for sheet metal materials using full field measurement. J Mater Process Technol 238:315–324
237. Marek A, Davis FM, Pierron F (2017) Sensitivity-based virtual fields for the non-linear virtual fields method. Comput Mech 60: 409–431
238. Teaca M, Charpentier I, Martiny M, Ferron G (2010) Identification of sheet metal plastic anisotropy using heterogeneous biaxial tensile tests. Int J Mech Sci 52:572–580
239. Ferron G, Makkouk R, Morreale J (1994) A parametric description of orthotropic plasticity in metal sheets. Int J Plast 10:431–449
240. Güner A, Soyarslan C, Brosius A, Tekkaya AE (2012) Characterization of anisotropy of sheet metals employing inhomogeneous strain fields for yld2000-2d yield function. Int J Solids Struct 49:3517–3527
241. Tardif N, Kyriakides S (2012) Determination of anisotropy and material hardening for aluminum sheet metal. Int J Solids Struct 49:3496–3506
242. Barlat F, Aretz H, Yoon JW, Karabin ME, Brem JC, Dick RE (2005) Linear transformation-based anisotropic yield functions. Int J Plast 21:1009–1039
243. Tsutamori H, Amaishi T, Chorman RR, Eder M, Vitzthum S, Volk V (2020) Evaluation of prediction accuracy for anisotropic yield functions using cruciform hole expansion test. J Manuf Mater Process 4:43–62
244. An Y, Vegter H, Carless L, Lambriks M (2011) A novel yield locus description by combining the Taylor and the relaxed Taylor theory for sheet steels. Int J Plast 27:1758–1780
245. Yoshida K, Ishii A, Tadano Y (2014) Work-hardening behavior of polycrystalline aluminum alloy under multiaxial stress paths. Int J Plast 53:17–39
246. Yamanaka A, Hashimoto K, Kawaguchi J, Sakurai T, Kuwabara T (2015) Material modeling and forming simulation of 5182 aluminum alloy sheet using numerical biaxial tensile test based on homogenized crystal plasticity finite element method. Keikinzoku/J Jpn Inst Light Metals 65:561–567
247. Coppieters S, Hakoyama T, Eyckens P, Nakano H, Van Bael A, Debruyne D, Kuwabara T (2019) On the synergy between physical and virtual sheet metal testing: calibration of anisotropic yield functions using a microstructure-based plasticity model. Int J Mat Form 12:741–759
248. Upadhyay MV, Patra A, Wen W, Panzner T, Van Petegem S, Tomé CN, Lebensohn RA, Van Swygenhoven H (2018) Mechanical response of stainless steel subjected to biaxial load path changes: cruciform experiments and multi-scale modeling. Int J Plast 108:144–168
249. Hama T, Kobuki A, Takuda (2017) Crystal-plasticity finite-element analysis of anisotropic deformation behavior in a commercially pure titanium grade 1 sheet. Int J Plast 91:77–108
250. Steglich D, Jeong Y, Andar MO, Kuwabara T (2012) Biaxial deformation behaviour of AZ31 magnesium alloy: crystal-plasticity-based prediction and experimental validation. Int J Solids Struct 49:3551–3561
251. Kim H, Barlat F, Lee Y, Zaman SB, Lee CS, Jeong Y (2018) A crystal plasticity model for describing the anisotropic hardening behavior of steel sheets during strain-path changes. Int J Plast 111: 85–106
252. Noma N, Kuwabara T (2012) Specimen geometry optimization for in-plane reverse loading test of sheet metal and experimental validation. Steel Res Int Spec Edition: 14th Metal Form 1283–1286
253. Verma RK, Chung K, Kuwabara T (2011) Effect of pre-strain on anisotropic hardening and springback behavior of an ultra low carbon automotive steel. ISIJ Int 51:482–490
254. Shirakami S, Yonemura S, Yoshida T, Suzuki N, Kuwabara T (2015) Work-hardening behavior of cold rolled interstitial-free steel sheet and dual phase high strength steel sheet subjected to two-stage, coaxial and non-coaxial tension/compression. Key Eng Mater 651-653:83–88
255. Shirakami S, Kuwabara T, Tsuru E (2017) Axial compressive deformation behavior and material modeling of steel pipe with bending deformation history. J Jpn Soc Technol Plast 58:692–698 (in Japanese)
256. Gröge R, Vitek V (2019) Impact of non-Schmid stress components present in the yield criterion for bcc metals on the activity of $\{110\}\langle 111\rangle$ slip systems. Comput Mater Sci 159:297–305
257. Ghaffari Tari D, Worswick MJ, Ali U, Gharghouri MA (2014) Mechanical response of AZ31B magnesium alloy: experimental characterization and material modeling considering proportional loading at room temperature. Int J Plast 55:247–267
258. Habib SA, Khan AS, Gnäupel-Herold T, Lloyd JT, Schoenfeld SE (2017) Anisotropy, tension-compression asymmetry and texture evolution of a rare-earth-containing magnesium alloy sheet, ZEK100, at different strain rates and temperatures: experiments and modeling. Int J Plast 95:163–190
259. Hama T, Kariyazaki Y, Hosokawa N, Fujimoto H, Takuda H (2012) Work-hardening behaviors of magnesium alloy sheet during in-plane cyclic loading. Mater Sci Eng A 551:209–217
260. Jia Y, Bai Y (2016) Experimental study on the mechanical properties of AZ31B-H24 magnesium alloy sheets under various loading conditions. Int J Fract 197:25–48
261. Li M, Lou XY, Kim JH, Wagoner RH (2010) An efficient constitutive model for room-temperature, low-rate plasticity of annealed Mg AZ31B sheet. Int J Plast 26:820–858
262. Hama T, Nagao H, Kobuki A, Fujimoto H, Takuda H (2015) Work-hardening and twinning behaviors in a commercially pure titanium sheet under various loading paths. Mater Sci Eng A 620: 390–398
263. Gilles G, Hammami W, Libertiaux V, Cazacu O, Yoon JH, Kuwabara T, Habraken AM, Duchene L (2011a) Experimental characterization and elasto-plastic modeling of the quasi-static mechanical response of TA-6 V at room temperature. Int J Solids Struct 48:1277–1289
264. Hammami W, Gilles G, Habraken AM, Duchêne L (2011) Phenomenological and crystal plasticity approaches to describe the mechanical behaviour of Ti6Al4V titanium alloy. Int J Mater Form 4:205–215

265. Dietrich L, Socha G, Kowalewski ZL (2014) Anti-buckling fixture for large deformation tension – compression cyclic loading of thin metal sheets. Strain 50:174–183
266. Marcadet SJ, Mohr D (2015) Effect of compression–tension loading reversal on the strain to fracture of dual phase steel sheets. Int J Plast 72:21–43
267. Lee MG, Kim JH, Kim D, Seo OS, Nguyen NT, Kim HY (2013) Anisotropic hardening of sheet metals at elevated temperature: tension-compressions test development and validation. Exp Mech 53:1039–1055
268. Zecevic M, Korkolis YP, Kuwabara T, Knezevic M (2016) Dual-phase steel sheets under cyclic tension–compression to large strains: experiments and crystal plasticity modeling. J Mech Phys Solids 96:65–87
269. Jeong Y, Gnäupel-Herold T, Barlat F, Iadicola M, Creuziger A, Lee MG (2015) Evaluation of biaxial flow stress based on elasto-viscoplastic self-consistent analysis of X-ray diffraction measurements. Int J Plast 66:103–118
270. Jeong Y, Iadicola MA, Gnäupel-Herold T, Creuziger A (2016) Multiaxial constitutive behavior of an interstitial-free steel: measurements through X-ray and digital image correlation. Acta Mater 112:84–93
271. Marciniak Z (1984) Assessment of material formability. Proc Int Conf Adv Techn Plasticity, Tokyo, pp 685–694
272. Soeiro JMC, Silva CMA, Silva MB, Martins PAF (2015) Revisiting the formability limits by fracture in sheet metal forming. J Mater Process Technol 217:184–192
273. Banabic D (2000) Forming limits of sheet metals. In: Banabic D (ed) Formability of metallic materials. Springer, Berlin, Heidelberg, pp 173–215
274. Banabic D (2000) Theoretical models of the FLD's. In: Banabic D (ed) Formability of metallic materials. Springer, Berlin, Heidelberg, pp 317–327
275. Banabic D (2016) Multiscale modelling in sheet metal forming. Springer, Berlin, Heidelberg
276. Felice L, Banabic D (2015) Formability and damage. In: Laperrière L, Reinhart G (eds) Encyclopedia of production engineering. Springer, Heidelberg, pp 539–547
277. Hora P, Krauer J (eds) (2006) Numerical and experimental methods in prediction of forming limits in sheet metal forming and tube hydroforming processes. FLC Conf, Zürich
278. Wagoner RH, Chan KS, Keeler SP (eds) (1989) Forming limit diagrams: concepts, methods, and applications. TMS, Warrendale
279. Xu Y (2006) Modern formability: measurement, Analysis and Applications. Hanser Gardner, Cincinnati
280. Embury JD, Duncan JL (1981) Formability maps. Annu Rev Mater Sci 11:505–521
281. Volk W, Suh J (2013) Prediction of formability for non-linear deformation history using generalized forming limit concept (GFLC). AIP Conf Proc 1567:556–561
282. Stoughton TB, Yoon JW (2011) A new approach for failure criterion for sheet metals. Int J Plast 27:440–459
283. Glover G, Duncan GL, Embury JD (1977) Failure maps for sheet metal. Metals Technol 4:153–159
284. Lloyd DJ, Sang H, Embury JD, Wycliffe P, LeRoy GH (1978) On the description of deformation at large imposed plastic strains. Mater Sci Eng 36:35–46
285. Arrieux R, Bedrin C, Boivin M (1982) Determination of an intrinsec forming limit stress diagram for isotropic sheets. In: proc. 12th IDDRG Conf. S-ta Margerita Ligure, pp 61-71
286. Simha CHM, Gholipour J, Bardelcik A, Worswick MJ (2007) Prediction of necking in tubular hydroforming using an extended stress-based FLC. Trans ASME J Eng Mater Technol 129:136–147
287. Simha CHM, Grantab R, Worswick MJ (2007) Computational analysis of stress-based forming limit curves. Int J Solids Struct 44:8663–8684
288. Müschenborn W, Sonne H (1975) Effects of the strain path on the limits of deformation of sheet metal (in German). Arch Eisenhüttenwesen:597–602
289. Volk W, Gaber W (2017) Investigation and compensation of bi-axial pre-strain during the standard Nakajima- and Marciniak-test using generalized forming limit concept. Process Eng 207:568–573
290. Yoshida K, Kuwabara T, Kuroda M (2007) Path-dependence of the forming limit stresses in a sheet metal. Int J Plast 23:361–384
291. Zeng D, Chappuis L, Xia Z, Zhu X (2009) A path independent forming limit criterion for sheet metal forming simulations. SAE Int J Mater Manuf 1:809–817
292. Dick RE, Yoon JW, Stoughton TB (2016) Path-independent forming limit models for multi-stage forming processes. Int J Mat Form 9:327–337
293. Stoughton TB (2000) A general forming limit criterion for sheet metal forming. Int J Mech Sci 42:1–27
294. Takashina K et al (1968) Relation between the manufacturing conditions and the average strain according to the scribed circle tests in steel sheets. La Metallurgia Ital 8:757–765
295. Veerman C et al (1971) Determination of appearing and admissible strains in cold-reduced sheets. Sheet Metal Ind 687-694
296. Bragard A, Baret JC, Bonnarens H (1972) A simplified technique to determine the FLD at onset of necking. CRM 33:53–63
297. d'Hayer R, Bragard A (1975) Determination of the limiting strains at the onset of necking. CRM 42:33–35
298. Hecker SS (1972) A simple forming limit curve technique and results on aluminum alloys. In: proc. IDDRG Congress, Amsterdam, pp 5.1–5.8
299. Kobayashi T, Ishigaki H, Tadayuki (1972) A effect of strain ratios on the deforming limit of steel sheet and its application to the actual press forming. In: Proc IDDRG Congress, Amsterdam, pp 8.1–8.4
300. Methods of determining the forming limit curve. IDDRG Meeting 1983, Zurich
301. Marron G et al (1997) A new necking criterion for the forming limit diagrams, IDDRG 1997 WG meeting, Haugesund
302. Volk W (2006) New experimental and numerical approach in the evaluation of the FLD with the FE-method. In: Hora P (ed) Numerical and experimental methods in prediction of forming limits in sheet forming and tube hydroforming processes. ETH, Zürich, pp 26–30
303. Volk W et al (2008) Benchmark 1. Virtual forming limit curves. Part A. physical tryout report. In: Hora P (ed) Proc NUMISHEET 2008 Conf (Part B Benchmark study), Interlaken, pp. 3–9
304. Volk W et al (2008) Benchmark 1. Virtual forming limit curves. Part B. benchmark analysis. In: Hora P (ed) Proc NUMISHEET 2008 Conf (Part B. Benchmark study), Interlaken, pp. 11–42
305. Hashemi R, Abrinia K, Assempour A (2013) The strain gradient approach to predict necking in tube hydroforming. J Manuf Process 15:51–55
306. Lumelskyj D, Rojek J, Banabic D, Lazarescu L (2017) Detection of strain localization in Nakazima formability test -experimental research and numerical simulation. Procedia Eng 183:89–94
307. Lumelskyj D, Rojek J, Banabic D, Lazarescu L (2017) Determination of forming limit curve by finite element method simulation. Procedia Manuf 27:78–82
308. Situ Q, Jain MK, Metzger DR (2011) Determination of forming limit diagrams of sheet materials with a hybrid experimental–numerical approach. Int J Mech Sci 53:707–719
309. Hotz W (2006) European efforts in standardization of FLC. In: Hora P (ed) Numerical and experimental methods in prediction of

forming limits in sheet forming and tube hydroforming processes. ETH Zürich, Zürich, pp 24–25
310. Hotz W, Timm J (2008) Experimental determination of forming limit curves (FLC). In: Hora P (ed.), Proc NUMISHEET 2008 Conf, Interlaken, pp. 271–278
311. Liebertz H et al (2004) Guideline for the determination of forming limit curves. In: Proc. IDDRG Conf, Sindelfilgen, pp. 216–224
312. Thoors H et al (2008) FLD assessment using the proposed new standard. IDDRG 2008 Int Conf, Olofström, pp. 25–35
313. Leppin C, Li J, Daniel D (2008) Application of a method to correct the effect of non-proportional strain paths on Nakajima test based forming limit curves. In: Hora P (ed), Proc NUMISHEET 2008 Conf, Interlaken, pp. 217–221
314. Hogström P, Ringsberg JW, Johnson E (2009) An experimental and numerical study of the effects of length scale and strain state on the necking and fracture behaviour in sheet metals. Int J Impact Eng 36:1194–1203
315. Dicecco S, Di Ciano M, Butcher C, Worswick M (2018) Die-quench formability of a developmental AA7xxx aluminum alloy sheet, proceedings international deep draw research group (IDDRG) 37th international conference, Waterloo, Ontario, June 3-7, 2018
316. Morales D, Martinez A, Vallellano C, Garcia-Lomas FJ (2009) Bending effect in the failure of stretch-bend metal sheets. Int J Mat Form 2:813–816
317. Silva MB, Martínez-Donaire AJ, Centeno G, Morales-Palma D, Vallellano C, Martins PAF (2015) Recent approaches for the determination of forming limits by necking and fracture in sheet metal forming. Procedia Eng 132:342–349
318. Zahedi A, Mollaei Dariani B, Mirnia MJ (2019) Experimental determination and numerical prediction of necking and fracture forming limit curves of laminated Al/cu sheets using a damage plasticity model. Int J Mech Sci 153–154:341–358
319. Iquilio RA et al (2019) Novel experimental method to determine the limit strain by means of thickness variation. Int J Mech Sci 153–154:208–218
320. Min J, Stoughton TB, Carsley JE, Lin J (2016) Compensation for process-dependent effects in the determination of localized necking limits. Int J Mech Sci 117:115–134
321. Min J, Stoughton TB, Carsley JE, Lin J (2017) A method of detecting the onset of localized necking based on surface geometry measurements. Exp Mech 57:521–535
322. Min J, Stoughton TB, Carsley JE, Lin J (2017) An improved curvature method of detecting the onset of localized necking in Marciniak tests and its extension to Nakazima tests. Int J Mech Sci 123:238–252
323. Elangovan K, Sathiya Narayanan C, Narayanasamy R (2010) Modelling of forming limit diagram of perforated commercial pure aluminium sheets using artificial neural network. Comput Mater Sci 47:1072–1078
324. Elangovan K, Sathiya Narayanan C, Narayanasamy R (2011) Modelling the correlation between the geometrical features and the forming limit strains of perforated Al 8011 sheets using artificial neural network. Int J Mater Form 4:389–399
325. Mitukiewicz G, Anantheshwara K, Zhou G, Mishra RK, Jain MK (2014) A new method of determining forming limit diagram for sheet materials by gas blow forming. J Mater Process Technol 214:2960–2970
326. Karadogan C, Tamer ME (2015) Development of a new and simplified procedure for the experimental determination of forming limit curves. CIRP Ann Manuf Technol 62:265–268
327. Marin J, Ulrich BH, Hughes WP (1951) Plastic stress-strain relations for 75S-T6 aluminum alloy subjected to biaxial tensile stresses. NACA report TN 2425
328. Yu Y, Wan M, Wu X-D, Zhou X-B (2002) Design of a cruciform biaxial tensile specimen for limit strain analysis by FEM. J Mater Process Technol 123:67–70
329. Cruciform Multiaxial Mechanical (2013) The National Institute of Standards and Technology https://www.nist.gov/programs-projects/cruciform-multiaxial-mechanical-testing
330. Shao Z, Li N, Lin J, Dean T (2016) Development of a new biaxial testing system for generating forming limit diagrams for sheet metals under hot stamping conditions. Exp Mech 56:1489–1500
331. Shao Z, Li N, Lin J, Dean T (2017) Formability evaluation for sheet metals under hot stamping conditions by a novel biaxial testing system and a new materials model. Int J Mech Sci 120:149–158
332. Ghosh AK, Hecker SS (1974) Stretching limits in sheet metals: in-plane versus out-of- plane deformation. Metall Trans A 5:2161–2164
333. Charpentier P (1975) Influence of punch curvature on stretching limits of sheet steel. Metall Mater Trans A 6:1665–1669
334. Martínez-Donaire AJ, Vallellano C, Morales D, Garcia-Lomas FJ (2010) Experimental detection of necking in stretch-bending conditions: a critical review and new methodology. Steel Res Int 81:785–788
335. Martínez-Palmeth LH, Martínez-Donaire AJ, Centeno G, García-Lomas FJ, Vallellano C (2013) Formability of automotive H240LA steel sheets in stretch–bending processes. Process Eng 63:669–677
336. Martínez-Palmeth LH, Martínez-Donaire AJ, Vallellano C (2019) Formability limits of high-strength H240LA steel sheets under stress/strain gradients. Mech Mater 132:47–56
337. Morales-Palma D, Vallellano C, García-Lomas F (2013) Assessment of the effect of the through-thickness strain/stress gradient on the formability of stretch-bend metal sheets. Mat Des 50:798–809
338. Vallellano C, Morales D, García-Lomas FJ (2008) On the study of the effect of bending in the formability of metal sheets. In: Proc Numisheet 2008 Conf Interlaken, Switzerland, pp 85–90
339. Atzema EH, Fictorie E, van den Boogaard AH, Droog JMM. (2010) The influence of curvature on FLC's of mild steel, (a)HSS and aluminium. In: Proc. IDDRG Conf, Graz, Austria, pp. 519–528
340. Martinez Lopez A, van den Boogaard AH (2011) Formability limit curves under stretch-bending. IDDRG 2011 Bilbao 1-8
341. Hou B, Perdahcioglu ES, van den Boogaard AH, Kitting D (2014) Study of instability and forming limit of sheet metal under stretch-bending. Key Eng Mater 611-612:84–91
342. Abbas A, Campoli G, Sinke J, Benedictus R (2011) Fracture in bending the straining limits of monolithic sheets and machined. Mater Des 32:1229–1241
343. Affronti E, Merklein M (2018) Analysis of the bending effects and the biaxial pre-straining in sheet metal stretch forming processes for the determination of the forming limits. Int J Mech Sci 138–139:295–309
344. Habibi M, Hashemi R, Ghazanfari A, Naghdabadi R, Assempour A (2016) Forming limit diagrams by including the M–K model in finite element simulation considering the effect of bending. J Mater Des App 232:625–636
345. Liewald M, Schleich R (2010) Development of an anisotropic failure criterion for characterising the influence of curvature on forming limits of aluminium sheet metal alloys. Int J Mater Form 3:1175–1178
346. Hu P, Liu W, Ying L, Zhang J, Wang D (2017) A thermal forming limit prediction method considering material damage for 22MnB5 sheet. Int J Adv Manuf Technol 92:627–638
347. Ma B, Wan M, Li XJ, Wu XD, Diao KS (2017) Evaluation of limit strain and temperature history in hot stamping of advanced high strength steels (AHSS). Int J Mech Sci 128–129:607–613

348. Mohamed MS, Foster AD, Lin J, Balint DS, Dean TA (2012) Investigation of deformation and failure features in hot stamping of AA6082: experimentation and modelling. Int J Mach Tools Manuf 53:27–38
349. Shao Z, Bai Q, Li N, Lin J, Shi Z, Stanton M, Watson D, Dean T (2018) Experimental investigation of forming limit curves and deformation features in warm forming of an aluminium alloy. J Eng Manuf 232:465–474
350. Zheng K, Politis DJ, Wang L, Lin J (2018) A review on forming techniques for manufacturing lightweight complex—shaped aluminium panel components. Int J Light Mater Manuf 1:55–80
351. Bariani PF, Bruschi S, Ghiotti A, Michieletto F (2013) Hot stamping of AA5083 aluminium alloy sheets. CIRP Ann Manuf Technol 62:251–254
352. Ding J, Zhang C, Chu X, Zhao G, Leotoing L, Guines D (2015) Investigation of the influence of the initial groove angle in the M–K model on limit strains and forming limit curves. Int J Mech Sci 98:59–69
353. Bagheriasl R, Worswick MJ (2015) Formability of AA3003 brazing sheet at elevated temperatures: limiting dome height tests and determination of forming limit diagrams. Int J Mater Form 8:229–244
354. Wang H, Luo Y, Friedman P, Chen M, Gao L (2012) Warm forming behavior of high strength aluminum alloy AA7075. Trans Nonferrous Metals Soc China 22:1–7
355. Wang H, Yan Y, Han F, Wan F (2017) Experimental and theoretical investigations of the forming limit of 5754O aluminum alloy sheet under different combined loading paths. Int J Mech Sci 133: 147–166
356. Xiao W, Wang B, Zheng K (2017) An experimental and numerical investigation on the formability of AA7075 sheet in hot stamping condition. Int J Adv Manuf Technol 92:3299–3309
357. Sorgente D, Scintilla LD, Palumbo G, Tricarico L (2010) Blow forming of AZ31 magnesium alloy at elevated temperatures. Int J Mater Form 3:13–19
358. Ghiotti A, Bruschi S (2010) A novel experimental set-up for warm incremental forming of AZ31B magnesium alloy sheets. Steel Res Int 81:950–953
359. Zhang H, Huang GS, Kong D, Sang G, Song B (2011) Influence of initial texture on formability of AZ31B magnesium alloy sheets at different temperatures. J Mater Process Technol 211:1575–1580
360. Huang GS, Zhang H, Gao XS, Song B, Zhang L (2011) Forming limit of textured AZ31B magnesium alloy sheet at different temperatures. Trans Nonferrous Metals Soc China 21:836–843
361. Ambrogio G, Filice L, Gagliardi F (2012) Formability of lightweight alloys by hot incremental sheet forming. Mater Des 34: 501–508
362. Boba M, Butcher C, Panahi N, Worswick MJ, Mishra R, Carter J (2017) Formability of magnesium-rare earth alloy ZEK100 sheet at elevated temperatures. Int J Mater Form 10:181–191
363. Berge F, Krüger L, Ullrich C (2014) Forming limit diagrams of twin-roll cast, rolled and heat-treated AZ31 as a function of temperature and loading rate. Mater Sci Eng A 614:27–35
364. Koh Y, Kim D, Seok DY, Bak J, Kim SW, Lee YS, Chung K (2015) Characterization of mechanical property of magnesium AZ31 alloy sheets for warm temperature forming. Int J Mech Sci 93:204–217
365. Kim SJ, Lee YS, Kim D (2016) Analysis of formability of ca-added magnesium alloy sheets at low temperatures. Mater Charact 113:152–159
366. Stutz L, Bohlen J, Kurz G, Letzig D, Kainer U (2011) Influence of the processing of magnesium alloys AZ31 and ZE10 on the sheet formability at elevated temperature. Key Eng Mater 473:335–342
367. Mekonen MN, Steglich D, Bohlen J, Stutz L, Letzig D, Mosler J (2013) Experimental and numerical investigation of Mg alloy sheet formability. Mater Sci Eng A 586:204–214
368. Yang H, Fan XG, Sun ZC, Guo LG, Zhan M (2011) Recent developments in plastic forming technology of titanium alloys. Sci China Technol Sci 54:490–501
369. Bodunrin MO, Chown LH, van der Merwe JW, Alaneme KA (2019) Hot working of Ti-6Al-4V with a complex initial microstructure. Int J Mater Form 12:857–874
370. Karbasian H, Tekkaya AE (2010) A review on hot stamping. J Mater Process Technol 210:2103–2118
371. Lihui L, Kangning L, Cai G, Yang X, Guo C, Bu G (2014) A critical review on special forming processes and associated research for lightweight components based on sheet and tube materials. Manuf Rev 1:9–20
372. Lin L (2015) Fundamentals of materials modelling for metals processing technologies: theories and applications. Imperial College Press, London
373. Drewes EJ, Martini A (1976) Einfluss der Umformgeschwindigkeit auf die Grenzformaenderungen und die Formaenderungsverteilung von Feinblech. Arch Eissenhuettenwessen 47:167–172
374. Ayres RA, Wenner ML (1978) Strain and strain–rate hardening effect on punch stretching of 5182-O aluminium at elevated temperature. Sheet Metal Ind 55:1208–1216
375. Percy JH (1980) The effect of strain rate on the FLD for sheet metal. CIRP Ann Manuf Technol 29:151–152
376. Li MY, Zhu X, Chu E (2012) Effect of strain rate sensitivity on FLDs—An instability approach. Int J Mech Sci 64:273–279
377. Yamashita M, Nikawa M, Kuroda T (2018) Effect of strain-rate on forming limit in biaxial stretching of aluminium sheet. Proc Manuf 15:877–883
378. Psyk V, Risch D, Kinsey BL, Tekkaya AE, Kleiner M (2011) Electromagnetic forming – a review. J Mater Process Technol 211:787–829
379. Smerd R, Winkler S, Salisbury C, Worswick MJ, Lloyd D, Finn M (2005) High strain rate tensile testing of automotive aluminum alloy sheet. Int J Impact Eng 32:541–560
380. Imbert J, Worswick M, Winkler S, Golovashchenko S, Dmitriev V (2005) Analysis of the increased formability of aluminum alloy sheet formed using electromagnetic forming. SAE technical paper series 2005-01-0082
381. Imbert J, Worswick M (2012) Reduction of a pre-formed radius in aluminium sheet using electromagnetic and conventional forming. J Mater Process Technol 212:1963–1972
382. Jacques N (2020) An analytical model for necking strains in stretched plates under dynamic biaxial loading. Int J Solids Struct. https://doi.org/10.1016/j.ijsolstr.2020.05.028
383. Nakazima K, Kikuma T, Hasuka K (1968) Study on the formability of steel sheets. Yamata Tech Rep 264:8517–8530
384. Graf AF, Hosford WF (1993) Effect of changing strain paths on forming limit diagrams of Al 2008-T4. Metall Trans A 24:2503–2512
385. Rojek J, Lumelskyy D, Pęcherski R, Grosman F, Tkocz M, Chorzępa W (2013) Forming limit curves for complex strain paths. Arch Metall Mater 58:587–593
386. El Fakir O, Wang LL, Balint D, Dear JP, Lin J (2014) Predicting effect of temperature, strain rate and strain path changes on forming limit of lightweight sheet metal alloys. Process Eng 81: 736–741
387. Mattiasson K, Jergéus J, DuBois P (2014) On the prediction of failure in metal sheets with special reference to strain path dependence. Int J Mech Sci 88:175–191
388. Suttner S, Merklein M (2015) Characterization of the shear stress state under non-proportional strain paths realized by biaxial stretching in the Marciniak test. Mater Today Proc 1:98–106

389. Nurcheshmeh M, Green DE (2016) Prediction of forming limit curves for nonlinear loading paths using quadratic and non-quadratic yield criteria and variable imperfection factor. Mater Des 91:248–255
390. Swift HW (1952) Plastic instability under plane stress. J Mech Phys Solid 1:1–16
391. Hill R (1952) On discontinous plastic states, with special reference to localized necking in thin sheets. J Mech Phys Solid 1:19–30
392. Hora P, Tong L (1994) Prediction methods for ductile sheet metal failure using FE-simulation. In: Proc. IDDRG Congress, Lisbon, pp. 363–375
393. Hora P, Tong L, Reissner J (1996) A prediction method for ductile sheet metal failure. In: Lee JK, Kinzel GL, Wagoner RH (eds), Proc NUMISHEET 1996 Conf, Dearborn, pp 252-256
394. Marciniak Z, Kuczynski K (1967) Limit strains in the processes of stretch forming sheet metal. Int J Mech Sci 9:609–620
395. Barata da Rocha A, Jalinier JM (1984) Plastic instability of sheet metals under simple and complex strain paths. Trans ISIJ 24:132–140
396. Stören S, Rice JR (1975) Localized necking in thin sheets. J Mech Phys Solids 23:421–441
397. Dudzinski D, Molinari A (1988) Instability of visco-plastic deformation in biaxial loading. C R Acad Sci Paris 307:1315–1321
398. Bressan JD, Williams JA (1983) The use of a shear instability criterion to predict local necking in sheet metal deformation. Int J Mech Sci 25:155–168
399. Stoughton TB (2008) Generalized metal failure criterion. In: Hora P (ed), Proc NUMISHEET 2008 Conf (Part B. Benchmark study), Interlaken, pp. 241–246
400. Banabic D, Kami A, Comsa DS, Eyckens P (2020) Developments of the Marciniak-Kuczynski model for sheet metal formability: a review. J Mater Process Technol (in press). https://doi.org/10.1016/j.jmatprotec.2019.116446
401. Bassani J, Hutchinson J, Neale K (1979) On the prediction of necking in anisotropic sheets. In: Lippmann H (ed) Metal forming plasticity. Springer, Berlin, pp 1–13
402. Bate P (1984) The prediction of limit strains in steel sheet using a discrete slip plasticity model. Int J Mech Sci 26:373–384
403. Asaro RJ, Needleman A (1985) Texture development and strain hardening in rate-dependent polycrystals. Acta Metall 33:923–953
404. van Houtte P, Toth LS (1993) Generalization of the Marciniak-Kuczynski defect model for predicting FLD. In: Lee WB (ed) Advances in engineering plasticity and its application. Elsevier, Amsterdam, pp 1013–1020
405. Wu PD, Neale KW, van der Giessen E (1997) On crystal plasticity FLD analysis. Proc R Soc Lond 453:1831–1848
406. Serenelli MJ, Bertinetti MA, Signorelli JW (2010) Investigation of the dislocation slip assumption on formability of BCC sheet metals. Int J Mech Sci 52:1723–1734
407. Serenelli MJ, Bertinetti MA, Signorelli JW (2011) Study of limit strains for FCC and BCC sheet metal using polycrystal plasticity. Int J Solids Struct 48:1109–1119
408. Signorelli JW, Serenelli MJ, Bertinetti MA (2012) Experimental and numerical study of the role of crystallographic texture on the formability of an electro-galvanized steel sheet. J Mater Process Technol 212:1367–1376
409. Inal K, Neale KW, Aboutajeddine A (2005) Forming limit comparisons for FCC and BCC sheets. Int J Plast 21:1255–1266
410. Inal K, Wu PD, Neale KW (2002) Instability and localized deformation in polycrystalline solids under plane-strain tension. Int J Solids Struct 39:983–1002
411. Nagra JS, Brahme A, Lebensohn RA, Inal K (2017) Efficient fast Fourier transform-based numerical implementation to simulate large strain behavior of polycrystalline materials. Int J Plast 98:65–82
412. Hancock J, Mackenzie A (1976) On the mechanisms of ductile failure in high-strength steels subjected to multi-axial stress-states. J Mech Phys Solids 24:147–160
413. Gurson AL (1975) Plastic flow and fracture behavior of ductile ma-terials incorporating void nucleation, growth and coalescence, PhD Diss, Brown University
414. Gurson AL (1977) Continuum theory of ductile rupture by void nucleation and growth part I-yield criteria and flow rules for porous ductile media. J Eng Mater Technol 99:2–15
415. Tvergaard V, Needleman A (1984) Analysis of the cup-cone fracture in a round tensile bar. Acta Metall 32:157–169
416. Richmond O, Smelser R (1985) Alcoa technical center memorandum
417. Leblond J, Perrin G, Suquet P (1994) Exact results and approximate models for porous viscoplastic solids. Int J Plast 10:213–235
418. Cazacu O, Revil-Baudard B, Lebensohn RA, Garajeu M (2013) On the combined effect of pressure and third invariant on yield-ing of porous solids with von Mises matrix. J Appl Mech 80:064501
419. Cazacu O, Revil-Baudard B, Chandola N, Kondo D (2014) New analytical criterion for porous solids with Tresca matrix under axisymmetric loadings. Int J Solids Struct 51:861–874
420. Cazacu O, Stewart JB (2009) Analytic plastic potential for porous aggregates with matrix exhibiting tension–compression asymmetry. J Mech Phys Solids 57:325–341
421. Benzerga, A. A, Besson, J. (2001). Plastic potentials for anisotropic porous solids. Eur J Mech-A/Solids, 20(3): 397–434
422. Stewart JB, Cazacu O (2011) Analytical yield criterion for an anisotropic material containing spherical voids and exhibiting tension–compression asymmetry. Int J Solids Struct 48:357–373
423. Thuillier S, Maire E, Brunet M (2012) Ductile damage in aluminium alloy thin sheets: correlation between micro-tomography observations and mechanical modeling. Mater Sci Eng A 558:217–225
424. Revil-Baudard B, Cazacu O, Thuillier S, Maire E (2013) Effect of stress triaxiality on porosity evolution in notched bars: quantitative agreement between a recent dilatational model and X-ray tomography data. Mech Res Commun 50:77–82
425. Maire E, Zhou S, Adrien J, Dimichiel M (2011) Damage quantification in aluminum alloys in situ tensile tests in X-ray tomography. Eng Fract Mech 78:2679–2690
426. Lemaitre J (2001) Continuous damage. In: Lemaitre J (ed) Handbook of materials behavior models. Academic Press, San Diego, pp 411–793
427. Lin J, Mohamed M, Balint D, Dean TA (2013) The development of continuum damage mechanics-based theories for predicting forming limit diagrams for hot stamping applications. Int J Damage Mech 23:684–701
428. Malcher L, Andrade Pires FM, César de Sá JMA (2014) An extended GTN model for ductile fracture under high and low stress triaxiality. Int J Plast 54:193–228
429. Yang XY, Lang LH, Liu KN, Guo C (2015) Modified MK model combined with ductile fracture criterion and its application in warm hydroforming. Trans Nonferrous Metals Soc China 25:3389–3398
430. Tang BT, Bruschi S, Ghiotti A, Bariani PF (2016) An improved damage evolution model to predict fracture of steel sheet at elevated temperature. J Mater Process Technol 228:76–87
431. Gologanu M, Comsa DS, Banabic D (2013) Theoretical model for forming limit diagram predictions without initial inhomogeneity. AIP Conf Proc 1532:245–253
432. Kami A, Dariani BM, Vanini AS, Comsa DS, Banabic D (2015) Numerical determination of the forming limit curves of anisotropic sheet metals using GTN damage model. J Mater Process Technol 216:472–483

433. Bai Y, Wierzbicki T (2008) A new model of metal plasticity and fracture with pressure and Lode dependence. Int J Plast 24:1071–1096
434. Bai Y, Wierzbicki T (2008) Forming severity concept for predicting sheet necking under complex loading histories. Int J Mech Sci 50:1012–1022
435. Bao Y, Wierzbicki T (2004) On fracture locus in the equivalent strain and stress triaxiality space. Int J Mech Sci 46:81–98
436. Bao Y, Wierzbicki T (2005) On the cut-off value of negative triaxiality for fracture. Eng Fract Mech 72:1049–1069
437. Bai Y, Wierzbicki T (2015) A comparative study of three groups of ductile fracture loci in the 3D space. Eng Fract Mech 135:147–167
438. Jia Y, Bai Y (2016) Ductile fracture prediction for metal sheets using all-strain-based anisotropic eMMC model. Int J Mech Sci 115-116:516–531
439. Li Y, Wierzbicki T (2010) Prediction of plane strain fracture of AHSS sheets with post-initiation softening. Int J Solids Struct 47: 2316–2327
440. Li Y, Luo M, Gerlach J, Wierzbicki T (2010) Prediction of shear-induced fracture in sheet metal forming. J Mater Process Technol 210:1858–1869
441. Luo M, Wierzbicki T (2010) Numerical failure analysis of a stretch-bending test on dual-phase steel sheets using a phenomenological fracture model. Int J Solids Struct 47:3084–3102
442. Wierzbicki T, Bao Y, Lee YW, Bai Y (2005) Calibration and evaluation of seven fracture models. Int J Mech Sci 47:719–743
443. Lou YS, Huh H, Lim S, Pack K (2012) New ductile fracture criterion for prediction of fracture forming limit diagrams of sheet metals. Int J Solids Struct 49:3605–3615
444. Lou YS, Yoon JW, Huh H (2014) Modeling of shear ductile fracture considering a changeable cut-off value for stress triaxiality. Int J Plast 54:56–80
445. Park N, Huh H, Lim SJ, Lou Y, Kang YS, Seo MH (2017) Fracture-based forming limit criteria for anisotropic materials in sheet metal forming. Int J Plast 96:1–35
446. Park N, Huh H, Yoon JW (2018) Anisotropic fracture forming limit diagram considering non-directionality of the equi-biaxial fracture strain. Int J Solids Struct 151:181–194
447. Li H, Fu MW, Lu J, Yang H (2011) Ductile fracture: experiments and computations. Int J Plast 27:147–180
448. Lou YS, Chen L, Clausmeyer T, Tekkaya EA, Yoon JW (2017) Modeling of ductile fracture from shear to balanced biaxial tension for sheet metals. Int J Solids Struct 112:169–184
449. Yoon, J.W, Lou, Y, Yoon, J and Glazoff, M.V. (2014) Asymmetric yield function based on the stress invariants for pressure sensitive metals. Int J Plast, 56 :184–202
450. Keeler SP (1970) La formabilité est améliorée par pression hydrostatique. Mach Mod:43–45
451. Banabic D, Soare S (2008) On the effect of the normal pressure upon the forming limit strains. In: Hora P (ed): Proc. NUMISHEET 2008 Conf., Interlaken, pp 199-204
452. Wu PD et al (2008) Effects of superimposed hydrostatic pressure on sheet metal formability. Int J Plast 25:1711–1725
453. Allwood JM, Shouler DR (2008) Generalised forming limit diagrams showing increased forming limits with non-planar stress states. Int J Plast 25:1207–1230
454. Liu B, Lang L, Zeng Y, Lin J (2012) Forming characteristic of sheet hydroforming under the influence of through-thickness normal stress. J Mater Process Technol 212:1875–1884
455. Zhang F, Chen J, Chen J, Lu J, Liu G, Yuan S (2012) Overview on constitutive modeling for hydroforming with the existence of through-thickness normal stress. J Mater Process Technol 212: 2228–2237
456. Zhang F, Chen J, Chen J (2014) Effect of through-thickness normal stress on forming limits under Yld2003 yield criterion and MK model. Int J Mech Sci 89:92–100
457. Nurcheshmeh M, Green DE (2014) The effect of normal stress on the formability of sheet metals under non-proportional loading. Int J Mech Sci 82:131–139
458. Lang L, Cai G, Liu K, Alexandrov S, Du P, Zheng H (2015) Investigation on the effect of through thickness normal stress on forming limit at elevated temperature by using modified M-K model. Int J Mater Form 8:211–228
459. Hashemi R, Abrinia K, Faraji G (2015) A methodology for determination of extended strain-based forming limit curve considering the effects of strain path and normal stress. J Mech Eng Sci 229: 1537–1547
460. Hashemi R, Abrinia K, Assempour A, Khakpour Nejadkhaki H, Shahbazi Mastanabad A (2016) Forming limit diagram of tubular hydroformed parts considering the through-thickness compressive normal stress. J Mater Design Appl 230:332–343
461. Mirfalah-Nasiri SM, Basti A, Hashemi R (2016) Forming limit curves analysis of aluminum alloy considering the through-thickness normal stress, anisotropic yield functions and strain rate. Int J Mech Sci 117:93–101
462. Mirfalah-Nasiri SM, Basti A, Hashemi R, Darvizeh A (2018) Effects of normal and through-thickness shear stresses on the forming limit curves of AA3104-H19 using advanced yield criteria. Int J Mech Sci 137:15–23
463. Ma B, Wan W, Zhang H, Gong XL, Wu XD (2018) Evaluation of the forming limit curve of medium steel plate based on nonconstant through-thickness normal stress. J Manuf Process 33:175–183
464. Bettaieb MB, Abed-Meraim F (2017) Theoretical and numerical investigation of the impact of out-of-plane compressive stress on sheet metal formability. Int J Mech Sci 130:244–257
465. Shi Y, Jin H, Wu PD, Lloyd DJ (2017) Effects of superimposed hydrostatic pressure on necking and fracture of tube under hydroforming. Int J Solids Struct 113–114:209–217
466. Hu Q, Li X, Chen J (2019) Forming limit evaluation by considering through-thickness normal stress: theory and modeling. Int J Mech Sci 155:187–196
467. Soare S, Barlat F (2014) About the influence of hydrostatic pressure on the yielding and flow of metallic polycrystals. J Mech Phys Solids 67:87–99
468. Eyckens P, Van Bael A, Van Houtte P (2009) Marciniak-Kuczynski type modelling of the effect of through-thickness shear on the forming limits of sheet metal. Int J Plast 25:2249–2268
469. Eyckens P, Van Bael A, Van Houtte P (2011) An extended Marciniak-Kuczynski model for anisotropic sheet subjected to monotonic strain paths with through-thickness shear. Int J Plast 27:1577–1597
470. Fatemi A, Dariani BM (2015) Forming limit prediction of anisotropic material subjected to normal and through thickness shear stresses using a modified M–K model. Int J Adv Manuf Technol 80:1497–1509
471. Darabi R, Deilami Azodi H, Bagherzadeh S (2017) Investigation into the effect of material properties and arrangement of each layer on the formability of bimetallic sheets. J Manuf Process 29:133–148
472. Kami A, Chung K, Banabic D (2017) Analytical and numerical studies on formability of metal/polymer/metal sandwich sheets. Rom J Technol Sci- Appl Mech 56:28–38
473. Sun T, Liang J, Guo X, Ren M, Wang L (2015) Optical measurement of forming limit and formability of cu/Al clad metals. J Mater Eng Perform 24:1426–1433
474. Kim YS, Yang SH (2017) Effect of plastic anisotropy on the formability of aluminum 6016-T4 sheet material. Chin J Mech Eng 30:625–631

475. Paraianu L, Dragos G, Bichis I, Comsa DS, Banabic D (2010) A new formulation of the modified maximum force criterion (MMFC). Int J Mater Form 3:243–246
476. Pham QT, Nguyen DT, Kim JJ, Kim YS (2019) A graphical method to estimate forming limit curve of sheet metals. Key Eng Mater 794:55–62
477. Xu ZT, Peng LF, Fu MW, Lai XM (2015) Size effect affected formability of sheet metals in micro/meso scale plastic deformation: experiment and modeling. Int J Plast 68:34–54
478. Hu Q, Zhang L, Ouyang Q, Li X, Zhu X, Chen J (2018) Prediction of forming limits for anisotropic materials with nonlinear strain paths by an instability approach. Int J Plast 103:143–167
479. Zajkani A, Bandizaki A (2017) An efficient model for diffuse to localized necking transition in rate-dependent bifurcation analysis of metallic sheets. Int J Mech Sci 133:794–803
480. Drucker DC (1951) A more fundamental approach to plastic stress-strain relations. Proc First US Nat Congr App Mech ASME New York pp 487–491
481. Hecker SS (1976) In: Stricklin A, Saczalski KC (eds) Experimental studies of yield phenomena in biaxially loaded metals. Constitutive equations in Viscoplasticity: computational and engineering aspects. ASME, New York, pp l–33
482. Stoughton TB (2002) A non-associated flow rule for sheet metal forming. Int J Plast 18:687–714
483. Stoughton TB, Yoon JW (2006) Review of Drucker's postulate and the issue of plastic stability in metal forming. Int J Plast 22: 391–433
484. Richmond O, Spitzig WA (1980) Pressure dependence and dilatancy of plastic flow, proc. IUTAM Conf, ASME, pp. 377–386
485. Aretz H (2005) A non-quadratic plane stress yield function for orthotropic sheet metals. J Mater Process Technol 168: 1–9
486. Choi H, Yoon JW (2019) Stress integration-based on finite difference method and its application for anisotropic plasticity and distortional hardening under associated and non-associated flow rules. Comput Methods Appl Mech Eng 345:123–160